OF MICHIGAN
FEB 10 1959
PHYSICS
LIBRARY

Journal of Research

of the

National Bureau of Standards

DECEMBER 1958

VOLUME 61 NUMBER 6

U. S. DEPARTMENT OF COMMERCE
Lewis L. Strauss, Secretary
NATIONAL BUREAU OF STANDARDS
A. V. Astin, Director

DECEMBER • 1958
VOLUME • 61
NUMBER • 6

JOURNAL OF RESEARCH
of the
NATIONAL BUREAU OF STANDARDS

The National Bureau of Standards

Functions and Activities

The functions of the National Bureau of Standards are set forth in the Act of Congress, March 3, 1901, as amended by Congress in Public Law 619, 1950. These include the development and maintenance of the national standards of measurement and the provision of means and methods for making measurements consistent with these standards; the determination of physical constants and properties of materials; the development of methods and instruments for testing materials, devices, and structures; advisory services to government agencies on scientific and technical problems; invention and development of devices to serve special needs of the Government; and the development of standard practices, codes, and specifications. The work includes basic and applied research, development, engineering, instrumentation, testing, evaluation, calibration services, and various consultation and information services. Research projects are also performed for other government agencies when the work relates to and supplements the basic program of the Bureau or when the Bureau's unique competence is required. The scope of activities is suggested by the listing of divisions and sections on the inside of the back cover.

Publications

The results of the Bureau's work take the form of either actual equipment and devices or published papers. These papers appear either in the Bureau's own series of publications or in the journals of professional and scientific societies. The Bureau itself publishes three monthly periodicals, available from the Government Printing Office: The Journal of Research, which presents complete papers reporting technical investigations; the Technical News Bulletin, which presents summary and preliminary reports on work in progress; and Basic Radio Propagation Predictions, which provides data for determining the best frequencies to use for radio communications throughout the world. There are also five series of nonperiodical publications: The Applied Mathematics Series, Circulars, Handbooks, Building Materials and Structures Reports, and Miscellaneous Publications.

Information on the Bureau's publications can be found in NBS Circular 460, Publications of the National Bureau of Standards ($1.25) and its Supplement ($1.50), available from the Superintendent of Documents, Government Printing Office, Washington 25, D. C.

Order all publications from the Superintendent of Documents
U. S. Government Printing Office, Washington 25, D. C.

Use of funds for printing this publication approved by the Director of the Bureau of the Budget (June 24, 1958)

Journal of Research of the National Bureau of Standards Vol. 61, No. 6, December 1958 Research Paper 2914

Term Analysis of the Second Spectrum of Rhenium (Re II)

William F. Meggers, Miguel A. Catalán,[1,2] and Manuel Sales[2]

Wavelengths and estimated intensities of approximately 2,000 spectral lines emitted by singly ionized rhenium atoms were available for this analysis. Observed Zeeman patterns for 220 Re II lines facilitated finding and interpreting the first energy levels. The analysis continued until 49 low-even, and 85 high-odd levels were found. Transitions between these groups of levels account for 1,014 Re II lines including about 70 percent of the total observed intensity. The ground state of Re^+ is described by the spectral term $5d^5(a^6S)6s\ a^7S_3$.

1. Introduction

The term analysis of the first spectrum of rhenium (Re I) progressed intermittently since it began in 1931; it culminated in a recent report [1][3] on the present state of its analysis and interpretation. Two decades elapsed before the term analysis of the second spectrum of rhenium (Re II) could begin. The delay is explained by the lack of basic observations on this spectrum. No useful description of the Re II spectrum was available until 1952 when Meggers [2] published a description of the arc and spark spectra of rhenium including wavelength and intensity data for approximately 6,000 lines, about 4,200 of which were assigned to Re I, and nearly 1,800 to Re II (and possibly Re III). The wavelengths of spark-enhanced rhenium lines reported in that paper ranged from 2000.47 A to 6026.60 A. The spark spectrum of rhenium, like that of any heavy metal, is rich in the ultraviolet but gradually fades in the visible region, and vanishes in the orange. Because this spectrum is strong in the ultraviolet it would be expected to extend far beyond the violet limit of observation with large spectrographs at atmospheric pressure. In order to record the spectrum in the shorter-wave range Catalán made arc and spark spectrograms with a vacuum spectrograph at Princeton University; these spectrograms were measured in Madrid by Sales who thus extended the wavelength and intensity data of rhenium spectra to about 1500 A.

The splitting of spectral lines by magnetic fields (Zeeman effect) is extremely useful in analyses of complex spectra because it reveals (by the number of components) the inner-quantum numbers (J) of both levels, and usually identifies (by the splitting factors, g) the term types (l) and the multiplicity (r). In 1940, Zeeman spectrograms of rhenium were made [3] with the Bitter magnet and grating spectrographs in the Spectroscopy Laboratory of the Massachusetts Institute of Technology, but these spectrograms never yielded any information about Re II. By courtesy of G. R. Harrison in 1949 Meggers made new Zeeman spectrograms with the M. I. T. equipment and measured them at the National Bureau of Standards. Wavelengths of the Zeeman patterns were computed, and from these the inner-quantum numbers and the magnetic splitting factors of the first Re II energy levels were derived in 1950. A preliminary announcement of the Zeeman effect and first spectral terms of Re II was made [4] in 1952. When 22 low-even and 20 high-odd levels were established, the entire mass of Zeeman data was transferred to Madrid where Catalán and Sales continued the analysis until 1954 when it included about 830 classified lines resulting from transitions between 47 low-even and 69 high-odd levels. Most of the Zeeman data were exploited in this analysis. A final search among wavenumbers, at the Bureau disclosed several additional (provisional) levels that combined 7 or more times with other levels, so that a total of about 1,000 Re II lines could be classified. Details concerning the classified lines of Re II, the energy levels, the Zeeman patterns and magnetic splitting factors, are given below, followed by a brief discussion of spectral terms, and electron configurations.

2. Basic Data of Re II

The basic data of Re II consist of measured wavelengths and estimated relative intensities of more than 2,000 lines emitted by electric arcs and sparks between metallic electrodes. Nearly 1,800 of these have wavelengths between 2000 A and 6000 A which have been published by Meggers [2]; more than 1,000 lines of shorter wavelength (to 1500 A) were observed with a vacuum spectrograph by Catalán, but only the classified lines will be reported in this paper. The wavelength measurements were complicated by the hyperfine structure (hfs) exhibited by many rhenium lines. This has been discussed in the paper Term Analysis of the First Spectrum of Rhenium [1] and need not be repeated here. It suffices to say that in the cases of resolved hfs we have quoted the average wavelength published by Meggers [2].

By comparing the intensities of lines emitted by arcs and sparks, it was usually possible to identify the lines emitted by neutral atoms and by ions. In general, the intensities of Re I lines are greater in arc than in spark spectra, whereas Re II (and possibly Re III) lines appear stronger (or only) in spark spectrograms. Unfortunately there are no reliable criteria for differentiating Re II and Re III, so all the lines enhanced in spark spectra above 2000 A were included in the Re II list although a few may belong

[1] Deceased.
[2] Instituto de Optica, Madrid, Spain.
[3] Figures in brackets indicate the literature references at the end of this paper.

486859—59——1

to Re III. In the vacuum ultraviolet the arc spectrogram showed many more lines than the spark and there was insufficient information to assign the lines to successive spectra; for this reason only those lines that appear to satisfy combinations of Re II levels are reported.

The Zeeman-effect spectrograms at 81,000 oersteds, previously described [1, 4] yielded information concerning some 220 Re II lines. The Zeeman patterns of 85 of these were adequately recorded and resolved to yield J- and g-values for both atomic energy levels responsible for producing a spectral line. These initiated this analysis and interpretation of the Re II spectrum. The Zeeman patterns are of types 1, 2, 3, and 7 according to the description given by Back and Landé [5]. Type 1 occurs when the J-values are unequal and the level with the larger J has the smaller g; the strongest p-component is not displaced, and the strongest n-components have the smallest displacement. Type 2 occurs when J and g change in the same direction, in which case the strongest p-component is not displaced, but the strongest n-components have the largest displacement. Type 3 results from equal J-values but unequal g-values which produce a maximum displacement of the strongest p-components, and the displacements of two pairs of strong n-components are exactly equal to the g-values of the combining levels. Type 7 has only one (undisplaced) p-component, and two displaced n-components, either because one of the J-values is zero, or the two g-values are equal.

When Zeeman patterns of types 1, 2, and 3 were not resolved, only the wavelengths corresponding to the maximum intensity in both polarizations were measured. Then if the line is classified and the g-value of one level is known, the other may be calculated.

3. Classified Lines of Re II

The classified lines of Re II are listed in table 1 where information is given as to estimated relative intensity [2], wavelength [2], vacuum wavenumber, spectral-term combination, and Zeeman effect. In column 1, the intensity numbers of many lines shorter than 2000 A are followed by the letter a which indicates that the line was observed only in the arc spectrum. Because it is impossible to assign term symbols to many Re II energy levels these are represented in column 4 by the first 4 digits of their numerical value referred to the ground state as zero. The daggers attached to 7 wavelengths in column 2 mean that the line was also classified as Re I [1]. An asterisk attached to the Zeeman type in column 5 means that the Zeeman effect disagrees with the term combination of column 4. Numbers in column 6 express the separation of the resolved Zeeman components, or Δg, in Lorentz units. In columns 7 and 8, instead of giving all the observed Zeeman components, only the strongest parallel (p) and normal (n) components are shown; this information, combined with the g-values of columns 9 and 10, and the corresponding J-values in column 4, permit the calculation of the complete pattern. In columns 9 and 10, the g-values in parentheses are mean values from resolved patterns adopted to compute the other g-values from unresolved patterns when the types are indicated in column 5 and the J-values are known from column 4. After the Zeeman data of Re II were fully exploited in establishing energy levels some further progress was made in searching for additional levels by means of coincidences between wavenumber differences and known level intervals. About 830 Re II lines were thus explained by the end of 1954, but 900 lines with wavelengths greater than 2000 A still remained unclassified. In 1955 this search was continued at the Bureau by Jack Tech who found many provisional odd levels, nine of which have been retained in this analysis. In the meantime the possibility of applying electronic digital computers to systematic searches for atomic energy levels in complex atomic spectra had been tested with Tc I by Bozman [6] who used the IBM–604, and with Ru I by Kessler, Prusch, and Stegun [7] who employed the SEAC. Since more than half of the known Re II lines (mostly of low intensity) were still unclassified it appeared desirable to enlist the aid of an electronic computer in a final search for energy levels. This was done with an IBM–704 computer which displaced the machines previously used at the Bureau. Coding this problem for IBM–704 was successfully carried out by W. R. Bozman and C. Coleman, and searches for new levels of Re II were made by them. The first computer search was for possibly undiscovered high-odd levels between 40000 and 80000 K ($=cm^{-1}$) that could combine with the 47 low-even levels (0 to 37000 K), according to the selection rule $\Delta J=0, \pm 1$. The second search started with intervals between the known odd levels (44000 to 77000 K) and sought new even levels, both lower and higher, that might combine with those of opposite parity and thus account for observed Re II lines. These systematic computer searches were both disappointing and illuminating. Several hundred hypothetical levels were found, but when their combinations were displayed in a square array, they usually appeared to have a random distribution, they generally involved only 6 or 7 lines, and they often used the same line in two or more places. In other words, the great majority of predicted levels appeared to be based on accidental coincidences. This conclusion was confirmed by calculation of the number of probable coincidences to be expected among 900 unclassified Re II lines.

S. A. Goudsmit is credited [8] with having devised the following approximate formula for the most probable number of accidental coincidences, C, caused by a random distribution of L spectrum lines extending over a range of I wavenumber units: $C=2\epsilon(L^2/I)\times(I-d)/I$ if all pairs of lines having a wavenumber difference between $(d-\epsilon)$ and $(d+\epsilon)$ are regarded as coincident. If d is small compared with I, the second term may be neglected. Given 900 Re II lines with wavenumbers between 20000 and 50000 K, a tolerance of ± 0.2 K for coincidence

yields 6 or more chance coincidences for each value of d, depending on the size of d. Hundreds of such coincidences were found among the unclassified Re II lines but the energy levels calculated from them were discarded unless they accounted for lines in a nonrandom fashion, or combined with at least 8 other levels. This resulted in the discovery of only 2 additional low-even levels, and 3 odd levels. The search for high-even levels revealed nothing that could not be explained by chance coincidences. For example, the fact that such tentative high-even levels usually combined only with high-odd levels indicated that they were fortuitous because the density of unclassified Re II lines happens to be greatest below 2500 A. This was disappointing because it destroyed any hope of finding one or more spectral series that might be extrapolated to its limit and give an approximate value of the ionization potential of Re^+. This experience is a warning that many false levels may be found in complex spectra by searching with wavenumber intervals, unless the tolerance on coincidences is reduced sufficiently to exclude most accidentals, or unless the levels can be verified by Zeeman data.

When frustration ended the search for energy levels it was seen that the accepted levels account for 1,014 Re II lines listed in table 1. Only 33 of these lines are doubly classified. Although only half of the rhenium spark lines with wavelengths greater than 2000 A are classified in this analysis, these account for about 70 percent of the total observed intensity, and include almost all lines of intensity greater than 30. The combinations $a\,^7S_3 - z\,^7P_{2,\,3,\,4}$ (2275.25, 2414.27, 1973.13 A), yield the strongest Re II lines, but whether they arise from an s–p or a d–p transition is still in doubt.

TABLE 1. *Classified lines of the second spectrum of rhenium* (Re II)

Intensity spark	Wavelength air	Wavenumber	Term combination	Zeeman type	Separation	Zeeman components		g	
						Strongest p	Strongest n	1st	2d
1	2	3	4	5	6	7	8	9	10
	A	*K*							
5*h*	5418.37	18450.60	$3699_5 - z\,^5F^0_5$	-----	------	------	----------	-------	------
5*h*	5286.68	18910.21	$a\,^3G_4 - z\,^7P^0_3$	-----	------	------	----------	-------	------
1*h*	5066.60	19731.60	$3731_3 - z\,^7D^0_3$	-----	------	------	----------	-------	------
4*cw*	4909.71	20362.12	$2907_2 - z\,^5P^0_1$	-----	------	------	----------	-------	------
10*cw*	4904.33	20384.46	$a\,^5P_3 - z\,^7P^0_3$	-----	------	------	----------	-------	------
10*c*	4853.73	20596.96	$a\,^5P_2 - z\,^7P^0_2$	-----	------	------	----------	-------	------
10*cw*	4703.70	21253.91	$a\,^3F_4 - z\,^7P^0_3$	-----	------	------	----------	-------	------
100*c*	4673.15	21392.85	$a\,^3F_2 - z\,^7P^0_2$	-----	------	------	----------	-------	------
8	4664.01	21434.78	$3493_2 - z\,^5D^0_1$	-----	------	------	----------	-------	------
30*c*	4584.49	21806.57	$a\,^5P_2 - z\,^7P^0_3$	-----	------	------	----------	-------	------
4*cw*	4542.89	22006.25	$3738_2 - z\,^3P^0_2$	-----	------	------	----------	-------	------
20	4520.97	22112.94	$3493_2 - z\,^7D^0_3$	-----	------	------	----------	-------	------
6	4502.98	22201.29	$3493_2 - z\,^5D^0_2$	-----	------	------	----------	-------	------
100*c*	4481.32	22308.59	$a\,^3F_3 - z\,^7P^0_2$	-----	------	------	----------	-------	------
5*h*	4475.73	22336.46	$3699_3 - z\,^5D^0_3$	-----	------	------	----------	-------	------
2*h*	4473.60	22347.09	$3731_3 - \mathit{5966}^0_3$	-----	------	------	----------	-------	------
10	4452.68	22452.08	$3022_3 - z\,^5P^0_2$	-----	------	------	----------	-------	------
4*h*	4429.76	22568.25	$3287_2 - z\,^5F^0_2$	-----	------	------	----------	-------	------
20	4423.02	22602.64	$a\,^3F_2 - z\,^7P^0_3$ $3699_3 - z\,^5F^0_4$	-----	------	------	----------	-------	------
3*cwl*	4409.56	22671.63	$2676_2 - z\,^5P^0_1$	-----	------	------	----------	-------	------
10*cwl*	4389.60	22774.72	$2666_1 - z\,^5P^0_1$	3	0.962	0.962w	1.462, 2.424	1.462	2.424
2	4384.44	22801.52	$3225_3 - z\,^7D^0_2$	-----	------	------	----------	-------	------
10*cwl*	4381.00	22819.43	$3098_4 - z\,^5P^0_3$	-----	------	------	----------	-------	------
6	4356.29	22948.86	$2972_2 - z\,^5P^0_2$	-----	------	------	----------	-------	------
2*h*	4335.23	23060.34	$3398_3 - z\,^7D^0_3$	-----	------	------	----------	-------	------
9	4330.69	23084.52	$3071_3 - z\,^5P^0_3$	-----	------	------	----------	-------	------
20*h*	4311.68	23186.29	$3225_3 - z\,^5F^0_2$	1	------	0w	1.105	(1.114)	1.09
4*h*	4248.27	23532.37	$3606_5 - z\,^5F^0_4$	-----	------	------	----------	-------	------
4*cw*	4240.18	23577.27	$3022_3 - z\,^5P^0_3$	-----	------	------	----------	-------	------
2*h*	4186.26	23880.95	$3316_4 - z\,^7D^0_3$	-----	------	------	----------	-------	------
5*Hw*	4149.46	24092.73	$3295_4 - z\,^7D^0_3$	-----	------	------	----------	-------	------
2*h*	4135.43	24174.46	$3287_2 - z\,^7D^0_3$	-----	------	------	----------	-------	------
20*h*	4091.96	24431.28	$3101_2 - z\,^5F^0_3$	3	.340	0.670	1.078, 1.418	1.418	1.078
2*h*	4088.69†	24450.83	$3493_2 - z\,^3P^0_2$	-----	------	------	----------	-------	------
2	4085.14	24472.06	$3295_4 - z\,^5F^0_3$	-----	------	------	----------	-------	------

TABLE 1. *Classified lines of the second spectrum of rhenium* (Re II)—Continued

Intensity spark	Wavelength air	Wavenumber	Term combination	Zeeman type	Separation	Zeeman components		g	
						Strongest p	Strongest n	1st	2d
1	2	3	4	5	6	7	8	9	10
	A	*K*							
2*h*	4051.45	24675.55	3738_2—*6205*$\frac{2}{2}$						
3	4043.10	24726.51	3071_3—$z\ ^5F^0_3$	2	0.180	0	1.624	1.264	1.084
3	4042.78	24728.47	3493_2—*5966*$\frac{3}{3}$	7a,1	------	0h	1.132	(1.23)	1.19
1*h*	4041.11	24738.69	3731_3—*6205*$\frac{2}{2}$						
5*h*	4032.35	24792.42	3225_3—$z\ ^7D^0_3$						
20*c*6	4031.42	24798.15	$a\ ^5G_3$—$z\ ^7P^0_2$						
2*h*	4025.56	24834.24	3022_3—$z\ ^7D^0_2$						
6*h*	4024.040	24843.63	3220_4—$z\ ^7D^0_3$						
10*h*	4020.860	24863.27	3606_5—$z\ ^5F^0_3$	3	------	0.193h	1.178w	(1.21)	1.16
4*h*	4018.016	24880.88	3225_3—$z\ ^5D^0_2$						
10*h*	4009.94	24930.98	2774_3—$z\ ^5P^0_2$	1	.616	0	0	1.232	1.848
3*Hw*	3988.63	25064.18	3699_3—*6205*$\frac{2}{2}$						
10*h*	3984.28	25091.54	$a\ ^5G_2$—$z\ ^7P^0_2$						
3*Hw*	3971.63	25171.50	3225_3—$z\ ^5F^0_2$						
2*Hw*	3964.11	25219.21	3022_3—$z\ ^5F^0_2$						
3*c*	3963.53	25222.95	3220_4—$z\ ^5F^0_3$						
5*h*	3939.381	25377.53	2977_0—$z\ ^7D^0_1$	7a	2.272	0	2.272	0/0	2.272
10*h*	3915.382	25533.08	3738_2—*6291*$\frac{3}{3}$	2	0.166	0	1.570	1.072	1.238
2*cwl*	3900.24	25632.18	2942_1—$z\ ^7D^0_2$						
2*h*	3893.59	25675.97	3398_2—*5966*$\frac{3}{3}$						
7*cws*	3888.92	25706.80	2809_4—$z\ ^5P^0_2$						
5*h*	3886.21	25724.72	3731_3—*6304*$\frac{3}{4}$						
6*Hw*	3873.501	25809.13	3731_3—*6312*$\frac{4}{4}$						
5*h*	3858.528	25909.26	2676_2—$z\ ^5P^0_2$						
2*h*	3856.72	25921.42	3699_3—*6291*$\frac{3}{3}$						
10*Hw*	3847.72	25982.05	2907_2—$z\ ^7D^0_2$						
10*h*	3839.540	26037.40	3101_2—$z\ ^7D^0_3$	1	------	0	0.572	(1.42)	1.14
20*cw*	3836.786	26056.09	2774_3—$z\ ^5P^0_3$						
2*h*	3832.92	26082.38	3738_2—*6346*$\frac{2}{2}$						
8*h*	3830.525	26098.69	$a\ ^5P_2$—$z\ ^5P^0_1$	1	0.758	0	.912	1.670	2.428
2*h*	3826.55	26125.79	3101_2—$z\ ^5D^0_2$						
2*Hw*	3825.30	26134.32	3699_3—*6312*$\frac{4}{4}$						
2	3821.43	26160.80	3316_4—$z\ ^5D^0_3$						
100*cw*	3800.95	26301.75	$a\ ^5G_2$—$z\ ^7P^0_3$	2	1.137	0	4.055	0.644	1.781
2	3791.57	26366.81	2907_2—$z\ ^5F^0_2$						
3*h*	3782.95	26426.89	3316_4—$z\ ^5F^0_4$						
2*h*	3776.70	26470.62	3699_3—*6346*$\frac{2}{2}$						
15*cw*	3773.018	26496.50	3316_4—*5966*$\frac{3}{3}$	2	------	0w	1.185h	(1.188)	1.189
1*h*	3758.51	26598.73	2977_0—$z\ ^5D^0_1$						
4*h*	3752.15	26643.82	2972_2—$z\ ^5D^0_1$						
200*h*	3742.257	26714.26	$a\ ^5S_2$—$z\ ^7P^0_3$	3	0.463	0.927	1.714, 2.177	1.714	2.177
5*Hcw*	3732.058	26787.24	$a\ ^5F_4$—$z\ ^7P^0_4$						
10*Hcw*	3731.662	26790.10	3287_2—*5966*$\frac{3}{3}$						
5*Hc*	3730.89	26795.64	3606_5—$z\ ^5D^0_4$						
10*h*	3714.51	26913.80	3022_3—$z\ ^5D^0_2$	2	------	0w	1.525	(1.398)	1.33
5*h*	3710.22	26944.91	2942_1—$z\ ^5D^0_1$						
30*h*	3698.565	27029.82	3738_2—*6441*$\frac{2}{2}$	3	.260	0.522	0.810, 1.070	1.070	0.810
20*h*	3697.932	27034.45	2676_2—$z\ ^5P^0_3$	2	.555	0	2.754	1.089	1.644
10*h*	3692.783	27072.14	3225_3—$z\ ^5D^0_3$	3	------	0.063	1.123	1.114	1.135
8*h*	3685.803	27123.41	3220_4—$z\ ^5D^0_3$	1	------	0w	0.928	(1.08)	1.13
15*cw*	3674.87	27204.10	3022_3—$z\ ^5F^0_3$	3	.325	0.975	1.056, 1.381	1.381	1.056
7*h*	3668.496	27251.37	3234_5—$z\ ^5F^0_4$	7	------	0h	1.125h	(1.15)	1.16
3*h*	3660.17	27313.36	2774_3—$z\ ^7D^0_2$						
7*h*	3656.834	27338.27	3225_3—$z\ ^5F^0_4$	2	------	0w	1.314	(1.114)	1.15
10*hc*	3647.544	27407.90	3225_3—*5966*$\frac{3}{3}$						

TABLE 1. *Classified lines of the second spectrum of rhenium* (Re II)—Continued

Intensity spark	Wavelength air	Wavenumber	Term combination	Zeeman type	Separation	Zeeman components		g	
						Strongest p	Strongest n	1st	2d
1	2	3	4	5	6	7	8	9	10
	A	*K*							
7*h*	3640. 75	27459. 05	3220_4—*5966*$^0_3$	-----	------	------	----------	-------	------
3*H*	3626. 80	27564. 66	$a\ ^3G_4$—$z\ ^5P^0_3$	-----	------	------	----------	-------	------
4*h*	3624. 11	27585. 12	3738_2—*6496*$^0_3$	-----	------	------	----------	-------	------
2*c*	3609. 330	27698. 07	2774_3—$z\ ^5F^0_2$	-----	------	------	----------	-------	------
3*h*	3601. 600	27757. 52	3316_4—$z\ ^5F^0_3$	7b	------	0	1. 182	(1. 188)	1. 187
1	3595. 600	27803. 84	2666_1—$z\ ^5D^0_0$	-----	------	------	----------	-------	------
6*h*	3581. 434	27913. 81	$a\ ^5P_3$—$z\ ^5P^0_2$	-----	------	------	----------	-------	------
300*cw*	3580. 15	27923. 82	$a\ ^5S_2$—$z\ ^7P^0_3$	7a,2	------	0w	1. 820	(1. 71)	1. 75
2*Hw*	3576. 93	27948. 96	3699_3—*6494*$^0_4$	-----	------	------	----------	-------	------
3*h*	3573. 263	27977. 64	3493_2—*6291*$^0_3$	-----	------	------	----------	-------	------
2*h*	3562. 634	28061. 11	2907_2—$z\ ^5D^0_2$	-----	------	------	----------	-------	------
2*h*	3561. 83	28067. 44	3398_3—*6205*$^0_2$	-----	------	------	----------	-------	------
7*h*	3556. 935	28106. 07	3493_2—*6304*$^0_3$	-----	------	------	----------	-------	------
3*cw*	3546. 33	28190. 11	3738_2—*6557*$^0_3$	-----	------	------	----------	-------	------
30*h*	3542. 735	28218. 71	3606_5—$z\ ^7D^0_5$	1*	------	0w	1. 044	-------	------
4*h*	3538. 36	28253. 61	3731_3—*6557*$^0_3$	-----	------	------	----------	-------	------
3*H*	3532. 69	28299. 0	3098_4—$z\ ^7D^0_4$	-----	------	------	----------	-------	------
3*h*	3530. 41	28317. 22	3101_2—$z\ ^5D^0_2$	-----	------	------	----------	-------	------
5*h*	3527. 118	28343. 64	3606_5—*6440*$^0_4$	-----	------	------	----------	-------	------
1*h*	3525. 64	28355. 54	3731_3—*6567*$^0_2$	-----	------	------	----------	-------	------
6	3523. 170	28375. 42	3101_2—$z\ ^3P^0_2$	3	------	0. 234	?	(1. 42)	1. 54
5	3509. 432	28486. 49	2666_1—$z\ ^7D^0_1$	3	0. 804	. 803	1. 466, 2. 270	1. 466	2. 270
7*h*	3497. 696	28582. 07	3234_5—$z\ ^5F^0_5$	-----	------	------	----------	-------	------
3*Hw*	3493. 863	28613. 43	3098_4—$z\ ^5F^0_4$	-----	------	------	----------	-------	------
40*h*	3486. 183	28676. 46	2676_2—$z\ ^5F^0_2$	7	------	0w	1. 088	(1. 09)	1. 08
4*cws*	3485. 35	28683. 31	3098_4—*5966*$^0_3$	-----	------	------	----------	-------	------
6	3473. 688	28779. 62	2666_1—$z\ ^5F^0_2$	-----	------	------	----------	-------	------
3*h*	3455. 680	28929. 57	3731_3—*6624*$^0_3$	-----	------	------	----------	-------	------
4*h*	3452. 649	28954. 97	2809_4—$z\ ^7D^0_3$	-----	------	------	----------	-------	------
30*c*	3446. 43	29007. 22	$a\ ^5D_3$—$z\ ^7P^0_2$	1	0. 700	0	0. 081	1. 481	2. 181
2*cw*	3440. 52	29057. 04	3022_3—$z\ ^7D^0_4$	-----	------	------	----------	-------	------
15*h*	3434. 834	29105. 14	3022_3—$z\ ^5D^0_3$	3	. 245	0. 730	1. 133, 1. 380	1. 380	1. 133
30*cws*	3433. 828	29113. 67	$a\ ^5D_1$—$z\ ^7P^0_2$	2	------	0	2. 869	1. 505	2. 187
2*h*	3427. 964	29163. 47	3022_3—$z\ ^3P^0_2$	-----	------	------	----------	-------	------
5	3417. 274	29254. 70	3699_3—*6624*$^0_3$	2*	. 207	0	1. 473	0. 852	1. 059
3	3411. 507	29304. 15	2774_3—$z\ ^7D^0_3$	-----	------	------	----------	-------	------
10*c*	3407. 79	29336. 11	$a\ ^5P_2$—$z\ ^5P^0_2$	-----	------	------	----------	-------	------
20	3403. 718	29371. 22	3022_3—$z\ ^5F^0_4$	1	. 213	0	0. 553	1 400	1. 188
2	3395. 650	29440. 99	3022_3—*5966*$^0_3$	-----	------	------	----------	-------	------
100*cw*	3379. 063	29585. 50	$a\ ^5D_2$—$z\ ^7P^0_2$	3	. 660	1. 317	1. 528, 2. 187	1. 528	2. 187
10*h*	3367. 924	29683. 36	2774_3—$z\ ^5F^0_3$	-----	------	------	----------	-------	------
2	3365. 168	29707. 66	2666_1—$z\ ^5D^0_1$	-----	------	------	----------	-------	------
2*h*	3360. 879	29745. 60	3316_4—*6291*$^0_3$	-----	------	------	----------	-------	------
20*c*	3338. 574	29944. 31	3098_4—$z\ ^5F^0_3$	-----	------	------	----------	-------	------
2*c*	3332. 849	29995. 73	3731_3—*6731*$^0_3$	-----	------	------	----------	-------	------
4	3331. 336	30009. 36	3731_3—*6732*$^0_4$	-----	------	------	----------	-------	------
4*cw*	3329. 412	30026. 70	2963_4—*5966*$^0_3$	2	------	0w	1. 090	1. 14	(1. 19)
1*h*	3324. 20	30073. 77	3493_2—*6501*$^0_1$	-----	------	------	----------	-------	------
30*cw*	3318. 780	30122. 89	$a\ ^3G_3$—$z\ ^5F^0_2$	-----	------	------	----------	-------	------
15*c*	3317. 754	30132. 20	$a\ ^3F_2$—$z\ ^5P^0_2$	3	0. 616	1. 231	1. 200, 1. 816	1. 200	1. 816
5	3308. 468	30216. 77	$a\ ^5D_3$—$z\ ^7P^0_3$	-----	------	------	----------	-------	------
20	3308. 38	30217. 57	$a\ ^5G_4$—$z\ ^7P^0_4$	-----	------	------	----------	-------	------
5*cw*	3304. 542	30252. 68	2907_2—$z\ ^5D^0_3$	-----	------	------	----------	-------	------
50*cw*	3303. 208	30264. 89	$a\ ^5D_4$—$z\ ^7P^0_3$	1	. 310	0	0. 556	1. 486	1. 796
1	3301. 274	30282. 61	2676_2—$z\ ^7D^0_3$	-----	------	------	----------	-------	------

TABLE 1. *Classified lines of the second spectrum of rhenium* (Re II)—Continued

Intensity spark	Wavelength air	Wave-number	Term combination	Zeeman type	Separation	Zeeman components		g	
						Strongest p	Strongest n	1st	2d
1	2	3	4	5	6	7	8	9	10
	A	*K*							
10*c*	3299. 790	30296. 24	$a\ ^5P_3$—$z\ ^7D^0_4$	1	. 386	0	0. 630	1. 403	1. 790
2*h*	3298. 535	30307. 76	3606_5—6637^0_4	-----	-----	-----	-----	-----	-----
5*cw*	3298. 184	30310. 98	2907_2—$z\ ^3P^0_2$	-----	-----	-----	-----	-----	-----
3	3286. 636	30417. 46	3398_3—6440^0_4	-----	-----	-----	-----	-----	-----
7*h*	3268. 278	30588. 34	2907_2—5966^0_3 3287_2—6346^0_2	-----	-----	-----	-----	-----	-----
3*h*	3263. 297	30635. 02	3493_2—6557^0_3	7a, 2	-----	0	1. 251	(1. 23)	1. 24
5*h*	3261. 424	30652. 62	3220_4—$z\ ^5D^0_4$	3	0. 206	0. 821	1. 085, 1. 291	1. 085	1. 291
9*h*	3254. 936	30713. 71	2977_0—6048^0_1	7a	1. 128	0	1. 128	0/0	1. 128
1	3252. 482	30736. 89	3493_2—6567^0_2	-----	-----	-----	-----	-----	-----
2	3251. 548†	30745. 71	$a\ ^5P_1$—$z\ ^5D^0_0$	-----	-----	-----	-----	-----	-----
1*h*	3250. 142	30759. 02	2972_2—6048^0_1	-----	-----	-----	-----	-----	-----
80	3246. 311	30795. 31	$a\ ^5D_2$—$z\ ^7P^0_3$	2	0. 263	0	2. 318	1. 528	1. 791
15*l*	3244. 464	30812. 84	$a\ ^3G_4$—$z\ ^7D^0_3$	7a, 2	-----	0	1. 101	(1. 12)	1. 11
10*cw*	3241. 910	30837. 12	3220_4—6304^0_3	-----	-----	-----	-----	-----	-----
1	3238. 470	30869. 88	3225_3—6312^0_4	-----	-----	-----	-----	-----	-----
2*H*	3229. 804	30952. 70	3398_3—6494^0_3	-----	-----	-----	-----	-----	-----
2	3227. 76	30972. 30	3738_2—6835^0_3	-----	-----	-----	-----	-----	-----
10*hl*	3226. 37	30985. 64	3606_5—6704^0_5	3*	. 181	0. 881	0. 96, 1. 14	0. 96	1. 14
3	3220. 258	31044. 45	3101_2—6205^0_2	-----	-----	-----	-----	-----	-----
50*c*	3219. 906	31047. 84	$a\ ^3F_3$—$z\ ^5P^0_2$	1	. 559	0	. 145	1. 263	1. 821
5*h*	3218. 653	31059. 93	2942_1—6048^0_1	-----	-----	-----	-----	-----	-----
6*h*	3213. 168	31112. 95	3316_4—$z\ ^7D^0_5$	-----	-----	-----	-----	-----	-----
1*h*	3203. 560	31206. 26	3225_3—6346^0_2	-----	-----	-----	-----	-----	-----
3	3198. 330	31257. 28	$a\ ^3F_2$—$z\ ^5P^0_3$	-----	-----	-----	-----	-----	-----
2*h*	3197. 59	31264. 52	3606_5—6732^0_4	-----	-----	-----	-----	-----	-----
15	3195. 206	31287. 84	2963_4—$z\ ^5F^0_5$	2	-----	0w	1. 365	1. 14	(1. 18)
1	3192. 852	31310. 91	3493_2—6624^0_3 3731_3—6862^0_2	-----	-----	-----	-----	-----	-----
2*h*	3175. 094	31486. 02	3738_2—6886^0_3	-----	-----	-----	-----	-----	-----
2*h*	3173. 604	31500. 80	2809_4—$z\ ^5F^0_4$	-----	-----	-----	-----	-----	-----
7*h*	3170. 074	31535. 88	3287_2—6441^0_2 $(2774_3$—$z\ ^7D^0_4)$	3	0. 247	0. 498	0. 813, 1. 060	1. 060	0. 813
8*h*	3166. 609	31570. 39	2809_4—5966^0_3	7a, 2	-----	0	1. 276h	(1. 22)	1. 20
1*H*	3155. 209	31684. 5	3398_3—6567^0_2	-----	-----	-----	-----	-----	-----
1	3151. 498	31721. 8	$a\ ^5P_1$—$z\ ^5F^0_2$	-----	-----	-----	-----	-----	-----
1*h*	3143. 974	31797. 7	3316_4—6496^0_3	-----	-----	-----	-----	-----	-----
2	3142. 018	31817. 5	$a\ ^3G_3$—$z\ ^5D^0_2$	-----	-----	-----	-----	-----	-----
6	3138. 796	31850. 2	2774_3—$z\ ^5F^0_4$	7a, 1	-----	0	1. 120	(1. 23)	1. 20
1*h*	3138. 663	31851. 5	3731_3—6917^0_2	-----	-----	-----	-----	-----	-----
4*cw*	3136. 178	31876. 7	3098_4—$z\ ^5D^0_4$	-----	-----	-----	-----	-----	-----
20	3131. 952	31919. 8	2774_3—5966^0_3	7, 3	-----	0	1. 200	(1. 23)	1. 18
7*h*	3130. 203	31937. 6	3234_5—$z\ ^7D^0_5$	-----	-----	-----	-----	-----	-----
2	3127. 521	31965. 0	3731_3—6928^0_4	-----	-----	-----	-----	-----	-----
2*h*	3123. 622	32004. 8	2314_1—$z\ ^7D^0_1$	-----	-----	-----	-----	-----	-----
2	3118. 002	32062. 6	3234_5—6440^0_4	-----	-----	-----	-----	-----	-----
3*c*	3117. 652	32066. 2	3287_2—6494^0_3	2	-----	0	1. 920w	1. 08	1. 36
2	3116. 720	32075. 7	3220_4—$z\ ^7D^0_3$	-----	-----	-----	-----	-----	-----
2*h*	3113. 350	32110. 5	3398_3—6610^0_3	-----	-----	-----	-----	-----	-----
2*h*	3110. 326	32141. 7	3071_3—$z\ ^5D^0_3$	-----	-----	-----	-----	-----	-----
2	3109. 983	32145. 2	3098_4—6312^0_4	-----	-----	-----	-----	-----	-----
6	3109. 576	32149. 4	3225_3—6440^0_4	-----	-----	-----	-----	-----	-----
2*h*	3109. 156	32153. 8	3225_3—6441^0_5	-----	-----	-----	-----	-----	-----
3*c*	3107. 298	32173. 0	$a\ ^3F_3$—$z\ ^5P^0_3$	-----	-----	-----	-----	-----	-----
2*h*	3106. 948	32176. 6	3699_3—6917^0_3	-----	-----	-----	-----	-----	-----
7*h*	3105. 082	32196. 0	3606_5—6825^0_5	-----	-----	-----	-----	-----	-----
20*c*	3103. 260	32214. 83	$a\ ^5S_2$—$z\ ^5P^0_1$	-----	-----	-----	-----	-----	-----
20	3103. 055	32216. 96							

TABLE 1. *Classified lines of the second spectrum of rhenium* (Re II)—Continued

Intensity spark	Wavelength air	Wavenumber	Term combination	Zeeman type	Separation	Zeeman components		g	
						Strongest p	Strongest n	1st	2d
1	2	3	4	5	6	7	8	9	10
	A	*K*							
2*cw*	3099. 064	32258. 5	3398_2—6624^3_3						
15	3096. 312	32287. 1	$a\ ^5P_3$—$z\ ^7D^3_3$	3	0. 282	0. 835	1. 138, 1. 420	1. 420	1. 138
4*cw*	3095. 314	32297. 6	2314_1—$z\ ^5F^2_2$						
3*c*	3092. 607	32325. 8	3071_3—6304^3_3						
10	3092. 288	32329. 2	2972_2—6205^2_2						
1	3091. 356	32338. 9	3493_2—6727^3_1						
6	3087. 854	32375. 6	$a\ ^5P_3$—$z\ ^5D^2_2$						
10	3080. 660	32451. 2	3101_2—6346^2_2	3		0. 148	1. 459w	1. 422	1. 496
4	3080. 048	32457. 6	3731_3—6977^4_4						
3*cw*	3074. 657	32514. 5	$a\ ^3F_2$—$z\ ^7D^2_2$						
15	3066. 020	32606. 1	$a\ ^3F_2$—$z\ ^7D^1_1$	1	1. 068	0	0. 138	1. 206	2. 274
15	3063. 762	32630. 2	2942_1—6205^2_2	1	0. 194	0	. 980	1. 368	1. 174
4	3061. 930	32649. 7	$a\ ^5P_1$—$z\ ^5D^1_1$	3	. 619	0. 763	1. 284, 1. 903	1. 903	1. 284
15	3058. 149	32690. 1	3022_3—6291^3_3	3	. 150	. 452	1. 246, 1. 396	1. 396	1. 246
2*h*	3057. 538	32696. 6	3287_2—6557^3_3						
5*h*	3055. 004	32723. 7	2666_1—$z\ ^3P^2_2$						
1	3053. 88	32735. 7	3220_4—6494^3_3 3699_3—6972^3_3						
5*cw*	3048. 036	32798. 5	3287_2—6567^2_2						
3*h*	3046. 644	32813. 5	3606_5—$6887^{3,4}_{3,4}$						
7	3044. 969	32831. 5	2809_4—$z\ ^5F^3_3$	1		0w	1. 027	(1. 22)	1. 18
1*h*	3039. 804	32887. 3	2762_4—6052^3_3						
2	3038. 812	32898. 1	2676_2—5966^3_3						
1	3038. 694	32899. 3	$a\ ^3F_2$—$z\ ^5F^2_2$						
10	3038. 368	32902. 9	3022_3—6312^4_4	1	0. 12	0	0. 921	1. 40	1. 28
3*h*	3035. 776	32931. 0	3316_4—6610^3_3						
15*cws*	3026. 555	33031. 3	$a\ ^5P_2$—$z\ ^5D^1_1$		. 38	0	2. 027h	1. 65	1. 27
3*c*	3025. 36	33044. 3	$a\ ^3G_4$—$z\ ^7D^4_4$						
2*c*	3022. 194	33079. 0	3316_4—6624^3_3						
7	3012. 36	33186. 9	2972_2—6291^3_3						
2*h*	3010. 977	33202. 2	3316_4—6637^4_4						
8*c*	3009. 362	33220. 0	2963_4—6285^4_4 3606_5—6928^4_4						
2*cw*	3008. 984	33224. 2	3287_2—6610^3_3						
8*c*	3008. 826	33225. 9	2314_1—$z\ ^5D^1_1$	3	. 187	0. 168h	1. 104, 1. 291	1. 104	1. 291
7*h*	3007. 62	33239. 2	3022_3—6346^2_2	1		0w	1. 168	(1. 398)	1. 51
3*c*	3002. 633†	33294. 4	$a\ ^3G_5$—$z\ ^7D^4_4$						
3*h*	3000. 828	33314. 5	3225_3—6557^3_3						
4*h*	2999. 947	33324. 2	3398_3—6731^3_3						
5*h*	2998. 700	33338. 1	3398_2—6732^4_4						
6	2996. 842	33358. 8	$a\ ^3G_4$—$z\ ^5F^4_4$						
2	2996. 182	33366. 1	3220_4—6557^3_3						
4	2996. 074†	33367. 3	3316_4—6653^3_3						
10*h*	2992. 746	33404. 4	2963_4—6304^3_3						
5*h*	2990. 926	33424. 7	3098_4—6440^4_4						
5	2990. 604	33428. 3	$a\ ^3G_4$—5966^3_3	1		0w	0. 962	(1. 12)	1. 17
3	2990. 433	33430. 3	$a\ ^3F_3$—$z\ ^7D^2_2$						
3	2985. 207	33488. 7	2963_4—6312^4_4						
50*c*	2980. 90	33537. 1	$a\ ^5G_3$—$z\ ^5P^2_2$	1	0. 710	0	1. 096, 1. 812	1. 110	1. 820
2*cw*	2977. 148	33579. 4	3295_4—6653^3_3						
10*cw*	2974. 563	33608. 1	$a\ ^3G_5$—$z\ ^5F^4_4$	7		0	1. 221	(1. 22)	1. 22
2*h*	2971. 734	33640. 6	2907_2—6271^1_1						
10*c*	2967. 415	33689. 9	3071_3—6440^4_4						
2*h*	2967. 018	33694. 1	3071_3—6441^3_3						
80*cw*	2957. 907	33797. 8	$a\ ^5P_2$—$z\ ^5D^3_3$	3	. 363	0. 725	1. 312, 1. 675	1. 675	1. 312
8*c*	2955. 730	33822. 7	2666_1—6048^1_1						
10*c*	2954. 99	33831. 2	$a\ ^5G_2$—$z\ ^5P^3_3$						

TABLE 1. *Classified lines of the second spectrum of rhenium* (Re II)—Continued

Intensity spark	Wavelength air	Wavenumber	Term combination	Zeeman type	Separation	Zeeman components		g	
						Strongest p	Strongest n	1st	2d
1	2	3	4	5	6	7	8	9	10
	A	*K*							
2*h*	2954. 454	33837. 3	2907_3—*6291*$\frac{3}{3}$	-----	-----	-----	-----	-----	-----
3*h*	2952. 982	33854. 2	3287_2—*6673*$\frac{3}{2}$	-----	-----	-----	-----	-----	-----
3*h*	2950. 731	33880. 0	3316_4—*6704*$\frac{5}{5}$	-----	-----	-----	-----	-----	-----
8*h*	2943. 794	33959. 9	3098_4—*6494*$\frac{3}{3}$	1	0. 158	0	0. 72	1. 197	1. 355
3*h*	2941. 141	33990. 5	3225_3—*6624*$\frac{3}{3}$	-----	-----	-----	-----	-----	-----
50*cl*	2940. 974	33992. 4	2314_1—$z\ ^5D^0_2$	2	0. 19	0	1. 463cw	1. 08	1. 27
3	2939. 557	34008. 8	$a\ ^3G_3$—$z\ ^5D^0_3$	-----	-----	-----	-----	-----	-----
40	2934. 529	34067. 1	$a\ ^3G_3$—$z\ ^3P^0_2$	1	.620	0	0. 900, 1. 519	0. 899	1. 519
7*h*	2933. 542	34078. 5	3731_3—*7139*$\frac{2}{2}$	-----	-----	-----	-----	-----	-----
6*h*	2932. 657	34088. 8	$a\ ^5P_2$—$z\ ^5F^0_3$	-----	-----	-----	-----	-----	-----
1*h*	2929. 044	34130. 8	3731_3—*7144*$\frac{3}{3}$	-----	-----	-----	-----	-----	-----
5*h*	2927. 852	34144. 8	3316_4—*6731*$\frac{3}{3}$	-----	-----	-----	-----	-----	-----
20*h*	2926. 661	34158. 7	3316_4—*6732*$\frac{4}{4}$	-----	-----	-----	-----	-----	-----
10*h*	2926. 134	34164. 8	3220_4—*6637*$\frac{4}{4}$	7*	-----	0	1. 071	-----	-----
10*h*	2925. 703	34169. 9	3234_5—*6651*$\frac{5}{5}$	3	-----	0. 164	1. 120	1. 11	1. 14
6*h*	2922. 694	34205. 0	3493_2—*6914*$\frac{3}{3}$	1	. 147	0	0. 789	1. 230	1. 083
1*h*	2917. 173	34269. 8	3220_4—*6647*$\frac{4}{4}$	-----	-----	-----	-----	-----	-----
20	2916. 731	34275. 0	$a\ ^3G_3$—$z\ ^5F^0_4$	2	. 267	0	1. 974	0. 910	1. 177
2*cwl*	2915. 643	34287. 7	$a\ ^5G_4$—*6052*$\frac{5}{5}$	-----	-----	-----	-----	-----	-----
5	2913. 639	34311. 3	2774_3—*6205*$\frac{2}{2}$	7*	-----	0	1. 227	-----	-----
3*h*	2912. 025	34330. 3	3220_4—*6653*$\frac{5}{5}$	-----	-----	-----	-----	-----	-----
7*hc*	2910. 818	34344. 6	$a\ ^3G_3$—*5966*$\frac{3}{3}$	-----	-----	-----	-----	-----	-----
4*hc*	2909. 127	34364. 5	3398_3—*6835*$\frac{3}{3}$	-----	-----	-----	-----	-----	-----
2	2907. 231	34387. 0	2907_2—*6346*$\frac{3}{3}$	-----	-----	-----	-----	-----	-----
2*h*	2906. 11	34400. 2	3287_2—*6727*$\frac{1}{1}$	-----	-----	-----	-----	-----	-----
2*cw*	2905. 854	34403. 2	3699_3—*7139*$\frac{2}{2}$	-----	-----	-----	-----	-----	-----
6*h*	2904. 982	34413. 5	3731_3—*7173*$\frac{3}{2}$	-----	-----	-----	-----	-----	-----
6	2902. 886	34438. 4	3287_2—*6731*$\frac{3}{3}$	-----	-----	-----	-----	-----	-----
6	2900. 012	34472. 5	3225_3—*6673*$\frac{2}{2}$	1?	0. 166	0	0. 776	1. 108	1. 274
10*c*	2897. 242	34505. 5	$a\ ^3F_2$—$z\ ^7D^0_3$	7*	-----	0h	1. 079h	-----	-----
3*h*	2892. 724	34559. 4	3101_2—*6557*$\frac{3}{3}$	-----	-----	-----	-----	-----	-----
10*c*	2892. 093	34566. 9	$a\ ^5P_3$—$z\ ^5D^0_3$	3	. 273	0. 826	1. 140, 1. 413	1. 413	1. 140
10*cw*	2889. 832	34594. 0	$a\ ^3F_2$—$z\ ^5D^0_2$	-----	-----	-----	-----	-----	-----
40*c*	2888. 06	34615. 3	$a\ ^5D_1$—$z\ ^5P^0_1$	3	. 907	. 909	1. 502, 2. 406	1. 500	2. 407
10*h*	2886. 774	34630. 6	3731_3—*7194*$\frac{2}{2}$	-----	-----	-----	-----	-----	-----
2*h*	2885. 710	34643. 4	2963_4—$z\ ^7D^0_5$	-----	-----	-----	-----	-----	-----
20*h*	2884. 244	34661. 0	3101_2—*6567*$\frac{3}{3}$	2*	-----	. 209	1. 295	-----	-----
2*h*	2882. 367	34683. 6	2972_2—*6440*$\frac{4}{4}$	-----	-----	-----	-----	-----	-----
60*h*	2881. 874	34689. 5	$a\ ^3G_4$—$z\ ^5F^0_5$	2	-----	0w	1. 390	(1. 12)	1. 18
8*h*	2880. 630	34704. 4	3234_5—*6704*$\frac{5}{5}$	-----	-----	-----	-----	-----	-----
3*h*	2877. 528	34741. 9	3022_3—*6496*$\frac{3}{3}$	-----	-----	-----	-----	-----	-----
30	2875. 698	34764. 0	2809_4—$z\ ^5D^0_4$	3	-----	0. 21	1. 26w	1. 23	1. 28
2	2871. 432	34815. 6	3731_3—*7213*$\frac{2}{2}$	-----	-----	-----	-----	-----	-----
2	2871. 102	34819. 6	2809_4—*6291*$\frac{3}{3}$	-----	-----	-----	-----	-----	-----
7*h*	2870. 000	34833. 0	$a\ ^5P_3$—$z\ ^5F^0_4$	1	0. 759	0	0. 445	1. 409	1. 168
4*c*	2869. 200	34842. 7	3220_4—*6704*$\frac{5}{5}$	-----	-----	-----	-----	-----	-----
2*H*	2866. 294	34878. 1	3398_3—*6886*$\frac{3}{3}$	-----	-----	-----	-----	-----	-----
3*h*	2865. 554	34887. 1	3398_3—*6887*$\frac{4}{4}$	-----	-----	-----	-----	-----	-----
10*h*	2864. 280	34902. 6	$a\ ^5P_3$—*5966*$\frac{3}{3}$	-----	-----	-----	-----	-----	-----
10*c*	2861. 260	34939. 4	$a\ ^3G_5$—$z\ ^5F^0_5$	7*	-----	0w	1. 028	-----	-----
20*h*	2860. 550	34948. 1	2809_4—*6304*$\frac{3}{3}$	1	-----	0w	0. 880	(1. 22)	1. 33
2	2859. 92	34955. 8	3699_3—*7194*$\frac{2}{2}$	-----	-----	-----	-----	-----	-----
15*cw*	2859. 87	34956. 4	$a\ ^5G_2$—$z\ ^5P^0_3$	2	. 998	0	3. 634	0. 640	1. 638
2*h*	2857. 662	34983. 4	3234_5—*6732*$\frac{4}{4}$	-----	-----	-----	-----	-----	-----
8*h*	2857. 575	34984. 5	2942_1—*6441*$\frac{2}{2}$	-----	-----	-----	-----	-----	-----

TABLE 1. *Classified lines of the second spectrum of rhenium* (Re II)—Continued

Intensity spark	Wavelength air	Wavenumber	Term combination	Zeeman type	Separation	Zeeman components		g	
						Strongest p	Strongest n	1st	2d
1	2	3	4	5	6	7	8	9	10
	A	*K*							
8*h*	2851. 720	35056. 3	3225_3—6731^3_3	3	. 10	0. 31		(1. 11)	1. 21
3	2850. 590	35070. 1	3225_3—6732^3_4						
6*c*	2849. 22	35087. 1	*a* $^5D_2$—*z* $^5P^\circ_1$	7*		0	1. 513		
10*h*	2848. 966	35090. 2	3316_4—6825^5_5	7a, 1		0	1. 119	(1. 188)	1. 17
7*h*	2847. 568	35107. 4	3220_4—6731^3_3						
1*h*	2844. 854	35140. 9	3699_3—7213^2_2						
5*h*	2843. 762	35154. 4	3738_2—7253^3_3						
2	2842. 588	35168. 9	2774_3—6291^5_5						
2*H*	2841. 669	35180. 3	3398_3—6917^2_2						
1	2841. 275	35185. 1	3316_4—6835^3_3						
4*h*	2840. 024	35200. 7	3493_2—7013^1_1						
4*cw*	2834. 782	35265. 7	3098_4—6624^3_3						
4*c*	2833. 05	35287. 3	2762_3—6291^3_3						
1*h*	2832. 857	35289. 7	2676_2—6205^2_2						
2*h*	2832. 540	35293. 6	3398_3—6928^4_4						
5*h*	2832. 245	35297. 4	2774_3—6304^3_3						
2*h*	2831. 854	35302. 2	3295_4—6825^5_5						
3*h*	2831. 752	35303. 4	2963_4—6494^3_3						
4*h*	2825. 50	35381. 6	2774_3—6312^4_4						
5*H*	2824. 939	35388. 6	*a* $^3F_4$—*z* $^7D^4_4$ 3098_4—6637^4_4						
5*h*	2824. 596	35392. 9	2666_1—6205^2_2	1	0. 27	0	0. 901	1. 44	1. 17
3*h*	2822. 341	35421. 2	*a* $^3F_3$—*z* $^7D^3_3$						
8	2821. 110	35436. 6	*a* $^3F_4$—*z* $^5D^3_3$	2		0w	1. 690	(1. 275)	1. 14
60*cwl*	2819. 779	35453. 4	*a* $^5S_2$—*z* $^5P^2_2$						
3*c*	2815. 31	35509. 6	*a* $^3F_3$—*z* $^5D^2_2$						
20*h*	2813. 53	35532. 1	3098_4—6651^3_3	7a, 1		0	1. 137	(1. 188)	1. 18
10*h*	2809. 435	35583. 9	2942_1—6501^1_1	3	0. 570	0. 574	0. 797, 1. 365	1. 366	0. 796
10*hl*	2803. 925	35653. 8	3071_3—6637^4_4	2	. 345	0	2. 522	1. 142	1. 487
20*c*	2803. 28	35662. 1	*a* $^5D_0$—*z* $^5P^1_1$	7a	2. 452	0	2. 452c	0/0	2. 452
1	2802. 97	35666. 0	*a* $^5P_1$—*z* $^3P^2_2$						
3*c*	2798. 918	35717. 6	3101_2—6673^3_3						
5*h*	2798. 870	35718. 2	2774_3—6346^2_2						
1*h*	2797. 208	35739. 4	3398_3—6972^3_3						
20*h*	2794. 632	35772. 4	*a* $^3F_4$—*5966*$^3_3$	2		0w	1. 527	(1. 275)	1. 191
5*h*	2789. 026	35844. 2	2972_2—6557^3_3						
10*h*	2782. 101	35933. 5	2907_2—6501^1_1 2963_4—6557^3_3						
50*c*	2777. 797	35989. 2	*a* $^5P_2$—*z* $^5D^3_3$	1	0. 54	0	0. 05	1. 68	1. 14
2*h*	2768. 177	36114. 2	3316_4—6928^4_4						
30*h*	2765. 69	36146. 6	3022_3—6637^4_4						
7*h*	2765. 30	36151. 7	3493_2—7108^2_2						
1*h*	2760. 494	36214. 7	2338_5—*z* $^5F^4_4$						
3*h*	2758. 418	36242. 0	2314_1—*z* $^3P^2_2$						
4*h*	2757. 700	36251. 4	3022_3—6647^3_4						
2	2756. 806	36263. 2	3101_2—6727^1_1						
10*h*	2755. 854	36275. 7	2676_2—6304^3_3						
100*cws*	2753. 638	36304. 9	*a* $^5G_3$—*z* $^5F^2_2$						
6*h*	2751. 620	36331. 5	3098_4—6731^3_3						
80*c*	2750. 564	36345. 5	3295_4—6930^3_3 3098_4—6732^3_4	1, 3*		0. 402	1. 141	1. 543	1. 677
20*d*	2748. 55	36372. 1	2972_2—6610^3_3						
30*c*	2741. 967†	36459. 4	3493_2—7139^2_2						
2*h*	2734. 43	36559. 9	3316_4—6972^3_3						
300*cl*	2733. 04	36578. 5	*a* $^5S_2$—*z* $^5P^3_3$	7a, 1		0w	1. 595w	(1. 71)	1. 67
6*cw*	2732. 398	36587. 1	*a* $^5G_4$—*z* $^7D^5_5$						
150*cwl*	2731. 562	36598. 3	*a* $^5G_2$—*z* $^5F^2_2$	3	0. 436	0. 873	0. 650, 1. 086	0. 650	1. 086
2	2730. 911	36607. 0	3316_4—6977^4_4						

TABLE 1. *Classified lines of the second spectrum of rhenium* (Re II)—Continued

Intensity spark	Wavelength air	Wavenumber	Term combination	Zeeman type	Separation	Zeeman components		g	
						Strongest *p*	Strongest *n*	1st	2d
1	2	3	4	5	6	7	8	9	10
	A	*K*							
10*h*	2730.658	36610.4	3071_3—*6732*$\frac{4}{4}$	-----	-----	-----	-----	-----	-----
			3225_3—*6886*$\frac{3}{3}$	-----	-----	-----	-----	-----	-----
10	2730.027	36618.9	3225_3—*6887*$\frac{4}{4}$	7a, 1	-----	0	1.053	(1.114)	1.10
2*h*	2729.803	36621.9	*a* $^3G_4$—*z* $^5D_4^0$	-----	-----	-----	-----	-----	-----
15*h*	2726.870	36661.3	2774_3—*6440*$\frac{4}{4}$	7b	-----	0	1.227	(1.23)	1.23
			3220_4—*6886*$\frac{3}{3}$	-----	-----	-----	-----	-----	-----
3*cl*	2726.57	36665.2	2774_3—*6441*$\frac{2}{2}$	-----	-----	-----	-----	-----	-----
3*h*	2724.253	36696.5	2676_2—*6346*$\frac{2}{2}$	-----	-----	-----	-----	-----	-----
3	2718.659	36772.0	3295_4—*6972*$\frac{3}{3}$	-----	-----	-----	-----	-----	-----
10*cw*	2717.670	36785.3	*a* $^3F_3$—*z* $^5D_3^0$	2	-----	0w	1.126	(1.20)	1.17
2*c*	2716.63	36799.5	2666_1—*6346*$\frac{2}{2}$	-----	-----	-----	-----	-----	-----
3	2716.144	36806.0	*a* $^3G_4$—*6304*$\frac{3}{3}$	-----	-----	-----	-----	-----	-----
3*h*	2713.828	36837.4	2963_4—*6647*$\frac{4}{4}$	-----	-----	-----	-----	-----	-----
15*c*	2713.375	36843.6	*a* $^3F_3$—*z* $^3P_2^0$	-----	-----	-----	-----	-----	-----
8*h*	2712.646	36853.5	3287_2—*6972*$\frac{3}{3}$	-----	-----	-----	-----	-----	-----
6*h*	2711.298	36871.8	2809_4—*6496*$\frac{3}{3}$	-----	-----	-----	-----	-----	-----
10*h*	2711.008	36875.7	2963_4—*6651*$\frac{5}{5}$	-----	-----	-----	-----	-----	-----
2*h*	2710.36	36884.6	3225_3—*6914*$\frac{3}{3}$	-----	-----	-----	-----	-----	-----
10*cw*	2709.91	36890.7	*a* $^3G_4$—*6312*$\frac{4}{4}$	-----	-----	-----	-----	-----	-----
4*h*	2708.322	36912.3	3225_3—*6917*$\frac{2}{2}$	7a, 1	-----	0	0.738	(1.114)	1.30
2*h*	2706.39	36938.7	3234_5—*6928*$\frac{4}{4}$	-----	-----	-----	-----	-----	-----
1*h*	2701.726	37002.4	2972_2—*6673*$\frac{2}{2}$	-----	-----	-----	-----	-----	-----
1*h*	2701.556	37004.8	3731_3—*7432*$\frac{2}{2}$	-----	-----	-----	-----	-----	-----
8*c*	2700.211	37023.2	2907_2—*6610*$\frac{3}{3}$	-----	-----	-----	-----	-----	-----
5	2700.027	37025.7	3225_3—*6928*$\frac{4}{4}$	-----	-----	-----	-----	-----	-----
5	2699.462	37033.5	*a* $^3F_4$—*z* $^5F_5^0$	-----	-----	-----	-----	-----	-----
3*h*	2696.298	37076.9	3220_4—*6928*$\frac{4}{4}$	-----	-----	-----	-----	-----	-----
1*h*	2695.41	37089.1	3022_3—*6731*$\frac{3}{3}$	-----	-----	-----	-----	-----	-----
30	2693.104	37120.9	*a* $^3F_2$—*5966*$\frac{3}{3}$	7a, 1	-----	0	1.166	(1.20)	1.19
30*cw*	2691.694	37140.3	*a* $^3G_5$—*6312*$\frac{4}{4}$	2	-----	0w	1.062	(1.26)	1.31
3*cW*	2691.262	37146.3	*a* $^5P_2$—*6048*$\frac{1}{1}$	-----	-----	-----	-----	-----	-----
3*h*	2687.592	37197.0	3493_2—*7213*$\frac{2}{2}$	-----	-----	-----	-----	-----	-----
3*h*	2683.688	37251.1	3738_2—*7463*$\frac{2}{2}$	-----	-----	-----	-----	-----	-----
6*h*	2682.888	37262.2	3287_2—*7013*$\frac{1}{1}$	1	0.561	0	0.515	1.076	1.637
5*H*	2681.838	37276.8	3098_4—*6825*$\frac{5}{5}$	-----	-----	-----	-----	-----	-----
2*h*	2677.231	37341.0	2314_1—*6048*$\frac{1}{1}$	-----	-----	-----	-----	-----	-----
3*h*	2669.354	37451.1	3234_5—*6979*$\frac{4}{4}$	-----	-----	-----	-----	-----	-----
4*h*	2667.893	37471.6	3225_3—*6972*$\frac{3}{3}$	-----	-----	-----	-----	-----	-----
4*H*	2667.54	37476.6	2809_4—*6557*$\frac{3}{3}$	-----	-----	-----	-----	-----	-----
1	2665.688	37502.6	2977_0—*6727*$\frac{1}{1}$	-----	-----	-----	-----	-----	-----
1	2664.556	37518.6	3225_3—*6977*$\frac{4}{4}$	-----	-----	-----	-----	-----	-----
1	2663.159	37538.2	3225_3—*6979*$\frac{4}{4}$?	-----	-----	-----	-----	-----	-----
4	2662.464	37548.0	2972_2—*6727*$\frac{1}{1}$	7b	-----	0	1.292	1.292	1.292
7	2660.928	37569.7	3220_4—*6977*$\frac{4}{4}$	-----	-----	-----	-----	-----	-----
4	2659.552	37589.2	3220_4—*6979*$\frac{4}{4}$	-----	-----	-----	-----	-----	-----
1	2659.236	37593.6	a^3G_3—*6291*$\frac{3}{3}$	-----	-----	-----	-----	-----	-----
3*c*	2655.048	37652.9	*a* $^3F_3$—*z* $^7D_4^0$	-----	-----	-----	-----	-----	-----
			2907_2—*6673*$\frac{2}{2}$	-----	-----	-----	-----	-----	-----
5*h*	2653.485	37675.1	2963_4—*6731*$\frac{3}{3}$	-----	-----	-----	-----	-----	-----
6*h*	2652.506	37689.0	2963_4—*6732*$\frac{4}{4}$	-----	-----	-----	-----	-----	-----
5	2651.662	37701.0	*a* $^3F_3$—*z* $^5D_3^0$	-----	-----	-----	-----	-----	-----
10*h*	2650.197	37721.8	*a* $^3G_3$—*6304*$\frac{3}{3}$	-----	-----	-----	-----	-----	-----
50*h*	2648.462	37746.5	*a* $^5D_3$—*z* $^5P_2^0$	-----	-----	-----	-----	-----	-----

TABLE 1. *Classified lines of the second spectrum of rhenium* (Re II)—Continued

Intensity spark	Wavelength air	Wavenumber	Term combination	Zeeman type	Separation	Zeeman components		g	
						Strongest p	Strongest n	1st	2d
1	2	3	4	5	6	7	8	9	10
	A	*K*							
20	2647. 578	37759. 2	$a\ ^3F_3$—$z\ ^3P^0_2$	1	0. 263	0	0. 731	1. 257	1. 520
5	2644. 266	37806. 4	$a\ ^3G_3$—*6312*$^0_4$	2	. 36	0	----------	(0. 90)	1. 26
30*cw*	2642. 25	37835. 4	$a\ ^5S_2$—$z\ ^7D^0_3$	3	-------	0w	1. 77	(1. 71)	1. 83
3	2641. 300	37848. 9	2942_1—*6727*$^0_1$	-----	-------	-------	----------	-------	-------
30	2641. 021	37852. 9	$a\ ^5D_1$—$z\ ^5P^0_2$	2	. 326	0	2. 148	1. 496	1. 822
7*h*	2638. 147	37894. 1	3098_4—*6887*$^0_4$	3	-------	0. 342	1. 22w	1. 18	1. 26
150*c*	2637. 006	37970. 5	$a\ ^5G_3$—$z\ ^5F^0_3$	7, 3	-------	0w	1. 136	(1. 12)	1. 15
200*cwl*	2635. 831	37927. 4	$a\ ^5S_2$—$z\ ^7D^0_1$	1	. 564	0	1. 143	1. 707	2. 271
2*h*	2634. 798	37942. 3	$a\ ^3F_2$—*6048*$^0_1$	-----	-------	-------	----------	-------	-------
8	2633. 084	37967. 0	$a\ ^3F_3$—$z\ ^5F^0_4$	1	-------	0w	0. 945	(1. 26)	1. 18
20*c*	2632. 16	37980. 3	$a\ ^3F_2$—*6052*$^0_3$	-----	-------	-------	----------	-------	-------
30?	2630. 861	37999. 1	$a\ ^5G_3$—$z\ ^5D^0_3$	1	0. 199	0	0. 692	1. 090	1. 289
8	2630. 436	38005. 2	2809_4—*6610*$^0_3$	-----	-------	-------	----------	-------	-------
100*h*	2628. 258	38036. 7	$a\ ^5P_3$—$z\ ^3P^0_3$	3	-------	0. 220w	1. 198w	1. 234	1. 161
3	2622. 276	38123. 5	3699_5—*7511*$^0_3$	-----	-------	-------	----------	-------	-------
3	2621. 870	38129. 3	3022_3—*6835*$^0_3$	-----	-------	-------	----------	-------	-------
2*h*	2620. 937	38142. 9	$a\ ^3G_3$—*6346*$^0_2$	-----	-------	-------	----------	-------	-------
10*hs*	2619. 805	38159. 4	3071_3—*6887*$^0_4$	-----	-------	-------	----------	-------	-------
4*h*	2619. 082	38169. 9	$a\ ^3G_4$—*6440*$^0_4$	-----	-------	-------	----------	-------	-------
150*cwl*	2616. 720	38204. 4	$a\ ^5G_2$—$z\ ^7D^0_3$	2	. 66	0	1. 131	0. 65	1. 131
5*h*	2615. 59	38220. 9	$a\ ^5S_2$—$z\ ^5F^0_2$	-----	-------	-------	----------	-------	-------
8*c*	2610. 874	38289. 9	$a\ ^5G_3$—$z\ ^5F^0_3$ 3101_2—*6930*$^0_3$	-----	-------	-------	----------	-------	-------
20*h*	2610. 545	38294. 8	$a\ ^3G_5$—$z\ ^7D^0_5$	-----	-------	-------	----------	-------	-------
2*h*	2610. 120	38301. 0	3098_4—*6928*$^0_4$	-----	-------	-------	----------	-------	-------
5	2609. 839	38305. 1	$a\ ^5G_5$—$z\ ^7D^0_4$	-----	-------	-------	----------	-------	-------
400	2608. 501	38324. 8	$a\ ^5D_2$—$z\ ^5P^0_2$	3	. 299	0. 595	1. 526, 1. 825	1. 526	1. 825
10	2606. 480	38354. 5	2774_3—*6610*$^0_3$	3	. 18	. 530	----------	(1. 23)	1. 41
8*h*	2593. 048	38553. 1	3225_3—*7081*$^0_3$	3	-------	. 116h	1. 154h	1. 13	1. 17
60*cd*	2588. 579	38619. 7	$a\ ^5G_5$—$z\ ^5F^0_4$	-----	-------	-------	----------	-------	-------
1	2586. 425	38651. 9	3022_3—*6887*$^0_4$	-----	-------	-------	----------	-------	-------
4	2583. 146	38700. 9	$a\ ^5P_3$—*6346*$^0_2$	-----	-------	-------	----------	-------	-------
7*cw*	2582. 870	38705. 1	$a\ ^3G_4$—*6494*$^0_3$	-----	-------	-------	----------	-------	-------
10*cWs*	2582. 111	38716. 4	$a\ ^5P_2$—*6205*$^0_2$	-----	-------	-------	----------	-------	-------
4*h*	2581. 166	38730. 6	2774_3—*6647*$^0_4$	-----	-------	-------	----------	-------	-------
15*hl*	2580. 311†	38743. 4	2762_3—*6637*$^0_4$	-----	-------	-------	----------	-------	-------
4*h*	2580. 102	38746. 6	3098_4—*6972*$^0_3$	-----	-------	-------	----------	-------	-------
20	2576. 238	38804. 7	2676_2—*6557*$^0_3$	2	-------	0w	1. 494	(1. 09)	1. 23
1*h*	2575. 664	38813. 3	3098_4—*6979*$^0_4$	-----	-------	-------	----------	-------	-------
30	2575. 317	38818. 5	$a\ ^5G_4$—$z\ ^7D^0_4$	-----	-------	-------	----------	-------	-------
5*h*	2572. 117	38866. 8	$a\ ^5G_4$—$z\ ^5D^0_3$	-----	-------	-------	----------	-------	-------
300*cw*	2571. 810	38871. 5	$a\ ^5D_3$—$z\ ^5P^0_3$	3	0. 21	0. 64w	1. 56w	1. 46	1. 67
3*h*	2570. 186	38896. 1	$a\ ^5G_6$—$z\ ^5F^0_5$	-----	-------	-------	----------	-------	-------
2*h*	2569. 828	38901. 5	2972_2—*6862*$^0_3$	-----	-------	-------	----------	-------	-------
3*h*	2569. 192	38911. 1	2314_1—*6205*$^0_2$	-----	-------	-------	----------	-------	-------
300	2568. 638	38919. 5	$a\ ^5D_4$—$z\ ^5P^0_3$	1	. 157	0	0. 925	1. 479	1. 636
4*hl*	2566. 92	38945. 5	3022_3—*6917*$^0_2$	-----	-------	-------	----------	-------	-------
60	2566. 366	38953. 9	2809_4—*6704*$^0_3$	2	-------	0w	1. 550	(1. 22)	1. 29
10	2565. 582	38965. 9	$a\ ^3F_4$—$z\ ^5D^0_4$	7b	-------	0	1. 283	1. 28	1. 28
4	2561. 920	39021. 5	$a\ ^3F_4$—*6291*$^0_3$	-----	-------	-------	----------	-------	-------
5*h*	2559. 478	39058. 8	3022_3—*6928*$^0_4$ 3071_3—*6977*$^0_4$	7a, 1	-------	0	1. 220	(1. 398)	1. 35
15	2557. 694	39086. 0	$a\ ^3G_3$—*6440*$^0_4$	2	0. 313	0	2. 146	0. 894	1. 207
20	2557. 414	39090. 3	$a\ ^3G_3$—*6441*$^0_3$	2	-------	0w	1. 050	(0. 90)	0. 82
200	2554. 630	39132. 9	$a\ ^5G_4$—$z\ ^5F^0_4$	7b	-------	0w	1. 183	1. 18	1. 18
100*cw*	2553. 588	39148. 8	$a\ ^5S_2$—$z\ ^5D^0_1$	-----	-------	-------	----------	-------	-------
100*cw*	2550. 091	39202. 5	$a\ ^5G_4$—*5966*$^0_3$	2	-------	0w	1. 207	(1. 18)	1. 17

TABLE 1. *Classified lines of the second spectrum of rhenium* (Re II)—Continued

Intensity spark	Wavelength air	Wavenumber	Term combination	Zeeman type	Separation	Zeeman components		g	
						Strongest p	Strongest n	1st	2d
1	2	3	4	5	6	7	8	9	10
	A	*K*							
3*h*	2548. 386	39228. 7	2963_4—*6886*$\frac{3}{3}$						
7	2548. 020	39234. 4	$a\ ^3F_4$—*6312*$\frac{4}{4}$	7b		0	1. 262	1. 26	1. 26
2	2546. 450	39258. 6	3287_2—*7213*$\frac{3}{2}$						
15*h*	2545. 258	39277. 0	2907_2—*6835*$\frac{3}{3}$						
4*h*	2541. 651	39332. 7	2676_2—*6610*$\frac{3}{3}$						
6	2541. 514	39334. 8	$a\ ^3G_4$—*6557*$\frac{5}{5}$						
3	2536. 398	39414. 2	2972_2—*6914*$\frac{3}{3}$						
80	2534. 099	39449. 9	$a\ ^5D_2$—$z\ ^5P_3^\circ$	2		0w	1. 900	(1. 53)	1. 65
5*h*	2532. 536	39474. 2	3225_4—*7173*$\frac{2}{2}$						
7*cw*	2532. 33	39477. 5	2338_5—$z\ ^5D_4^\circ$						
3	2526. 536	39568. 0	2774_5—*6731*$\frac{3}{3}$						
10	2526. 32	39571. 4	2314_1—*6271*$\frac{1}{1}$	3	0. 43	0. 42	1. 11, 1. 55	1. 11	1. 54
4	2525. 653	39581. 8	2774_5—*6732*$\frac{4}{4}$						
10*h*	2521. 691	39644. 0	$a\ ^5D_1$—$z\ ^5D_0^\circ$ $a\ ^5P_3$—*6440*$\frac{4}{4}$						
2*h*	2520. 658	39660. 3	3287_2—*7253*$\frac{2}{2}$						
10*hw*	2518. 720	39690. 8	3225_3—*7194*$\frac{2}{2}$						
2*h*	2517. 99	39702. 2	$a\ ^5P_2$—*6304*$\frac{3}{3}$						
2*h*	2515. 190	39746. 5	2338_5—*6312*$\frac{4}{4}$						
2	2512. 414	39790. 4	2907_2—*6886*$\frac{3}{3}$						
10	2511. 250	39808. 8	3738_2—*7719*$\frac{3}{3}$	7*		0	1. 156		
20*cw*	2510. 11	39826. 8	$a\ ^5S_2$—$z\ ^7D_3^\circ$						
2*h*	2509. 50	39836. 6	3097_3—*7681*$\frac{3}{3}$						
5*c*	2507. 854	39862. 7	$a\ ^3G_4$—*6610*$\frac{3}{3}$						
10	2506. 999	39876. 3	3225_3—*7213*$\frac{2}{2}$						
4	2505. 210	39904. 8	3731_3—*7722*$\frac{3}{3}$						
30*c*	2504. 595	39914. 6	$a\ ^5S_2$—$z\ ^5D_2^\circ$						
200*cw*	2502. 348	39950. 4	$a\ ^5G_5$—$z\ ^5F_5^\circ$	3		0. 391w	1. 239w	1. 28	1. 20
2	2501. 05	39971. 2	3287_2—*7284*$\frac{3}{3}$						
1	2498. 566	40010. 9	$a\ ^3G_4$—*6624*$\frac{3}{3}$						
3*h*	2495. 386	40061. 9	$a\ ^5G_4$—*6052*$\frac{3}{3}$						
7	2495. 141	40065. 8	2666_1—*6673*$\frac{2}{2}$						
1	2494. 609	40074. 4	3606_5—*7613*$\frac{4}{4}$ 3398_3—*7406*$\frac{3}{4}$						
1	2494. 517	40075. 8	3101_2—*7108*$\frac{2}{2}$						
3*h*	2494. 217	40080. 7	3398_3—*7407*$\frac{3}{3}$						
2	2493. 597	40090. 62	2963_4—*6972*$\frac{3}{3}$						
1	2493. 461	40092. 8	2907_2—*6917*$\frac{2}{2}$						
10	2491. 234	40128. 7	$a\ ^5D_3$—$z\ ^7D_2^\circ$	1	0. 319	0	0. 838	1. 476	1. 795
1	2490. 91	40133. 9	$a\ ^3G_4$—*6637*$\frac{4}{4}$						
3*h*	2490. 40	40142. 1	$a\ ^5G_3$—$z\ ^7D_4^\circ$						
50	2490. 161	40145. 9	3098_4—*7112*$\frac{4}{4}$						
4	2489. 482	40156. 9	2963_4—*6979*$\frac{4}{4}$						
30*l*	2489. 04	40164. 0	2809_4—*6825*$\frac{3}{3}$	1		0w	. 934	(1. 22)	1. 16
6*c*	2488. 104	40179. 1	$a\ ^5P_3$—*6494*$\frac{3}{3}$						
4*cwl*	2486. 46	40205. 7	$a\ ^5S_2$—$z\ ^5F_3^\circ$						
2	2484. 406	40238. 9	$a\ ^3G_4$—*6647*$\frac{4}{4}$						
8*cw*	2481. 98	40278. 2	3225_3—*7253*$\frac{2}{2}$						
6	2480. 631	40300. 2	3493_2—*7523*$\frac{2}{2}$						
4	2479. 541	40317. 9	2314_1—*6346*$\frac{2}{2}$						
80	2478. 99	40326. 8	$a\ ^5D_1$—$z\ ^7D_1^\circ$	3	0. 777	0. 778	1. 498, 2. 274	1. 498	2. 274
10*cl*	2478. 545	40334. 1	3398_3—*7432*$\frac{2}{2}$						
10*c*	2476. 332	40370. 1	$a\ ^3F_2$—*6291*$\frac{3}{3}$	7		0	1. 340		
5*h*	2475. 470	40384. 2	3101_2—*7139*$\frac{2}{2}$ 3316_4—*7355*$\frac{3}{3}$						
30	2475. 172	40389. 0	$a\ ^3F_4$—$z\ ^7D_5^\circ$	2		0w	1. 443	(1. 275)	1. 31
1	2472. 78	40428. 1	$a\ ^3F_3$—*6205*$\frac{2}{2}$						
20	2471. 049	40456. 4	$a\ ^5G_3$—$z\ ^5F_4^\circ$	7a, 2		0	1. 264	(1. 12)	1. 16

TABLE 1. *Classified lines of the second spectrum of rhenium* (Re II)—Continued

Intensity spark	Wavelength air	Wavenumber	Term combination	Zeeman type	Separation	Zeeman components		g	
						Strongest p	Strongest n	1st	2d
1	2	3	4	5	6	7	8	9	10
	A	*K*							
50	2470.610	40463.6	$a\ ^5G_4$—$z\ ^5F_5^0$	7b	.....	0	1.178	1.18	1.18
100*cwl*	2469.356	40484.1	$a\ ^5G_2$—$z\ ^5D_3^0$	2	.50	0	2.150	0.650	1.150
7	2468.480	40498.5	$a\ ^3F_2$—6304_3^0	.....	.....	.....	.....	.....	.....
20*cl*	2467.85	40508.8	2676_2—6727_1^0	.....	.....	.....	.....	.....	.....
100*c*	2467.574	40513.4	$a\ ^5D_3$—$z\ ^5F_2^0$	2	.412	0	2.320	1.492	1.080
20*c*	2466.810	40525.9	$a\ ^5G_3$—5966_3^0	.....	.....	.....	.....	.....	.....
20*c*	2465.80	40542.5	$a\ ^5G_2$—$z\ ^3P_2^0$	.....	.....	.....	.....	.....	.....
2	2462.658	40594.2	3738_2—7797_3^0	.....	.....	.....	.....	.....	.....
1	2459.89	40640.0	3220_4—7284_3^0	.....	.....	.....	.....	.....	.....
8	2458.833	40657.4	3731_3—7797_3^0	.....	.....	.....	.....	.....	.....
100*c*	2455.827	40707.2	$a\ ^5D_2$—$z\ ^7D_2^0$	3	0.298	0.672	1.526, 1.824	1.526	1.824
2	2455.63	40710.5	2942_1—7013_1^0	.....	.....	.....	.....	.....	.....
10	2455.097	40719.3	3101_2—7173_2^0	.....	.....	.....	.....	.....	.....
7	2450.320	40798.6	$a\ ^5D_2$—$z\ ^7D_1^0$	1	.741	0	0.754	1.528	2.269
20*c*	2449.523†	40811.9	$a\ ^3G_4$—6704_5^0	.....	.....	.....	.....	.....	.....
100*c*	2449.033	40820.1	$a\ ^5G_2$—5966_3^0	2	.543	0	2.260	0.631	1.174
20	2444.54	40895.1	3316_4—7406_4^0	.....	.....	.....	.....	.....	.....
7*h*	2444.14	40901.8	3316_4—7407_3^0	.....	.....	.....	.....	.....	.....
10	2443.10	40919.2	$a\ ^3F_2$—6346_2^0	3	.289	0.579	1.198, 1.487	1.198	1.487
1	2442.64	40926.9	$a\ ^3G_3$—6624_3^0	.....	.....	.....	.....	.....	.....
1	2442.08	40936.3	3101_2—7194_2^0	.....	.....	.....	.....	.....	.....
8	2438.20	41001.4	2762_3—6862_2^0	.....	.....	.....	.....	.....	.....
10	2437.43	41014.4	3071_3—7173_2^0	.....	.....	.....	.....	.....	.....
10	2436.74	41026.0	2338_5—6440_4^0	7a, 1	.....	0	1.095	(1.19)	1.21
15	2435.31	41050.1	$a\ ^3G_3$—6637_4^0	1*	.....	0w	1.14	.....	.....
20*cw*	2434.62	41061.7	$a\ ^3G_5$—6704_5^0	.....	.....	.....	.....	.....	.....
40	2433.741	41076.5	$a\ ^3G_4$—6731_3^0	.....	.....	.....	.....	.....	.....
5	2433.365	41082.9	2972_2—7081_3^0	.....	.....	.....	.....	.....	.....
10*c*	2432.87	41091.2	$a\ ^3G_4$—6732_4^0 $(a\ ^5D_2$—$z\ ^5F_2^0)$	.....	.....	.....	.....	.....	.....
5	2431.068	41121.7	2774_3—6886_3^0 3101_2—7213_2^0	.....	.....	.....	.....	.....	.....
2	2430.750	41127.1	3398_3—7511_3^0	.....	.....	.....	.....	.....	.....
40	2430.515	41131.1	2774_3—6887_4^0	.....	.....	.....	.....	.....	.....
4	2429.097	41155.1	$a\ ^3G_3$—6647_4^0	.....	.....	.....	.....	.....	.....
15	2427.148	41188.1	2809_4—6928_4^0	3	.....	0.160	1.231d	1.21	1.25
9	2422.60	41265.4	2314_1—6441_2^0	1	0.28	0	0.530	1.09	0.81
60	2421.41	41285.6	$a\ ^3F_3$—6291_3^0	7, 3	.....	0c	1.249	(1.26)	1.24
15	2418.392	41337.2	$a\ ^5P_3$—6610_3^0	7, 3	.....	0c	1.405	(1.41)	1.40
30	2418.201	41340.5	$a\ ^3G_5$—6732_4^0	2	.....	0w	1.505	(1.22)	1.15
2	2417.815	41347.1	3220_4—7355_5^0	.....	.....	.....	.....	.....	.....
6	2417.026	41360.6	2972_2—7108_1^0	.....	.....	.....	.....	.....	.....
40	2416.265	41373.6	$a\ ^5D_0$—$z\ ^7D_1^0$	7a	2.272	0	2.272	0/0	2.272
7	2414.198	41409.0	$a\ ^3G_3$—6673_3^0	1	0.37	0	.....	(0.90)	1.27
3*c*	2412.974	41430.0	3493_2—7636_3^0	.....	.....	.....	.....	.....	.....
20*c*	2411.947	41447.7	3287_2—7432_2^0	.....	.....	.....	.....	.....	.....
7	2409.777	41485.0	$a\ ^5P_3$—6624_3^0	.....	.....	.....	.....	.....	.....
20	2408.989	41498.6	$a\ ^3F_3$—6312_4^0	7a, 2	.....	0	1.300	(1.26)	1.27
5	2408.23	41511.7	3295_4—7446_3^0	.....	.....	.....	.....	.....	.....
2	2406.11	41548.3	$a\ ^5D_1$—$z\ ^5D_1^0$	.....	.....	.....	.....	.....	.....
7	2403.87	41586.9	2676_2—6835_3^0	.....	.....	.....	.....	.....	.....
50*c*	2403.036	41601.4	$a\ ^5P_2$—6494_3^0	1	0.306	0	0.750	1.668	1.362
10*cw*	2398.58	41678.7	$a\ ^3F_4$—6557_3^0	.....	.....	.....	.....	.....	.....
60	2398.420	41681.4	2809_4—6977_4^0	7, 3	.....	0w	1.231d	(1.22)	1.24
1	2396.22	41719.7	3234_5—7406_4^0	.....	.....	.....	.....	.....	.....
3	2395.96	41724.2	3022_3—7194_2^0	.....	.....	.....	.....	.....	.....
	2395.41	41733.8	2907_2—7081_3^0	.....	.....	.....	.....	.....	.....

TABLE 1. *Classified lines of the second spectrum of rhenium* (Re II)—Continued

Intensity spark	Wavelength air	Wavenumber	Term combination	Zeeman type	Separation	Zeeman components		g	
						Strongest p	Strongest n	1st	2d
1	2	3	4	5	6	7	8	9	10
	A	*K*							
30	2389. 62	41834. 9	$a\ ^3F_3$—6346^3_2	1	. 231	0	0. 809	1. 271	1. 502
5*c*	2388. 319	41857. 7	3220_4—7406^4_3	-----	------	------	----------	------	------
2	2387. 92	41864. 7	2314_1—6501^1_1	-----	------	------	----------	------	------
100*cw*	2386. 895	41882. 7	$a\ ^5G_5$—$z\ ^5D^4_4$	2	------	0w	1. 303	(1. 26)	1. 25
15*c*	2385. 362	41909. 6	3022_3—7213^2_2	-----	------	------	----------	------	------
10	2382. 07	41967. 4	$a\ ^5P_3$—6673^2_2	-----	------	------	----------	------	------
2	2380. 63	41992. 9	$a\ ^3G_3$—6731^3_3	-----	------	------	----------	------	------
5*c*	2379. 992	42004. 1	2972_2—7173^2_2	-----	------	------	----------	------	------
3	2379. 587	42011. 3	2907_2—7108^2_2	-----	------	------	----------	------	------
20	2379. 101	42019. 8	$a\ ^5D_2$—$z\ ^5D^1_1$	2	0. 234	0	1. 766	1. 532	1. 298
4	2378. 98	42021. 8	$a\ ^3G_4$—6825^3_3	-----	------	------	----------	------	------
20	2378. 526	42030. 0	2774_3—6977^4_4	7a, 2	------	0w	1. 301h	(1. 23)	1. 25
3	2374. 57	42100. 0	2676_2—6886^3_3	-----	------	------	----------	------	------
50	2373. 476	42119. 4	$a\ ^5D_3$—$z\ ^7D^3_3$	3	. 351	1. 053	1. 126, 1. 485	1. 481	1. 130
4	2371. 842	42148. 4	2762_3—6977^4_4	-----	------	------	----------	------	------
1	2371. 69	42151. 2	$a\ ^5G_5$—6312^4_4	-----	------	------	----------	------	------
100	2370. 762	42167. 7	$a\ ^5D_4$—$z\ ^7D^3_3$	2	. 343	0	2. 508	1. 479	1. 136
50*c*	2368. 527	42208. 1	$a\ ^5D_3$—$z\ ^5D^2_2$	1*	------	0w	1. 008	------	------
1	2367. 75	42221. 4	2972_2—7194^2_2	-----	------	------	----------	------	------
4*c*	2367. 16	42231. 9	$a\ ^5P_2$—6557^3_3	-----	------	------	----------	------	------
40	2366. 078	42251. 1	$a\ ^5G_6$—$z\ ^7D^5_5$	1	------	0w	0. 899	(1. 24)	1. 31
1	2364. 91	42272. 0	$a\ ^3G_5$—6825^5_5	-----	------	------	----------	------	------
5	2364. 125	42286. 0	3493_2—7722^3_3	-----	------	------	----------	------	------
10	2362. 54	42314. 4	$a\ ^5D_1$—$z\ ^5D^2_2$	-----	------	------	----------	------	------
10*c*	2361. 47	42333. 6	$a\ ^5P_2$—6567^2_2	-----	------	------	----------	------	------
5	2359. 157	42375. 1	2676_2—6914^3_3 3225_3—7463^3_3	-----	------	------	----------	------	------
3	2358. 022	42395. 4	$a\ ^5G_4$—$z\ ^5D^4_4$	-----	------	------	----------	------	------
10*cw*	2357. 91	42397. 5	$a\ ^3F_2$—6494^3_3	-----	------	------	----------	------	------
3	2357. 66	42402. 0	2676_2—6917^2_2	-----	------	------	----------	------	------
40*c*	2355. 423	42442. 2	$a\ ^5S_2$—5966^3_3	1	0. 528	0	0. 110c	1. 694	1. 166
2	2351. 925	42505. 3	2666_1—6917^3_2	-----	------	------	----------	------	------
3	2350. 653	42528. 3	2314_1—6567^2_2	-----	------	------	----------	------	------
3	2349. 94	42541. 2	3101_2—7355^3_3	-----	------	------	----------	------	------
10*cl*	2349. 61	42547. 2	$a\ ^5D_4$—$z\ ^5F^3_3$	-----	------	------	----------	------	------
20	2346. 987	42594. 8	$a\ ^5D_0$—$z\ ^5D^1_1$	-----	------	------	----------	------	------
10*c*	2345. 51	42621. 6	3022_3—7284^3_3	-----	------	------	----------	------	------
1	2344. 544	42639. 1	$a\ ^3G_4$—6887^4_4	-----	------	------	----------	------	------
10	2341. 31	42698. 0	$a\ ^5D_2$—$z\ ^7D^3_3$	-----	------	------	----------	------	------
20	2340. 344	42715. 7	2809_4—7081^5_5	-----	------	------	----------	------	------
50	2336. 923	42778. 2	$a\ ^3F_3$—6440^4_4	7a, 1	------	0w	1. 101w	(1. 26)	1. 22
15	2336. 47	42786. 4	$a\ ^5D_2$—$z\ ^5D^2_2$	-----	------	------	----------	------	------
1	2333. 75	42836. 3	3071_3—7355^3_3	-----	------	------	----------	------	------
2	2332. 51	42859. 0	3225_3—7511^3_3	-----	------	------	----------	------	------
10	2331. 81	42871. 9	2907_2—7194^2_2	-----	------	------	----------	------	------
10	2330. 878	42889. 1	$a\ ^3G_5$—6887^4_4	-----	------	------	----------	------	------
8*cw*	2329. 89	42907. 2	$a\ ^5P_2$—6624^3_3	-----	------	------	----------	------	------
2*c*	2325. 424	42989. 7	2338_5—6637^4_4	-----	------	------	----------	------	------
10*c*	2324. 45	43007. 8	$a\ ^5P_1$—6673^2_2	-----	------	------	----------	------	------
60	2323. 409	43027. 0	$a\ ^3F_2$—6557^3_3	2	------	0w	1. 427	(1. 20)	1. 28
10	2321. 75	43057. 8	3101_2—7407^3_3	-----	------	------	----------	------	------
20	2317. 889	43129. 4	$a\ ^3F_2$—6567^2_2	-----	------	------	----------	------	------
10*c*	2316. 49	43155. 5	2338_5—6653^5_5 $a\ ^3F_4$—6704^5_5	-----	------	------	----------	------	------
2	2315. 186	43179. 8	3295_4—7613^4_4	-----	------	------	----------	------	------
2	2314. 209	43198. 0	3316_4—7636^3_3	-----	------	------	----------	------	------
3*c*	2310. 703	43263. 6	$a\ ^5S_2$—6048^1_1	-----	------	------	----------	------	------

TABLE 1. *Classified lines of the second spectrum of rhenium* (Re II)—Continued

Intensity spark	Wavelength air	Wavenumber	Term combination	Zeeman type	Separation	Zeeman components		g	
						Strongest *p*	Strongest *n*	1st	2d
1	2	3	4	5	6	7	8	9	10
	A	*K*							
3	2308. 972	43296. 0	$a\ ^3G_5$—6928°_4	-----	------	------	----------	------	------
15	2308. 658	43301. 89	$a\ ^5S_2$—6052°_3	-----	------	------	----------	------	------
20*c*	2308. 45	43305. 8	$a\ ^5G_3$—$z\ ^7D^\circ_5$	-----	------	------	----------	------	------
10	2308. 060	43313. 1	$a\ ^3F_3$—6494°_3	-----	------	------	----------	------	------
5	2307. 215	43329. 0	3022_3—7355°_3	-----	------	------	----------	------	------
4	2306. 268	43346. 8	3071_3—7406°_4	-----	------	------	----------	------	------
2	2305. 934	43353. 0	3071_3—7407°_3	-----	------	------	----------	------	------
8	2305. 021	43370. 2	2676_2—7013°_1	-----	------	------	----------	------	------
30*cw*	2303. 993	43389. 5	$a\ ^5P_3$—6673°_2	-----	------	------	----------	------	------
6	2302. 345	43420. 6	$a\ ^3F_4$—6731°_3	-----	------	------	----------	------	------
40*c*	2301. 815	43430. 6	$a\ ^5G_5$—6440°_4	7a, 2	------	0h	1. 357	(1. 26)	1. 23
7	2301. 612	43434. 4	$a\ ^3F_4$—6732°_4	-----	------	------	----------	------	------
10	2298. 586	43491. 6	a^3G_4—6972°_3 3287_2—7636°_3	-----	------	------	----------	------	------
100*cw*	2298. 094	43500. 9	2762_3—7112°_4	7a, 2	------	0w	1. 314	1. 15	(1. 19)
1	2296. 09	43538. 8	$a\ ^3G_4$—6977°_4	-----	------	------	----------	------	------
3	2295. 217	43555. 4	$a\ ^3G_3$—6887°_4 $a\ ^3F_3$—6610°_3	-----	------	------	----------	------	------
15	2295. 060	43558. 4	$a\ ^3G_4$—6979°_4	-----	------	------	----------	------	------
10	2293. 678	43584. 7	2314_1—6673°_2	-----	------	------	----------	------	------
10	2290. 196	43650. 9	2774_3—7139°_2	-----	------	------	----------	------	------
60	2286. 608	43719. 4	$a\ ^5G_3$—$z\ ^5D^\circ_4$	7a, 2	------	0w	1. 626	(1. 12)	1. 25
1	2283. 69	43775. 2	$a\ ^5G_3$—6291°_3	-----	------	------	----------	------	------
20	2282. 980	43788. 9	$a\ ^3G_3$—6977°_4	-----	------	------	----------	------	------
10	2281. 406	43819. 1	$a\ ^5G_4$—$z\ ^7D^\circ_5$	-----	------	------	----------	------	------
1	2281. 07	43825. 4	2972_2—7355°_3	-----	------	------	----------	------	------
2	2280. 00	43846. 1	3022_3—7407°_3	-----	------	------	----------	------	------
1	2279. 87	43848. 5	$a\ ^3G_3$—6917°_2	-----	------	------	----------	------	------
2	2278. 948	43866. 3	$a\ ^5P_3$—6862°_2	-----	------	------	----------	------	------
1	2278. 635	43872. 4	$a\ ^5G_2$—6271°_1	-----	------	------	----------	------	------
10	2277. 012	43903. 6	$a\ ^5G_3$—6304°_3	-----	------	------	----------	------	------
1	2276. 41	43915. 3	3071_3—7463°_3	-----	------	------	----------	------	------
500*c*	2275. 25	43937. 7	$a\ ^7S_3$—$z\ ^7P^\circ_2$	2*	------	0w	2. 00	------	------
10	2273. 98	43962. 2	$a\ ^3G_3$—6928°_4	-----	------	------	----------	------	------
50	2272. 644	43988. 0	$a\ ^5G_3$—6312°_4	-----	------	------	----------	------	------
5	2270. 928	44021. 2	3316_4—7719°_3	-----	------	------	----------	------	------
10	2269. 793	44043. 3	2676_2—7081°_3	-----	------	------	----------	------	------
2	2269. 228	44054. 2	3316_4—7722°_3	-----	------	------	----------	------	------
40*c*	2268. 46	44069. 2	$a\ ^5G_2$—6291°_3	-----	------	------	----------	------	------
2	2266. 387	44109 4	3225_3—7636°_3	-----	------	------	----------	------	------
10	2266. 18	44113. 5	$a\ ^5P_3$—6887°_4	-----	------	------	----------	------	------
3*h*	2265. 10	44134. 5	3098_4—7511°_3	-----	------	------	----------	------	------
9*c*	2263. 748	44160. 8	3220_4—7636°_3	-----	------	------	----------	------	------
50*c*	2261. 846	44198. 0	$a\ ^5G_2$—6304°_3	-----	------	------	----------	------	------
30	2260. 500	44224. 3	3101_2—7523°_2	-----	------	------	----------	------	------
8	2258. 55	44262. 5	3097_3—7523°_2	-----	------	------	----------	------	------
15	2254. 196	44348. 0	3287_2—7722°_3	-----	------	------	----------	------	------
8	2253. 28	44366. 0	$a\ ^3F_4$—6825°_5	-----	------	------	----------	------	------
2	2252. 61	44379. 2	$a\ ^5P_3$—6914°_3	-----	------	------	----------	------	------
10	2252. 154	44388. 1	2774_3—7213°_2	-----	------	------	----------	------	------
40	2251. 593	44399. 2	$a\ ^5D_3$—$z\ ^5D^\circ_3$ $a\ ^5D_4$—$z\ ^7D^\circ_4$	-----	------	------	----------	------	------
15	2251. 148	44408. 0	$a\ ^3G_3$—6972°_3 3022_3—7463°_3	-----	------	------	----------	------	------

TABLE 1. *Classified lines of the second spectrum of rhenium* (Re II)—Continued

Intensity spark	Wavelength air	Wavenumber	Term combination	Zeeman type	Separation	Zeeman components		g	
						Strongest p	Strongest n	1st	2d
1	2	3	4	5	6	7	8	9	10
	A	*K*							
15	2250. 273	44425. 3	2963_4—*7406*$\frac{3}{4}$	-----	-----	-----	-----	-----	-----
50	2248. 63	44457. 7	*a* $^5D_3$—*z* $^3P_2^\circ$	-----	-----	-----	-----	-----	-----
10	2247. 948	44471. 2	*a* $^3F_3$—*6610*$\frac{3}{3}$	-----	-----	-----	-----	-----	-----
9	2247. 544	44479. 2	*a* $^5G_4$—*6494*$\frac{3}{3}$	-----	-----	-----	-----	-----	-----
10	2247. 326	44483. 5	*a* $^5G_6$—*6651*$\frac{5}{5}$	-----	-----	-----	-----	-----	-----
9*c*	2245. 43	44521. 0	*a* $^5P_3$—*6928*$\frac{4}{4}$	-----	-----	-----	-----	-----	-----
4	2244. 500	44539. 5	*a* $^5P_3$—*6930*$\frac{3}{3}$	-----	-----	-----	-----	-----	-----
5	2240. 00	44628. 9	2676_2—*7139*$\frac{2}{2}$	-----	-----	-----	-----	-----	-----
10	2238. 169	44665. 5	*a* $^5D_3$—*z* $^5F_4^\circ$	-----	-----	-----	-----	-----	-----
100*c*	2235. 803	44712. 7	*a* $^5D_4$—*z* $^5F_4^\circ$	-----	-----	-----	-----	-----	-----
10	2234. 865	44731. 5	*a* $^3F_2$—*6727*$\frac{1}{1}$	-----	-----	-----	-----	-----	-----
3	2232. 964	44769. 6	*a* $^3F_2$—*6731*$\frac{2}{3}$	-----	-----	-----	-----	-----	-----
50	2232. 292	44783. 0	*a* $^5D_4$—*5966*$\frac{3}{3}$	-----	-----	-----	-----	-----	-----
8*c*	2231. 127	44806. 5	3316_4—*7797*$\frac{3}{3}$	-----	-----	-----	-----	-----	-----
20	2229. 104	44847. 1	*a* $^3F_3$—*6647*$\frac{4}{4}$	-----	-----	-----	-----	-----	-----
20	2226. 048	44908. 7	2762_3—*7253*$\frac{2}{2}$	-----	-----	-----	-----	-----	-----
7	2224. 851	44932. 8	3225_3—*7719*$\frac{3}{3}$	-----	-----	-----	-----	-----	-----
5	2223. 20	44966. 3	*a* $^5P_3$—*6972*$\frac{3}{3}$	-----	-----	-----	-----	-----	-----
7*c*	2221. 845	44993. 6	2907_2—*7407*$\frac{3}{3}$	-----	-----	-----	-----	-----	-----
5	2220. 920	45012. 3	3022_3—*7523*$\frac{2}{2}$	-----	-----	-----	-----	-----	-----
2	2220. 69	45017. 0	3220_4—*7722*$\frac{3}{3}$	-----	-----	-----	-----	-----	-----
1	2219. 75	45036. 2	*a* $^5D_2$—*z* $^3P_2^\circ$	-----	-----	-----	-----	-----	-----
5*c*	2216. 52	45101. 7	*a* $^3F_3$—*6673*$\frac{2}{2}$	-----	-----	-----	-----	-----	-----
50	2216. 161	45109. 0	*a* $^5G_4$—*6557*$\frac{3}{3}$	-----	-----	-----	-----	-----	-----
1000*cw*	2214. 261	45147. 7	*a* $^7S_3$—*z* $^7P_3^\circ$	3	-----	0. 545	1. 884w	1. 975	1. 793
7	2209. 320	45248. 6	*a* $^3F_4$—*6914*$\frac{3}{3}$	-----	-----	-----	-----	-----	-----
2	2208. 188	45271. 9	*a* $^5G_3$—*6441*$\frac{3}{3}$	-----	-----	-----	-----	-----	-----
3	2207. 376	45288. 5	*a* $^5P_2$—*6862*$\frac{3}{3}$	-----	-----	-----	-----	-----	-----
40	2206. 154	45313. 6	*a* $^5D_2$—*5966*$\frac{3}{3}$	-----	-----	-----	-----	-----	-----
20	2203. 579	45366. 5	2676_2—*7213*$\frac{2}{2}$	-----	-----	-----	-----	-----	-----
2	2202. 695	45384. 7	3098_4—*7636*$\frac{3}{3}$	-----	-----	-----	-----	-----	-----
10	2202. 19	45395. 1	*a* $^5G_5$—*6637*$\frac{4}{4}$	-----	-----	-----	-----	-----	-----
3	2199. 113	45458. 6	2809_4—*7355*$\frac{3}{3}$	-----	-----	-----	-----	-----	-----
15	2197. 928	45483. 2	2314_1—*6862*$\frac{2}{2}$	-----	-----	-----	-----	-----	-----
4	2197. 610	45489. 8	*a* $^3G_3$—*7081*$\frac{3}{3}$	-----	-----	-----	-----	-----	-----
10	2197. 373	45494. 6	*a* $^5S_2$—*6271*$\frac{1}{1}$	-----	-----	-----	-----	-----	-----
30*c*	2197. 130	45499. 7	*a* $^5G_5$—*6647*$\frac{4}{4}$	-----	-----	-----	-----	-----	-----
40	2195. 284	45537. 9	*a* $^5G_5$—*6651*$\frac{5}{5}$	-----	-----	-----	-----	-----	-----
10	2194. 433	45555. 6	2907_2—*7463*$\frac{3}{3}$	-----	-----	-----	-----	-----	-----
15*c*	2193. 933	45566. 0	*a* $^5G_2$—*6441*$\frac{2}{2}$	-----	-----	-----	-----	-----	-----
20*c*	2192. 567	45594. 4	*a* $^5D_3$—*6052*$\frac{3}{3}$	-----	-----	-----	-----	-----	-----
50	2190. 260	45642. 41	*a* $^5D_4$—*6052*$\frac{3}{3}$	-----	-----	-----	-----	-----	-----
10	2188. 221	45684. 9	*a* $^3F_3$—*6731*$\frac{3}{3}$	-----	-----	-----	-----	-----	-----
4	2187. 556	45698. 8	*a* $^3F_3$—*6732*$\frac{4}{4}$	-----	-----	-----	-----	-----	-----
1	2184. 19	45769. 1	2676_2—*7253*$\frac{2}{2}$ 3220_4—*7797*$\frac{3}{3}$	-----	-----	-----	-----	-----	-----
15*c*	2183. 443	45784. 8	*a* $^5G_4$—*6624*$\frac{3}{3}$	-----	-----	-----	-----	-----	-----
2	2182. 374	45807. 3	*a* $^3G_3$—*7112*$\frac{4}{4}$	-----	-----	-----	-----	-----	-----
100*cw*	2181. 77	45819. 9	*a* $^5S_2$—*6304*$\frac{3}{3}$	-----	-----	-----	-----	-----	-----
4	2181. 430	45827. 1	*a* $^5G_3$—*6496*$\frac{3}{3}$	-----	-----	-----	-----	-----	-----
10	2180. 804	45840. 3	2879_3—*7463*$\frac{3}{3}$	-----	-----	-----	-----	-----	-----
20	2178. 778	45882. 9	*a* $^3F_4$—*6977*$\frac{4}{4}$	-----	-----	-----	-----	-----	-----
100	2177. 851	45902. 4	2338_5—*6928*$\frac{4}{4}$	-----	-----	-----	-----	-----	-----
20	2177. 579	45908. 1	*a* $^5G_4$—*6637*$\frac{4}{4}$	-----	-----	-----	-----	-----	-----
4	2177. 382	45912. 3	3022_3—*7613*$\frac{4}{4}$	-----	-----	-----	-----	-----	-----
4	2174. 692	45969. 1	2809_4—*7406*$\frac{3}{4}$	-----	-----	-----	-----	-----	-----

TABLE 1. *Classified lines of the second spectrum of rhenium* (Re II)—Continued

Intensity spark	Wavelength air	Wavenumber	Term combination	Intensity spark	Wavelength air	Wavenumber	Term combination
1	2	3	4	1	2	3	4
	A	*K*			*A*	*K*	
30	2172. 618	46013. 0	$a\ ^5G_4$—*6647*$^5_4$	80	2085. 76	47928. 8	$a\ ^5D_3$—*z* $^5D^5_4$
2	2172. 094	46024. 1	2314_1—*6917*$^3_2$	40*c*	2085. 14	47943. 1	2314_1—*7108*$^1_1$
4	2171. 145	46044. 2	$a\ ^5D_4$—*z* $^5F^3_3$	80	2083. 67	47976. 8	$a\ ^5D_4$—*z* $^5D^5_4$
10	2170. 970	46047. 9	*a* $^5P_3$—*7081*$^3_3$	20	2083. 342	47984. 5	$a\ ^5D_3$—*6291*$^3_3$
50	2170. 806	46051. 4	$a\ ^5G_4$—*6651*$^3_3$	100*c*	2082. 234	48010. 0	$a\ ^5P_1$—*7173*$^2_2$
2	2169. 77	46073. 4	$a\ ^5G_4$—*6653*$^5_5$	40	2081. 26	48032. 4	$a\ ^5D_4$—*6291*$^3_3$
5	2169. 240	46084. 6	$a\ ^3F_2$—*6862*$^3_2$	8	2079. 33	48077. 1	$a\ ^3G_5$—*7406*$^4_4$
40	2166. 880	46134. 8	$a\ ^5D_2$—*6048*$^1_1$	8	2079. 05	48083. 6	$a\ ^5P_3$—*7284*$^3_3$
2	2166. 52	46142. 5	3022_3—*7636*$^3_3$	7	2078. 33	48100. 1	$a\ ^3F_3$—*6972*$^3_3$
7	2163. 07	46216. 08	3097_3—*7719*$^3_3$	20	2077. 78	48113. 1	$a\ ^5D_3$—*6304*$^3_3$
10	2161. 914	46240. 7	$a\ ^5S_2$—*6346*$^2_2$ 3098_4—*7722*$^3_3$	20*c*	2076. 30	48147. 3	$a\ ^3F_3$—*6977*$^4_4$
				50*c*	2075. 70	48161. 2	$a\ ^5D_4$—*6304*$^3_3$
20	2158. 292	46318. 4	2774_3—*7406*$^4_4$	20	2075. 11	48174. 8	$a\ ^5G_3$—*6731*$^3_3$?
4*cs*	2158. 05	46323. 5	$a\ ^3F_2$—*6886*$^3_3$	15*c*	2072. 88	48226. 7	$a\ ^5P_1$—*7194*$^2_2$
2	2156. 103	46365. 4	$a\ ^5P_3$—*7112*$^4_4$	30	2072. 62	48232. 8	$a\ ^3G_3$—*7355*$^3_3$
3*c*	2153. 79	46415. 1	$a\ ^5P_1$—*7013*$^1_1$ 2338_5—*6979*$^4_4$	20	2072. 09	48245. 1	$a\ ^5D_4$—*6312*$^4_4$
				10	2071. 175	48266. 4	$a\ ^3F_2$—*7081*$^3_3$
2	2152. 98	46432. 6	$a\ ^5G_3$—*6557*$^3_3$	60*c*	2069. 42	48307. 2	$a\ ^5G_5$—*6928*$^4_4$
5	2152. 79	46436. 7	2762_3—*7406*$^4_4$	40*c*	2067. 64	48348. 9	$a\ ^5S_2$—*6557*$^3_3$
4	2149. 59†	46505. 8	3071_3—*7722*$^3_3$	30*c*	2066. 91	48366. 0	$a\ ^5D_2$—*6271*$^1_1$
20	2148. 261	46534. 6	$a\ ^5G_3$—*6567*$^2_2$				
3	2148. 13	46537. 5	2809_4—*7463*$^3_3$	15	2065. 83	48391. 2	2774_3—*7613*$^4_4$ $a\ ^5P_2$—*7173*$^2_2$
30	2145. 90	46585. 8	$a\ ^5G_4$—*6704*$^3_3$	3	2065. 64	48395. 7	$a\ ^3G_4$—*7463*$^3_3$
30	2144. 085	46625. 2	$a\ ^3F_2$—*6917*$^3_2$	30	2064. 87	48413. 7	$a\ ^5G_4$—*6887*$^4_4$
8*h*	2143. 96	46627. 9	$a\ ^3G_3$—*7194*$^2_2$	20	2064. 16	48430. 4	$a\ ^5G_2$—*6727*$^1_1$
4	2140. 190	46710. 1	$a\ ^5D_0$—*6048*$^1_1$	80	2059. 75	48534. 0	$a\ ^5D_3$—*6346*$^2_2$
3	2139. 45	46726. 1	$a\ ^5G_2$—*6557*$^3_3$				
				5	2059. 33	48544. 0	$a\ ^3F_2$—*7108*$^2_2$
4	2136. 701	46786. 3	2676_2—*7355*$^3_3$	15	2058. 520	48563. 0	$a\ ^5D_2$—*6291*$^3_3$
5	2136. 22	46796. 8	$a\ ^5P_2$—*7013*$^1_1$	5	2058. 10	48572. 9	2666_1—*7523*$^2_2$
10*c*	2134. 773	46828. 6	$a\ ^5G_2$—*6567*$^2_2$	15*c*	2056. 59	48608. 6	$a\ ^5P_2$—*7194*$^2_2$
20	2133. 776	46850. 4	$a\ ^5G_4$—*6731*$^3_3$	20	2055. 25	48640. 3	$a\ ^5D_1$—*6346*$^2_2$
9	2133. 122	46864. 8	$a\ ^5G_4$—*6732*$^4_4$				
				50	2053. 597	48679. 4	$a\ ^5G_4$—*6914*$^3_3$
6	2128. 773	46960. 05	$a\ ^5G_3$—*6610*$^3_3$	10	2053. 10	48691. 2	$a\ ^5D_2$—*6304*$^3_3$
4	2128. 53	46965. 9	3022_3—*7719*$^3_3$	15	2050. 64	48749. 6	$a\ ^3G_3$—*7407*$^3_3$
8	2128. 392	46969. 0	$a\ ^5P_3$—*7173*$^2_2$	3	2048. 380	48803. 3	2314_1—*7194*$^2_2$
2	2127. 28	46993. 5	3098_4—*7797*$^3_3$	6	2047. 955	48813. 5	$a\ ^5P_1$—*7253*$^2_2$
3	2126. 96	47000. 6	$a\ ^3F_3$—*6862*$^4_4$				
				7	2047. 67	48820. 3	$a\ ^5G_4$—*6928*$^4_4$
4	2126. 73	47005. 7	2762_3—*7463*$^3_3$	6*h*	2046. 318	48852. 5	$a\ ^3F_2$—*7139*$^2_2$
20	2122. 081	47108. 6	$a\ ^5G_3$—*6624*$^3_3$	40	2042. 64	48940. 4	$a\ ^5D_0$—*6271*$^1_1$
10	2121. 27	47126. 7	$a\ ^5D_3$—*6205*$^2_2$	2	2040. 64	48988. 4	2314_1—*7213*$^2_2$
1	2119. 67	47162. 2	2762_3—*7463*$^3_3$	15	2036. 20	49095. 3	2809_4—*7719*$^3_3$
15	2118. 671	47184. 4	$a\ ^3F_2$—*6972*$^3_3$				
				10	2035. 51	49111. 8	$a\ ^5D_2$—*6346*$^2_2$
5	2118. 54	47187. 4	$a\ ^5S_2$—*6441*$^2_2$	2	2034. 824	49128. 5	2809_4—*7722*$^3_3$
7	2116. 23	47238. 9	$a\ ^3F_3$—*6886*$^3_3$	20	2034. 020	49147. 9	$a\ ^3G_3$—*7446*$^3_3$
20*c*	2115. 51	47255. 0	$a\ ^5G_2$—*6610*$^3_3$	20	2032. 59	49182. 5	2879_3—*7797*$^3_3$
100	2114. 25	47283. 1	$a\ ^5G_5$—*6825*$^5_5$	30	2032. 02	49196. 1	$a\ ^5P_2$—*7253*$^2_2$
60	2111. 854	47336. 7	$a\ ^5G_3$—*6647*$^4_4$				
				9	2027. 69	49301. 3	$a\ ^5P_3$—*7406*$^4_4$
4	2102. 28	47552. 3	2963_4—*7719*$^3_3$	3	2027. 45	49307. 2	$a\ ^5P_3$—*7407*$^3_3$
8	2100. 85	47584. 7	2963_4—*7722*$^3_3$	10	2027. 29	49311. 1	$a\ ^3G_3$—*7463*$^3_3$
7	2100. 58	47590. 7	$a\ ^5G_3$—*6673*$^2_2$	10	2026. 40	49332. 5	$a\ ^7G_4$—*6979*$^4_4$
10	2097. 77	47654. 5	$a\ ^3F_3$—*6928*$^4_4$	4	2024. 05	49389. 8	2314_1—*7253*$^2_2$
15	2093. 792	47747. 3	2338_5—*7112*$^4_4$	200	2023. 644	49399. 8	$a\ ^5D_4$—*z* $^7D^5_4$
7	2091. 920	47787. 7	$a\ ^5S_2$—*6501*$^1_1$	10*c*	2020. 475	49477. 3	$a\ ^5D_3$—*6440*$^4_4$ 2774_3—*7722*$^3_3$
30	2091. 535	47796. 5	$a\ ^5G_4$—*6825*$^5_5$				
60*c*	2090. 20	47827. 1	$a\ ^3G_4$—*7406*$^4_4$	4*c*	2020. 34	49480. 7	$a\ ^5D_3$—*6441*$^2_2$
30*c*	2087. 67	47884. 9	$a\ ^5G_2$—*6673*$^2_2$	10	2019. 97	49489. 7	$a\ ^5G_3$—*6862*$^3_2$
10	2087. 30	47893. 4	$a\ ^5D_1$—*6271*$^1_1$	30*c*	2019. 28	49506. 7	$a\ ^5S_2$—*6673*$^2_2$

TABLE 1. *Classified lines of the second spectrum of rhenium* (Re II)—Continued

Intensity spark	Wavelength air	Wave-number	Term combination	Intensity spark	Wavelength vac	Wave-number	Term combination
1	2	3	4	1	2	3	4
	A	*B*			*A*	*B*	
40	2018.54	49524.8	$a\ ^5D_4$—6440$\frac{3}{4}$	3*a*	1927.912	51869.6	$a\ ^3G_3$—7719$\frac{3}{3}$
6	2017.08	49560.6	$a\ ^5P_3$—7432$\frac{2}{2}$	5*a*	1926.93	51896.0	$a\ ^5D_2$—6624$\frac{3}{3}$ $a\ ^5P_3$—7523$\frac{2}{2}$
9	2015.91	49589.4	$a\ ^3F_2$—7213$\frac{3}{2}$				
4	2013.02	49660.6	2389_4—7355$\frac{3}{3}$	5*a*	1926.569	51905.7	$a\ ^5D_1$—6673$\frac{2}{2}$
10	2011.82	49706.2	$a\ ^5P_3$—7446$\frac{3}{3}$	5*a*	1926.096	51918.5	$a\ ^5S_2$—6914$\frac{1}{2}$
				15*a*	1925.05	51946.7	$a\ ^5S_2$—6917$\frac{1}{2}$
100	2009.92	49737.1	$a\ ^5G_3$—6887$\frac{4}{4}$				
2	2008.67	49768.1	$a\ ^3F_3$—7139$\frac{3}{2}$	5*a*	1913.60	52257.5	$a\ ^5G_3$—7139$\frac{3}{2}$
6	2004.14	49880.6	2809_4—7797$\frac{3}{3}$	12*a*	1908.98	52384.0	$a\ ^5D_3$—6731$\frac{3}{3}$ $a\ ^5G_4$—7284$\frac{1}{1}$
				10*a*	1908.48	52397.7	$a\ ^5D_3$—6732$\frac{2}{1}$
	vac			6*a*	1907.385	52427.8	$a\ ^5P_3$—7719$\frac{3}{3}$
25	1999.50	50012.5	$a\ ^5D_3$—6494$\frac{3}{3}$	5*a*	1907.10	52435.6	$a\ ^3F_3$—7406$\frac{4}{3}$
3*a*	1998.77	50030.8	$a\ ^5G_2$—6887$\frac{4}{3}$ $a\ ^5G_3$—6917$\frac{2}{2}$	10*a*	1906.73	52445.8	$a\ ^5D_4$—6732$\frac{1}{0}$
				15	1906.49	52452.4	$a\ ^5D_1$—6727$\frac{1}{1}$
				3*a*	1906.19	52460.7	$a\ ^5P_3$—7722$\frac{3}{3}$
30	1997.60	50060.1	$a\ ^5D_4$—6494$\frac{3}{3}$	5*a*	1905.689	52474.5	$a\ ^3F_4$—7636$\frac{3}{3}$?
1*a*	1996.663	50083.5	$a\ ^5D_4$—6496$\frac{3}{3}$	12*ha*	1904.55	52505.8	$a\ ^5S_2$—6972$\frac{1}{2}$
10*a*	1995.87	50103.5	$a\ ^3F_3$—7173$\frac{2}{2}$				
3*a*	1994.785	50130.7	$a\ ^3G_4$—7636$\frac{3}{3}$	2*a*	1902.916	52550.9	$a\ ^5G_2$—7139$\frac{3}{2}$
25	1994.24	50144.4	$a\ ^5G_3$—6928$\frac{4}{4}$	5*a*	1901.40	52592.8	$a\ ^5G_3$—7173$\frac{2}{2}$
				10*a*	1899.14	52655.4	$a\ ^3G_3$—7797$\frac{3}{3}$
3*a*	1993.480	50163.5	$a\ ^5G_3$—6930$\frac{3}{3}$	100	1898.36	52677.0	$a\ ^7S_3$—$z\ ^5P_2^0$
6*a*	1993.189	50170.9	$a\ ^3F_4$—7406$\frac{4}{3}$	3*a*	1897.825	52691.9	$a\ ^3F_2$—7523$\frac{2}{2}$
12*cwa*	1992.53	50187.5	$a\ ^5D_1$—6501$\frac{1}{1}$				
15*a*	1988.19	50297.0	$a\ ^5G_2$—6914$\frac{3}{3}$	20	1893.60	52809.5	$a\ ^5G_3$—7194$\frac{3}{3}$
2*a*	1987.984	50302.2	$a\ ^3F_2$—7284$\frac{3}{3}$	20	1889.85	52914.3	$a\ ^5S_2$—7013$\frac{1}{1}$
				10*a*	1888.17	52961.3	$a\ ^5D_2$—6731$\frac{3}{3}$
10*da*	1985.95	50353.7	$a\ ^5P_3$—7511$\frac{3}{3}$	1*a*	1886.650	53004.0	$a\ ^3F_3$—7463$\frac{3}{3}$
10*a*	1981.89	50456.9	$a\ ^5G_2$—6930$\frac{3}{3}$	10*a*	1885.843	53026.7	$a\ ^5P_2$—7636$\frac{3}{3}$
5*a*	1981.217	50474.0	$a\ ^5P_3$—7523$\frac{2}{2}$				
15	1976.67	50590.1	$a\ ^5D_2$—6494$\frac{3}{3}$	3*a*	1883.546	53091.3	$a\ ^5G_4$—7355$\frac{4}{3}$
5*a*	1974.86	50636.5	$a\ ^5G_3$—6977$\frac{4}{4}$	10*a*	1883.12	53103.4	$a\ ^5G_2$—7194$\frac{2}{2}$
				20	1879.26	53212.4	$a\ ^5P_3$—7797$\frac{3}{3}$
25	1974.65	50641.9	$a\ ^5D_3$—6557$\frac{3}{3}$	10*a*	1876.58	53288.4	$a\ ^5G_2$—7213$\frac{2}{2}$
5*a*	1973.986	50658.9	$a\ ^5D_2$—6501$\frac{1}{1}$	1*a*	1875.118	53330.0	$a\ ^3F_4$—7722$\frac{5}{4}$
150	1973.13	50680.9	$a\ ^7S_3$—$z\ ^7P_4^0$				
3*a*	1972.776	50690.0	$a\ ^5D_4$—6557$\frac{3}{3}$	100*ha*	1871.812	53424.2	$a\ ^5D_3$—6835$\frac{3}{3}$
5*a*	1970.84	50739.8	$a\ ^3F_4$—7463$\frac{3}{3}$	1*a*	1869.172	53499.6	$a\ ^5D_0$—6727$\frac{1}{1}$
				1*a*	1865.657	53600.4	$a\ ^5G_4$—7406$\frac{4}{3}$
10*a*	1970.68	50743.9	$a\ ^5D_3$—6567$\frac{2}{2}$	1*a*	1862.219	53699.4	$a\ ^5D_3$—6862$\frac{4}{3}$
10*a*	1966.55	50850.5	$a\ ^5D_1$—6567$\frac{2}{2}$	10*a*	1861.94	53707.4	$a\ ^5G_3$—7284$\frac{3}{3}$
3*a*	1962.58	50953.3	$a\ ^3G_4$—7719$\frac{3}{3}$				
25	1954.29	51169.5	$a\ ^5D_3$—6610$\frac{3}{3}$	200	1858.65	53802.5	$a\ ^7S_3$—$z\ ^5P_3^0$
1*a*	1952.830	51207.7	2676_2—7797$\frac{3}{3}$	5*a*	1856.49	53865.1	$a\ ^5S_2$—7108$\frac{1}{1}$
				25	1854.00	53937.4	$a\ ^5D_2$—6886$\frac{3}{3}$
12*a*	1952.45	51217.7	$a\ ^5D_4$—6610$\frac{3}{3}$ $a\ ^3F_3$—7284$\frac{3}{3}$	40	1853.70	53946.2	$a\ ^5D_3$—6887$\frac{4}{3}$
				40	1852.35	53985.5	$a\ ^5D_4$—6886$\frac{3}{3}$
20	1951.84	51233.7	$a\ ^5D_0$—6501$\frac{1}{1}$	5*a*	1851.81	54001.2	$a\ ^5G_2$—7284$\frac{3}{3}$
3*a*	1948.65	51317.6	$a\ ^5D_3$—6624$\frac{3}{3}$	20	1849.04	54082.1	$a\ ^3F_4$—7797$\frac{3}{3}$
25	1948.48	51322.1	$a\ ^5D_2$—6567$\frac{2}{2}$	6*a*	1846.060	54169.4	$a\ ^5G_4$—7463$\frac{3}{3}$
12*a*	1944.02	51439.8	$a\ ^5D_3$—6637$\frac{4}{4}$	4*a*	1845.916	54173.6	$a\ ^5S_2$—7139$\frac{2}{2}$
				15*a*	1844.61	54212.0	$a\ ^5D_3$—6914$\frac{3}{3}$
15*a*	1942.19	51488.3	$a\ ^5D_4$—6637$\frac{4}{4}$	12*a*	1842.98	54259.9	$a\ ^5D_4$—6914$\frac{3}{3}$
5*a*	1940.769	51526.0	$a\ ^3F_2$—7407$\frac{3}{3}$	12*a*	1840.05	54346.3	$a\ ^5D_1$—6917$\frac{2}{1}$
25	1940.04	51545.3	$a\ ^5D_3$—6647$\frac{4}{4}$	18	1839.81	54353.4	$a\ ^5D_3$—6928$\frac{4}{4}$
30*a*	1938.224	51593.6	$a\ ^5D_4$—6647$\frac{4}{4}$	8*a*	1838.198	54401.1	$a\ ^5D_4$—6928$\frac{4}{4}$
1*a*	1937.857	51603.4	$a\ ^5P_3$—7636$\frac{3}{3}$	3*a*	1837.73	54415.0	$a\ ^5G_3$—7355$\frac{4}{3}$
20	1936.79	51631.8	$a\ ^5D_4$—6651$\frac{5}{5}$	10*a*	1837.56	54420.0	$a\ ^5D_4$—6930$\frac{3}{3}$
10*a*	1935.94	51654.5	$a\ ^5D_4$—6653$\frac{3}{3}$	100*a*	1834.319	54516.1	$a\ ^5D_2$—6886$\frac{3}{3}$
20*h*	1935.32	51671.0	$a\ ^5G_3$—7081$\frac{3}{3}$	5*a*	1830.32	54635.3	$a\ ^5P_2$—7797$\frac{3}{3}$
25	1932.43	51748.3	$a\ ^5D_2$—6610$\frac{3}{3}$	5*a*	1829.992	54645.05	$a\ ^3F_2$—7719$\frac{3}{3}$
4*a*	1931.372	51776.7	$\frac{1}{4}$ $a\ ^5P_2$—7511$\frac{3}{3}$	20	1825.13	54790.6	$a\ ^5D_2$—6914$\frac{3}{3}$

TABLE 1. *Classified lines of the second specturum of rhenium* (Re II)—Continued

Intensity spark	Wavelength vac	Wave-number	Term combination	Intensity spark	Wavelength vac	Wave-number	Term combination
1	2	3	4	1	2	3	4
	A	*B*			*A*	*B*	
5*a*	1824. 85	54799. 0	*a* $^5D_3$—*6972*$\frac{3}{3}$	3*da*	1748. 129	57204. 0	*a* $^5D_3$—*7213*$\frac{2}{2}$
12*a*	1823. 28	54846. 2	*a* $^5D_4$—*6972*$\frac{3}{3}$ *a* $^5D_3$—*6977*$\frac{1}{1}$	3*a*	1747. 42	57227. 2	*a* $^5G_3$—*7636*$\frac{3}{3}$
3*da*	1821. 681	54894. 3	*a* $^5D_4$—*6977*$\frac{1}{1}$	5*ha*	1744. 853	57311. 4	*a* $^5D_0$—*7108*$\frac{1}{1}$
18	1821. 03	54914. 0	*a* $^5D_4$—*6979*$\frac{4}{4}$	5*a*	1738. 74	57512. 9	*a* $^5G_4$—*7797*$\frac{3}{3}$
50	1816. 19	55060. 3	*a* $^7S_3$—*z* $^7D_2^3$	2*a*	1738. 458	57522. 2	*a* $^5G_2$—*7636*$\frac{1}{1}$
1*a*	1812. 149	55183. 1	*a* $^5G_3$—*7432*$\frac{2}{2}$	5*a*	1735. 93	57606. 0	*a* $^5D_3$—*7253*$\frac{2}{2}$
10*a*	1810. 80	55224. 2	*a* $^5G_2$—*7407*$\frac{3}{3}$?	100	1725. 20	57964. 3	*a* $^5D_4$—*7284*$\frac{3}{3}$
1*a*	1807. 873	55313. 6	*a* $^5D_1$—*7013*$\frac{1}{1}$	5*a*	1704. 40	58671. 7	*a* $^5D_4$—*7355*$\frac{3}{3}$
5*a*	1807. 37	55329. 0	*a* $^5G_3$—*7446*$\frac{3}{3}$	1*a*	1690. 903	59140. 0	*a* $^5D_3$—*7407*$\frac{3}{3}$
5*a*	1802. 54	55477. 3	*a* $^5G_2$—*7432*$\frac{2}{2}$	40	1686. 87	59281. 4	*a* $^7S_3$—*z* $^7D_4^4$
10*a*	1797. 82	55622. 9	*a* $^5S_2$—*7284*$\frac{3}{3}$	60	1685. 49	59329. 9	*a* $^7S_3$—*z* $^5D_3^3$
10*a*	1796. 184	55673. 6	*a* $^5G_4$—*7613*$\frac{4}{4}$	25	1683. 86	59387. 4	*a* $^7S_3$—*z* $^3P_2^2$
50*a*	1792. 53	55787. 1	*a* $^5G_3$—*7463*$\frac{3}{3}$	10*a*	1680. 67	59500. 1	*a* $^5D_1$—*7432*$\frac{2}{2}$
3*a*	1787. 994	55928. 6	*a* $^5D_4$—*7081*$\frac{3}{3}$	30	1677. 98	59595. 5	*a* $^7S_3$—*z* $^5F_4^4$
5*a*	1777. 11	56271. 1	*a* $^5G_2$—*7511*$\frac{3}{3}$	50	1676. 01	59665. 5	*a* $^7S_3$—*5966*$\frac{3}{3}$
2*a*	1771. 202	56458. 8	*a* $^5D_2$—*7081*$\frac{3}{3}$	25	1666. 66	60000. 2	*a* $^5S_2$—*7722*$\frac{3}{3}$
10*a*	1770. 97	56466. 2	*a* $^5D_3$—*7139*$\frac{2}{2}$	15*a*	1646. 05	60751. 5	*a* $^5S_2$—*7797*$\frac{3}{3}$
3*a*	1767. 65	56572. 3	*a* $^5D_1$—*7139*$\frac{2}{2}$	15*a*	1632. 53	61254. 6	*a* $^5D_4$—*7613*$\frac{4}{4}$
5*a*	1762. 84	56726. 6	*a* $^5G_4$—*7719*$\frac{3}{3}$?	20*a*	1590. 87	62858. 7	*a* $^7S_3$—*z* $^5D_2^3$
5*a*	1762. 56	56735. 7	*a* $^5D_2$—*7108*$\frac{1}{1}$?	3*a*	1584. 97	63092. 7	*a* $^5D_4$—*7797*$\frac{3}{3}$
5*a*	1759. 13	56846. 3	*a* $^5S_2$—*7407*$\frac{3}{3}$	12	1584. 10	63127. 3	*a* $^7S_3$—*6312*$\frac{4}{4}$
3*a*	1753. 83	57018. 1	*a* $^5D_3$—*7194*$\frac{2}{2}$	30	1552. 65	64406. 0	*a* $^7S_3$—*6440*$\frac{4}{4}$
2*a*	1753. 020	57044. 4	*a* $^5D_2$—*7139*$\frac{2}{2}$	3	1539. 84	64941. 8	*a* $^7S_3$—*6494*$\frac{3}{3}$
18	1752. 85	57049. 9	*a* $^7S_3$—*z* $^7D_3^3$	5	1525. 03	65572. 5	*a* $^7S_3$—*6557*$\frac{3}{3}$
200	1750. 14	57138. 3	*a* $^7S_3$—*z* $^5D_2^2$				

4. Energy Levels of Re II

This term analysis of the second spectrum of rhenium yielded more or less information concerning 49 even and 83 odd energy levels as shown in table 2. In column 3, CS stands for Catalán and Sales, M for Meggers, and T for Tech. During the course of the analysis deliberate effort was made to group the levels in spectral terms according to the general rules governing g- values, and level intervals. In the case of Re I [1] the interpretation of levels was guided by that for Mn I, and similar clues as to the interpretation of Re II were sought by comparison with the homologous spectra Mn II [9], and Tc II [10]. Indeed the ground states of these three homologous spectra are identical, $d^5(a^6S)s\,a^7S_3=0.0$, except that the principal quantum numbers of d and s electrons increase by one unit in successive periods. Likewise the companion term $d^5(a^6S)s\,a^5S_2$ is comparable in the three spectra except that it increases from 9472.9 K in Mn II, to 12617.2 K in Tc II, to 17223.5 K in Re II. The analogies end here, for the next even level, $a\,^5D_4$, in Mn II starts at 14325.6 K, in Tc II at 3461.3 K, and in Re II at 14882.6 K. In Mn II and Tc II these levels certainly arise from d^6 because they are completely inverted. If the $a\,^5D$ term of Re II arose from d^6 it would have very large negative intervals but since its intervals are relatively small and predominantly positive it must be ascribed to d^4s^2. Theoretically, of course, d^6 and d^4s^2 produce the same number and types of spectral terms, viz, ^{5}D, ^{3}(HGFDP)^1(IGFDS)^3(FP)^1(GDS), composed of 34 energy levels. A much larger family of even terms consisting of 74 levels theoretically arises from the d^5s configuration which produces ^{7}S, ^{5}S, ^{5}(GD) ^{3}(GD) ^{3}(IGFDS)^1(IGFDS) ^{5}(FP) ^{3}(FP) ^{3}(HGFDP) ^{1}(HGFDP) ^{3}D, ^{1}D. Thus the total number of levels expected from these two configurations of optical electrons is 108, whereas only 49 have been found in Re II. Moreover, the intervals between levels and terms is so large that strong configuration interaction may account for large deviations from Landé g-values, and for many interval and intensity anomalies. For these reasons in Atomic Energy Levels [10, p. 168] electron configurations and spectral term designations were cautiously given for only 6 low-even terms of Re II. Rather than list the remainder as miscellaneous levels in table 2, the advice of R. E. Trees was taken to attempt to group the levels and assign term symbols in a probable but provisional manner. However, since some terms are incomplete and many higher ones are missing, the provisionally designated terms have been omitted in the term combinations

TABLE 2. *Energy levels and spectral terms of Re II*

Config.	Desig.	Finder	J	Level value	Interval	Obs. g
$5d^5(^6S)6s$	$a\ ^7S$	M 50	3	0.0		2.05
$5d^4\ 6s^2$	$a\ ^5D$	M 50	0	13777.3		0/0
					1046.7	
		M 50	1	14824.0		1.50
					−471.8	
		M 50	2	14352.2		1.53
					578.3	
		M 50	3	14930.5		1.48
					−47.9	
		M 50	4	14882.6		1.48
$5d^5(^6S)6s$	$a\ ^5S$	M 50	2	17223.5		1.71
$5d^5(^4G)6s$	$a\ ^5G$	M 50	2	18845.8		0.64
					293.9	
		M 50	3	19139.7		1.12
					1323.5	
		M 50	4	20463.2		1.18
					513.2	
		CS 54	5	20976.4		1.26
					1254.7	
		CS 54	6	22031.1		1.24
$5d^5(^4P)6s$	$a\ ^5P$	CS 54	1	23722.4		1.903
					−381.6	
		M 50	2	23340.8		1.67
					1422.3	
		M 50	3	24763.1		1.41
$5d^4\ 6s^2$	$a\ ^3F$	M 50	2	22544.7		1.20
					−915.6	
		M 50	3	21629.1		1.26
					2264.4	
		CS 54	4	23893.5		1.275
			4			
$5d^4\ 6s^2$	$a\ ^3H$	CS 54	5	23381.2		1.19
			6			
$5d^4\ 6s^2$	$a\ ^3G$	M 50	3	25321.2		0.90
					916.1	
		CS 54	4	26237.3		1.12
					−249.8	
		CS 54	5	25987.5		1.22
$5d^4\ 6s^2$	$a\ ^3P$		0			
		CS 50	1	26664.3		1.46
			2			
$5d^4\ 6s^2$	$a\ ^3D$	M 50	1	23146.2		1.10
					3621.4	
		M 50	2	26767.6		1.09
					987.4	
		M 50	3	27746.0		1.23
$5d^5(a\ ^2F)6s$	$b\ ^3F$	CS 54	4	28095.3		1.22
					467.6	
		M 57	3	27627.7		
					−1449.6	
		M 50	2	29077.3		
$5d^5(^4D)6s$	$b\ ^5D$	M 50	0	29773.2		0/0
					−346.0	
		CS 54	1	29427.2		1.368
					1585.6	
		M 50	2	31012.8		1.42
					−788.0	
		M 50	3	30224.8		1.398
					2732.5	
		CS 54	4	32957.3		1.54
$5d^4\ 6s^2$	$a\ ^1G$	M 57	4	29638.9		
$5d^5(^2D)6s$	$b\ ^3D$		1			
		CS 54	2	29728.1		1.292
			3			
$5d^5(^4F)6s$	$a\ ^5F$		5			
		CS 54	4	30982.5		1.188
					265.0	
		CS 54	3	30717.5		1.26
					−2158.3	
		CS 54	2	32875.8		1.06
			1			
$5d^5(^4G)6s$	$b\ ^3G$	CS 54	3	32257.8		1.114
					−51.3	
		CS 54	4	32206.5		1.08
		CS 54	5	32344.7	138.2	
$5d^5(a\ ^2G)6s$	$c\ ^3G$	CS 54	3	33089.8		1.15
					−820.5	
		CS 54	4	33169.3		1.188
					2894.2	
		CS 54	5	36063.5		1.21
$5d^5(^4D)6s$	$b\ ^3D$		1			
		CS 54	2	34937.2		1.23
					2056.2	
		CS 54	3	36993.4		
$5d^5(b\ ^2F)6s$	$c\ ^3F$		4			
		CS 54	3	37318.5		
					−63.5	
		CS 54	2	37382.0		1.071
$5d^4\ 6s(^6D)6p$	$z\ ^7P°$	M 50	2	45867.7		2.19
					1209.8	
		M 50	3	45147.5		1.79
					5533.4	
		CS 54	4	50680.9		

Config.	Desig.	Finder	J	Level value	Interval	Obs. g
$5d^4\ 6s(^6D)6p$	$z\ ^5P°$	M 50	1	49459.3		2.42
					3237.7	
		M 50	2	52677.0		1.82
					1125.1	
		M 50	3	53802.1		1.66
$5d^4\ 6s(^6D)6p$	$z\ ^5D°$	T 55	0	54468.0		
					1904.1	
		M 50	1	56372.1		1.291
					766.5	
		M 50	2	57138.6		1.30
					2191.3	
		M 50	3	59329.9		1.145
					3529.1	
		CS 54	4	62859.0		1.27
$5d^4\ 6s(^6D)6p$	$z\ ^7D°$	M 50	1	55150.8		2.27
					−91.6	
		M 50	2	55059.2		1.81
					1991.0	
		M 50	3	57050.2		1.135
					2231.6	
		CS 54	4	59281.8		1.625
					5090.5	
		CS 54	5	64282.3		1.31
$5d^4\ 6s(^6D)6p$	$z\ ^5F°$	M 50	2	55444.0	1985.4	1.083
		CS 54	3	57429.4		1.056
					2166.7	
		M 50	4	59596.1		1.177
					1330.7	
		CS 54	5	60926.8		1.18
		M 50	2	59588.2		1.520
		M 50	3	59665.8		1.19
		CS 54	1	60487.2		1.128
		M 57	3	60525.0		
		CS 54	2	62057.3		1.17
		CS 54	1	62717.8		1.52
		M 56	3	62914.9		1.243
		CS 54	3	63045.2		1.34
		CS 54	4	63127.7		1.27
		M 50	2	63464.2		1.56
		M 50	4	64407.2		1.21
		CS 54	2	64411.4		0.812
		M 50	3	64942.2		1.36
		T 55	3	64966.9		
		CS 54	1	65011.0		0.796
		CS 54	3	65572.5		1.28
		CS 54	2	65674.0		
		CS 54	3	66100.5		1.40
		CS 54	3	66248.1		
		CS 54	4	66581.2		1.38
		CS 54	4	66476.2		
		CS 54	5	66514.6		1.18
		CS 54	5	66556.7		
		CS 54	2	66730.5		1.274
		T 55	5	67049.1		1.29
		CS 54	1	67276.1		1.292
		CS 54	3	67314.0		1.194
		CS 54	4	67328.1		1.15
		CS 54	5	68259.5		1.16
		T 55	3	68554.3		
		M 57	2	68629.4		
		CS 54	3	68868.0		
		CS 54	4	68876.7		
		CS 54	3	69142.5		1.083
		CS 54	2	69170.0		1.30
		CS 54	4	69285.6		1.35
		CS 54	3	69302.8		1.677
		CS 54	3	69729.2		
		CS 54	4	69776.3		1.25
		CS 54	4	69796.2		
		CS 54	1	70137.8		1.637
		T 55	3	70811.0		1.17
		T 55	1	71088.7		
		CS 54	4	71128.5		1.19
		CS 54	2	71396.8		
		M 57	2	71732.1		
		CS 54	2	71949.0		1.40
		CS 54	2	72154.3		
		CS 54	2	72526.3		
		CS 54	3	72846.6		
		CS 54	3	73553.9		
		T 55	4	74064.4		
		CS 54	3	74070.8		
		CS 54	2	74325.5		
		CS 54	3	74469.2		
		T 55	3	74683.0		
		CS 54	3	75117.0		
		CS 54	2	75237.1		
		CS 54	4	76157.1		
		CS 54	3	76567.2		
		T 55	3	77190.7		
		M 57	3	77225.4		
		T 55	3	77975.9		

of table 1 where they are represented by the first four digits of the energy levels.

According to the above, the low even terms of Re II resemble those of the isoelectronic spectrum W I [10, p. 156] more closely than those of the homologous spectrum Mn II. For the same reason, it appears that the lower odd terms of *Re* II should be attributed to $d^4\ s\ p$, as in W I, rather than to $d^5\ p$, as in Mn II. This arrangement avoids double electron jumps to produce the strong Re II lines involving $d^4\ s^2\ a\ ^5\mathrm{D}$. It also explains why $d^5(^4P)p\ y\ ^5\overline{P}^o_3$ could not be found [10] despite diligent search; the two other levels, 55059.2 and 55150.8, assigned to this term have been reassigned to $d^4 s(^6\mathrm{D})p\ z\ ^7\mathrm{D}$, and the doubtful designations, $z\ ^5\mathrm{G}^\circ$ and $z\ ^3P^\circ$ have been abandoned. Beyond the first five odd terms shown in table 2, no attempt to group and designate the remaining levels has been made, because to do so would be highly arbitrary.

Since no spectral series could be found among the available lines of Re II, we tentatively adopt the ionization potential of 16.6 ± 0.5 electron v extrapolated by Finkelnburg and Humbach [11]. This corresponds to a series limit at about 133900 K.

5. References

[1] P. F. A. Klinkenberg, W. F. Meggers, R. Velasco, and M. A. Catalán, J. Research NBS **59,** 319 (1957) RP2804.
[2] W. F. Meggers, J. Research NBS **49,** 187 (1952) RP2355.
[3] G. R. Harrison, Repts. on Progr. in Phys. **8,** 212 (1941).
[4] W. F. Meggers, M. A. Catalán, and R. Velasco, J. Opt. Soc. Am. **42,** 288 (1952).
[5] E. Back and A. Landé, Zeeman effekt und Multiplettstruktur der Spektrallinien, p. 168 (Julius Springer, Berlin, Germany (1925).
[6] W. R. Bozman, J. Opt. Soc. Am. **44,** 824 (1954).
[7] K. G. Kessler, S. B. Prusch, and I. A. Stegun, J. Opt. Soc. Am. **46,** 1043 (1956).
[8] G. R. Harrison, Rev. Sci. Instr. **4,** 581 (1933).
[9] C. E. Moore, Atomic Energy Levels, NBS Circ. 467 **2,** 32 (1952).
[10] C. E. Moore, Atomic Energy Levels, NBS Circ. 467 **3,** 19 (1958).
[11] W. Finkelnburg and W. Humbach, Naturwiss. **42,** 35 (1955).

WASHINGTON, July 16, 1958.

Journal of Research of the National Bureau of Standards Vol. 61, No. 6, December 1958 Research Paper 2915

Density Formula for Alkali Silicate Glasses From Annealing to Glass-Processing Temperatures

Leroy W. Tilton

An additive formula is given for the computation of specific volumes of molten and compacted alkali silicate binary glasses with modifiers up to 50-mole percent and from annealing temperatures (400° or 500° C) to 1,400° C. The effective partial volumes, v_s, for the silica are postulated as

$$(1/v_s)=2.198+r_m C_s(1723-t),$$

where r_m is the mole fraction of nonsilica and C_s is a constant to be evaluated from glass-density data. This is based on the idea that silica networks can contract in volume as temperatures are lowered provided, and in proportion as, modifier ions are present in the glass. The effective partial volumes of R_2O, the nonsilica, are assumed as linear functions of temperature but not of the fraction of silica present.

Computed and observed densities agree within approximately 1 percent. The effective volumes of nonsilica are somewhat smaller than published estimates for the oxides themselves, as should be expected because of interpenetrations.

Previous formulas for the computation of densities of glasses have related principally to variations in composition. The formula proposed by Stevels [1] [1] is based on ideas of structure and has very few constants. It assumes for restricted ranges in composition that volume is independent of the nature of the cation. As modified by Stanworth [2] it shows that volume is dependent on the size of the cations, the glass volumes being larger as cation radii are larger.

The additive formula proposed by Huggins [3] has many constants, and it is notably successful. That work is of considerable interest to anyone interested in structure because Huggins finds that the addition of every cation oxide molecule linearly increases the volume of a glass per oxygen atom, regardless of previous additions. However, at least for R_2O silicate glasses, it can be shown that the linearity is not dependent on the referral to oxygen, and his corresponding partial volumes of nonsilica (not referred to oxygen) also are found to be linear if plotted against mole fraction of the added oxide.[2]

The Huggins formula is of further interest because the partial volumes used for silica are almost identical in the presence of various kinds of nonsilicas and are so treated except for the presence of a few elements, notably boron. Most interesting of all in connection with the present paper, his partial molar volumes (P. M. V.) attributable to silica [3] decrease as larger amounts of modifier are added. The Huggins stepwise procedure in dealing with the silica component is roughly equivalent to the procedure mentioned by LeChatelier [13], namely an arbitrary dual calculation of the volumes attributable to silica, partly from the density of silica glass and partly from that of the crystalline silica phases. Biltz and Weibke [14] proceeded in a slightly less arbitrary manner and calculated volumes of "average mols" of glass by the additive rule after taking into account the specific volumes of certain crystal phases that could be derived from the equilibrium diagrams and therefore might be presumed to exist in the liquid silicates.

The procedures mentioned are certainly not inconsistent with a conclusion from data on annealing [4] that the nonsilica particles, chiefly in proportion to their mere number, seem to govern the extent of partial collapse of the silica framework. A decrease in the bond angle Si–O–Si, where the tetrahedra are connected, was suggested.

The object of this paper is to see if the additivity of volumes in alkali silicate glasses at high temperatures is compatible with the idea of a silica that is continuously variable in density as a function of both temperature and modifier content. The following considerations also are relevant to the development of the proposed formula:

(1) A bond-angle theory of annealing [4];
(2) Known linear variations of densities of glasses at equilibrium in the annealing ranges [4];
(3) Shermer's [7] curves for densities of molten glasses as functions of composition, showing (qualitatively [4]) the marked increases in expansivities as cation is added to silica;
(4) White's [8] finding that densities of molten alkali silicates vary nearly linearly with temperature over a 400° C range;
(5) White's report that the silicon-oxygen structure in molten silicates is not only similar to that in vitreous silica but is independent of the kind of cations present; and
(6) White's report that the partial molar volumes of silica are identical for the alkali silicates and decrease as cation is added.

[1] Figures in brackets indicate the literature references at the end of this paper.
[2] Although the Huggins partial volumes for silica (whether or not referred to oxygen) are more nearly representable by a smooth curve when plotted against mole fraction of silica than against the Si to O ratio (used by Huggins), their better representation by segments of straight lines can still be shown. The Huggins special points of intersection correspond to compositions where there are integral numbers of cations per cage according to vitron theory [5, 6].
[3] Computable from Huggins' table 1 as P. M. V.$=2b_{Si}+c_{Si}$. See White [8], p. 24 to 28.
[4] The slopes of Shermer's density curves from room temperature to 400° C are about ½ as steep as is indicated by the coefficients in his table 1.

The basis for development is the well-known additivity of volumes, so that the specific volume of a glass may be written:

$$V_g=\frac{1}{d}=s_w v_S+r_w v_R, \tag{1}$$

where v_S and v_R are *effective* partial specific volumes attributable to the silica network and the nonsilica modifier, respectively, and s_w and r_w are the respective weight fractions.

For each modifier oxide, the effective density is assumed as a linear function of temperature

$$(1/v_R)=A_R+B_R(1{,}400-t),$$

where 1,400° C is used because it will be desired later to compare directly the empirically determined A constants with White's estimates at 1,400° C.

The problem, then, is to find a suitable expression for v_S, the effective volume of the silica. As a first approximation one might use v_S as a constant independent of temperature and modifier concentration. If this be done then it is found necessary to express each of three values of v_R not only as a function of temperature but of modifier content. It is simpler to assume that only silica volume, v_S, is a function of modifier content.

It is desired that $1/v_S$ have the value 2.198 g/cm^3 at 1,723° C, the melting point, and at all temperatures in the absence of modifier oxides; also that it decrease monotonically with temperature for a given degree of modification, and increase with modification at constant temperatures other than 1,723° C.

Hence it is postulated that in the presence of any alkali modifier

$$(1/v_S)=2.198+r_m C_S(1{,}723-t), \tag{2}$$

where r_m is the mole fraction of nonsilica and C_S is a constant to be evaluated from the glass-density data.

Other procedures can, of course, be followed in seeking to express as a continuous function the changes with temperature and modification that seem necessary for successfully computing glass densities. It seems preferable to follow precedent in attributing the changes mainly to the silica component [3, 13, 14], as mentioned above.

The assumption of eq (2) leads to much lower and more reasonable temperature coefficients, B, for v_R than would otherwise be found necessary in eq (3). Incidentally, the form of eq (2) accords with ideas previously expressed [4] concerning the nature of the structural rearrangements and volume changes in silicate glasses in their annealing ranges, namely that the silicon-oxygen bond is temperature sensitive (undergoes more electron cloud distortion, and becomes more angularly directed) in proportion as nonsilica particles (metal ions) are present. The operation of formula (1) together with the auxiliary eq (2) and (3), depends importantly on the use of the factor r_m as included in eq (2) for evaluating the effective partial specific volume, v_S of the silica.

In eq (2) the constant C_S is the slope or the temperature-contraction rate, $-\Delta d/\Delta t$, for a network of vitreous silica collapsed as fully as can be accomplished by the presence of alkali ions. In other words, the slopes of a family of curves of the effective partial densities of silica itself (but permeated with alkali modifiers) versus temperature are expressed by $-r_m C_S$ and the partial derivative of such slopes with respect to r_m is $-C_S$.

From experiments [4] on volume changes of complex glasses in their annealing ranges only, and thus for an average of numerous types of modifiers, a value of $C_S=+0.00057$ might be expected.[5] Actually, for use in eq (2) for computing densities of alkali silicates in the annealing range and up to 1,400° C, a still lower value of $+0.00040$ is now *empirically* recommended (after several trials with larger slopes [6]).

The constants A and B were successively determined from the glass densities after assuming various values of C_S. A value $C_S=0.00040$ was found to give the best fitting curves when residuals were averaged for all three modifiers at four temperatures, namely annealing, 900°, 1,150°, and 1,400° C.

The "observed" values for molten glasses are computed [7] from those that White [8] tabulated at 1,400° C with coefficients for other temperatures from near 1,000° to 1,500° C. White shows that his results at 1,400° C are in fair agreement with those by Heidtkamp and Endell [9] and those by Shartsis, Spinner, and Capps [10]. The "observed" values for compacted glasses at room temperature and at their critical temperatures are based on the densities published by Young, Glaze, Faick, and Finn [11] and on thermal coefficients tabulated by Shermer [7] and by Schmid, Finn, and Young [12].

The best effective densities, $1/v_R$, for use in eq (1) are

$$\begin{aligned} 1/v_{Li}&=1.700+0.000332\ (1{,}400-t),\\ 1/v_{Na}&=2.117+0.000416\ (1{,}400-t),\\ 1/v_K&=2.066+0.000428\ (1{,}400-t). \end{aligned} \tag{3}$$

This implies that the effective densities of the oxides in the silicates at 1,400° C are 1.70, 2.12, and 2.07 which are 10, 12, and 14 percent higher than the densities computable for the oxides themselves from volume estimates as given by White [8] for Li_2O, Na_2O, and K_2O, respectively. These percentages can be considered to some extent indicative of inter-

[5] From eq (1) of the reference cited $(\Delta n/\Delta t)=-0.00010 r_m$ and from the Newton-Laplace relation between refractive index and density, namely $(n^2-1)=dC$, one finds by differentiation that $(\Delta d/\Delta n)=1/0.176$. Hence $(\Delta d/\Delta t)=-0.00057\ r_m$ for a silica network stabilized by the presence of various metallic ions, and $C_S=-(\partial^2 d/\partial\Delta t\partial r_m)=+0.00057$. This value of C_S extrapolates to a molar volume of 18.7 cm^3 for stabilized silica network at absolute zero, as compared with 27.3 cm^3 for metastable silica glass. This would be silica with 39-percent voids, even if one may consider oxygen and silicon as solid spheres with radii, 1.31 and 0.29 Å, respectively. Such a condition is then not unreasonable because it is intermediate between the known conditions for densest packing of spheres (26-% voids) and for most open packing (48-% voids).

[6] It can be shown that the higher value of $C_S=0.00057$ can be used if a threshold value of $r_m=0.12$ is assumed for the beginning of configurational thermal expansion. See White [8] p. 106.

[7] The computations are in several cases extrapolations from White's data to temperatures below the liquidii, particularly for lithia and potash glasses at 900° C.

Table 1. *Comparison of computed and observed densities*

Mole per-cent R_2O	Annealing temperature			900° C			1,150° C			1,400° C		
	Computed	Observed	(c−o)×10³	Computed	Observed	(c−o)×10³	Computed	Observed	(c−o)×10³	Computed	Observed	(c−o)×10³
						$Li_2O{\cdot}S_iO_2$						
10	2. 232	2. 239	−7	2. 213	----	----	2. 183	----	----	2. 180	----	----
20	2. 263	2. 275	−12	2. 215	2. 206	+9	2. 181	2. 187	−6	2. 152	2. 169	−17
30	2. 283	2. 298	−15	2. 208	2. 216	−8	2. 164	2. 177	−13	2. 120	2. 138	−18
40	2. 299	2. 313	−14	2. 197	2. 194	+3	2. 138	2. 146	−8	2. 083	2. 098	−15
50	2. 298	----	----	2. 172	2. 167	+5	2. 104	2. 111	−7	2. 040	2. 055	−15
60	----	----	----	2. 137	2. 108	+29	2. 062	2. 044	+18	1. 988	1. 980	+8
						$Na_2O{\cdot}S_iO_2$						
10	2. 272	2. 276	−4	2. 242	----	----	2. 223	----	----	2. 202	2. 210	−8
20	2. 342	2. 354	−12	2. 278	2. 271	+7	2. 241	2. 247	−6	2. 202	2. 222	−20
30	2. 404	2. 420	−16	2. 306	2. 308	−2	2. 252	2. 259	−7	2. 200	2. 210	−10
40	2. 457	2. 468	−11	2. 331	2. 322	+9	2. 263	2. 261	+2	2. 194	2. 201	−7
50	2. 496	2. 514	−18	2. 344	2. 336	+8	2. 267	2. 264	+3	2. 187	2. 192	−5
60	2. 524	----	----	2. 352	2. 323	+29	2. 264	2. 243	+21	2. 176	2. 163	+13
						$K_2O{\cdot}S_iO_2$						
10	2. 283	2. 282	+1	2. 242	2. 216	+26	2. 217	2. 216	+1	2. 191	2. 216	−25
20	2. 352	2. 355	−3	2. 271	2. 262	+9	2. 225	2. 223	+2	2. 179	2. 184	−5
30	2. 413	2. 405	+8	2. 293	2. 284	+9	2. 229	2. 220	+9	2. 166	2. 156	+10
40	2. 457	----	----	2. 307	2. 290	+17	2. 230	2. 213	+17	2. 151	2. 136	+15
50	2. 491	----	----	2. 313	----	----	2. 226	----	----	2. 140	----	----

penetration of the silica network cavities with these modifiers. Correspondingly, in eq (3) the temperature coefficients of density are 6, 8, and 16 percent higher than those computable from differencing White's estimates of oxide volumes at room temperature and at 1,400° C.

The complete formula yields densities of which two-thirds agree with observed densities within one-half percent over the range 1,400° to 400° or 500° C for both molten glasses and those in the annealing ranges, as shown in table 1.

From the residuals, c-o, in table 1 it is evident that the proposed density formula fits the data fairly well over the long range in temperature. This is illustrated in figures 1, 2, and 3 where, for the three systems, rough comparisons are also made with data by observers other than White. The slopes in figures 1, 2, and 3 show how regularly the expansivities increase as modifiers are added. The approximate constancy of expansivity from annealing temperatures to those of molten glasses accords with the idea that glass structure does not change fundamentally within these temperature ranges.

When more numerous and more precise data become available it may be found, for glasses nearly saturated with modifiers, that observed densities in the annealing ranges differ systematically from those computed by this formula as adjusted to fit densities not only for annealing ranges but for molten glasses also. This expectation is based on the postulated characteristics of vitrons. Saturated cages of vitrons [5, 6] cannot be expected to respond as freely to bond-angle contraction during cooling as is assumed for unsaturated cages considered in this simple formula. The resulting stresses that develop on further cooling may eventually cause some breaking of bonds so that the delayed bond-angle contraction can then proceed. Some indication of such systematic tendencies is shown by the predominantly positive residuals in the 900° column of table 1, and the almost exclusively negative residuals in the annealing-temperature column.

As modifiers are added, there is in these residuals another and more definite systematic trend. The computed densities must be regarded as averages over the composition ranges because the formula has no terms relating to degree of saturation. The computed densities are too low at low modifier content and become too high at higher percentages of nonsilica particularly for molten glasses at highest temperatures listed. This is clearly indicated in figure 4.

It will be noticed that maximum excess of observed densities tends to shift toward higher percentage modifications in the order K_2O, Na_2O, Li_2O. Indeed the maxima for K_2O and Na_2O occur at lower percentages than 16.7 and 23.1, respectively, at which it has been suggested that complete inclosure of oxygen in the dodecahedral cages should cease and the breaking of oxygen bridges should begin. It happens also, that the excesses change to deficiencies not far from the percentages 28.6, 37.5, and 50 that have been identified with complete saturation of the cages.

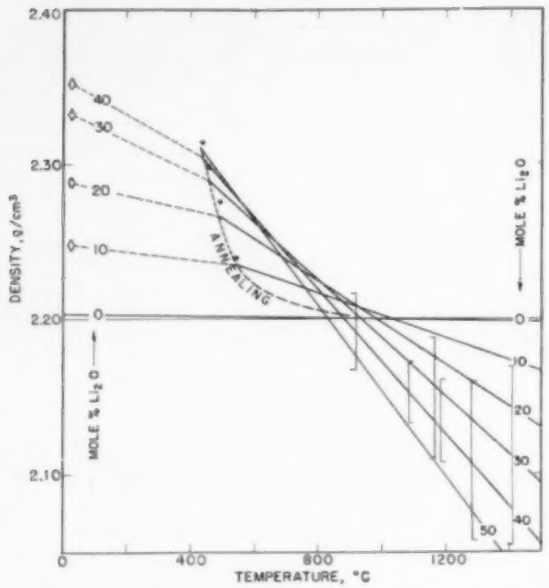

FIGURE 1. *Densities of lithia silicate glasses as functions of temperature.*

Full lines represent computations by the proposed formula. Diamonds represent observed values at room temperature by Young et al. [11]. Dotted lines lead to densities computed by formula at the annealing temperatures. Filled circles represent densities computed for annealing temperatures by use of room temperature densities and expansivities as measured by Schmid et al. [12] and by Shermer [7]. The total ranges in White's [8] observed values, for 20- to 50-mole percent of Li_2O, are indicated by brackets open to the left. The ranges in observed data by Shartsis et al. [10], 20-odd to 40-odd mole percent of Li_2O, are shown by right-face brackets. Shermer's similar diagram from observed data suggests a minimum spread in crossings of lines just below 800° C.

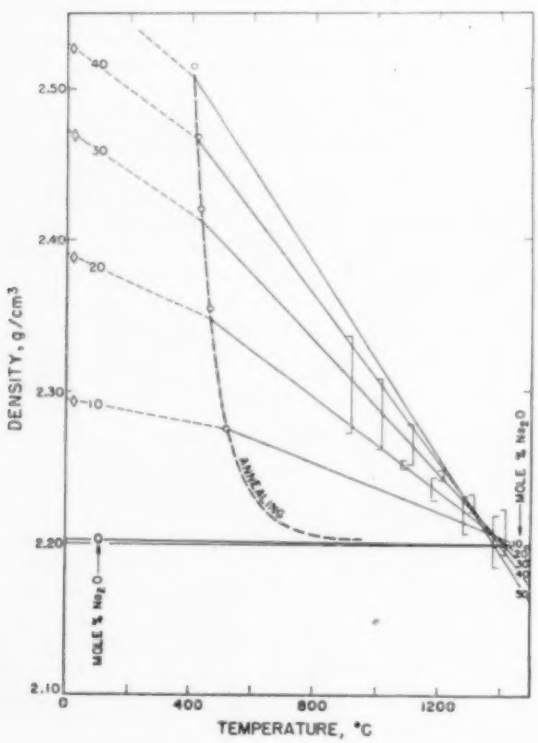

FIGURE 2. *Densities of soda silicate glasses as functions of temperature.*

The left-face brackets represent data by White [8] for 20- to 50-mole percent of Na_2O. The right-face brackets represent data by Heidtkamp and Endell [9] for 20- to 50-mole percent of Na_2O (except at 1,100° C where their modifier range is only 30 to 50 percent). Shermer's [7] diagram suggests minimum spread in crossings just below 1,350° C.

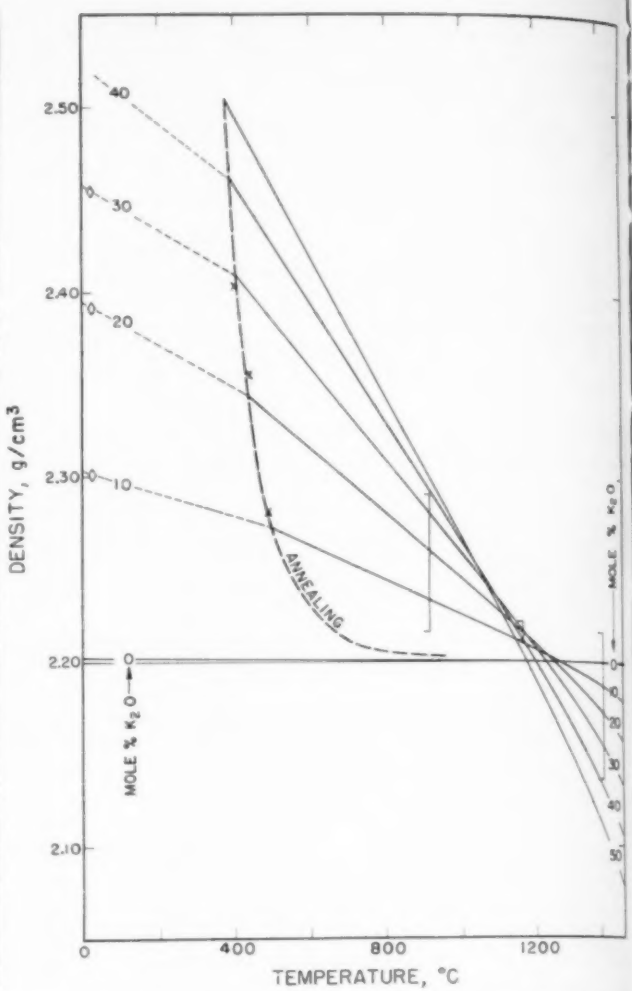

FIGURE 3. *Densities of potash silicate glasses as functions of temperature.*

The brackets indicate data by White [8] for 10- to 40-mole percent of K_2O. Shermer's diagram suggests minimum spread in crossings near 1,100° C.

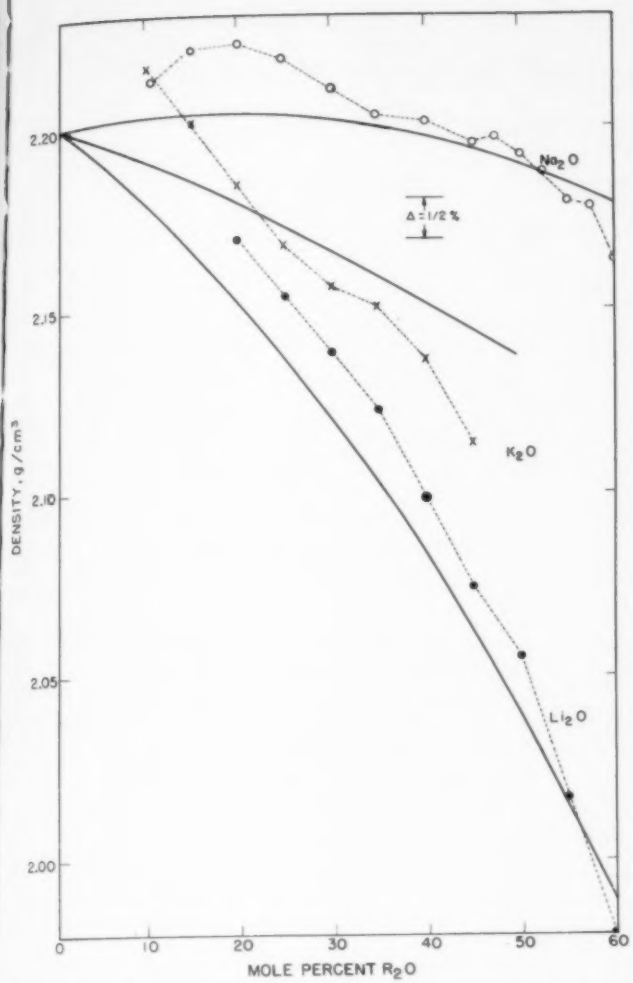

FIGURE 4. *Comparison of computed and observed densities of binary silicate glasses at 1,400° C.*

Full lines represent computed densities. Dotted lines connect densities observed by White [8]. Since the simple formula has no terms relating to saturation of the cavities, it is to be expected that (with an average adjustment) excess of observed values should be found principally at nonsilica contents below 28.6-, 37.5-, and 50-mole percent for K_2O, Na_2O, and Li_2O, respectively, because these are the percentages tentatively assigned for complete saturation according to vitron theory [5, 6].

WASHINGTON, April 10, 1958.

In addition to the results listed in table 1, data for two ternary glasses investigated by White were used. Each contained 60-mole percent of SiO_2 and 20 percent of Li_2O. For one with 20 percent of Na_2O the computed and observed densities at 1,400° C were 2.147 and 2.155; similarly for one with 20 percent of K_2O, 2.123, and 2.126, respectively.

In resumé the following points are emphasized:

(1) A simple additive formula [1], if written in accord with an effective partial value of silica as postulated by eq (2), represents the data on alkali silicates approximately as well as they are known. The systematic trends in the residuals seem qualitatively in accord with expectations from vitron theory.

(2) The use of a factor r_m in eq (2) is analogous to Huggins' [3] use for silica of a parameter variable with modifier concentration. The need for such a procedure was indirectly implied by White [8] and by Callow [15]. (See considerations as above listed.)

(3) The empirically determined constant, C_s, for silica in eq (2) is reasonable in that it is interpretable as a temperature collapse rate for silica network that extrapolates to reasonable volumes at 0° K.

(4) The empirically determined constants for nonsilica in eq (3) are reasonable in that they approximate the densities of the oxides and their temperature coefficients within 10 or 15 percent of estimated values.

It would appear from the analysis in this paper that to a first approximation the sensitive-bond-angle concept for silica with alkali modifiers is semiquantitatively compatible with our knowledge of the densities of alklali silicate glasses.

References

[1] J. M. Stevels, J. Soc. Glass Technol. **30,** 31 (1946).
[2] J. E. Stanworth, J. Soc. Glass Technol. **30,** 54 (1946).
[3] M. L. Huggins, J. Opt. Soc. Am. **30,** 420 (1940).
[4] L. W. Tilton, J. Soc. Glass Technol. **40,** 338T (1956).
[5] L. W. Tilton, J. Research NBS **59,** 139 (1957) RP2782.
[6] L. W. Tilton, J. Research NBS **60,** 351 (1958) RP2854.
[7] H. F. Shermer, J. Research NBS **57,** 97 (1956) RP2698.
[8] J. L. White (Ph. D. Thesis, Univ. of California 1955).
[9] G. Heidtkamp and K. Endell, Glastech. Ber. **14,** 89 (1936).
[10] L. Shartsis, S. Spinner, and W. Capps, J. Am. Ceram. Soc. **35,** 155 (1952).
[11] J. C. Young, F. W. Glaze, C. A. Faick, and A. N. Finn, J. Research NBS **22,** 453 (1939) RP1197.
[12] B. C. Schmid, A. N. Finn, J. C. Young, J. Research NBS **12,** 421 (1934) RP667.
[13] H. LeChatelier, Kieselsaüre und Silikate, p. 240 (Leipzig, 1920).
[14] W. Biltz and F. Weibke, Z. anorg. allgem. Chem. **203,** 345 (1932).
[15] R. W. Callow, J. Soc. Glass Technol. **36,** 137 (1952).

Journal of Research of the National Bureau of Standards Vol. 61, No. 6, December 1958 Research Paper 2916

Thermodynamic Properties of Gases at High Temperature:

1. Chemical Equilibrium Among Molecules, Atoms, and Atomic Ions Considered as Clusters

Harold W. Woolley

The equilibrium thermodynamic properties of gaseous mixtures at high temperatures are treated by an extension of the cluster theory of Ursell, omitting the assumption of additivity of pair energies. An effective partition function is introduced, which is a convenient function in expressing the increase of the partition function for the entire gas due to the joining together of the parts of the cluster. The law of mass action and the dependence of second and third virial coefficients upon the cluster integrals for pairs and triples of molecules in a mixture have been obtained therefrom. Extension to a partially ionized gas is made by incorporating Mayer's cluster-based extension of the Debye-Hückel theory.

1. Introduction

The calculation of the thermodynamic properties of gases at high temperatures involves a number of special problems which may well be disregarded at more moderate temperatures. The thermodynamic functions for a gaseous constituent in a mixture in chemical equilibrium are usually calculated from a partition function definable as a sum of Boltzmann factors for all states of the elementary unit of the constituent. The states of a single isolated molecule, atom, or atomic ion may be arranged in some kind of joint or compound progression of quantum numbers up through a range of moderate energies. For still greater energies, however, the number of states associated with the physical system comprising the constituent is enormously greater, with the states forming a continuum of values nominally of infinite extent, as the constituent dissociates, rather than occurring discretely. At some elevated temperature and beyond, the usual criterion for neglect of high-energy states based on the smallness of the Boltzmann factor is not fulfilled below the dissociation limit. The infinity of states immediately encountered at this energy does not permit the continuation of the same type of sum of states to indefinitely higher energies. A common procedure for avoiding the divergence which threatens to occur involves the termination of the sum of states at the dissociation energy or the inclusion of only that limited group of states above dissociation which still imply some of the typical structure of the undissociated constituent.

A different procedure for avoiding this divergence difficulty is to be discussed, involving the use of a method thought to have the merit of formal correctness, although it is admittedly not the only type of analysis with this appropriate feature. For this purpose, a special kind of partition function will be used, here to be termed an "effective partition function". These effective partition functions are related to the increase in the occupancy of states of a combined unit due to the joining together of parts of the unit, putting it together from any of all of the ways in which the unit may be considered as separated into component parts. The present procedure comprises an analysis using clusters of the Ursell type [1] [1] to specify the net thermodynamic effects of particle groupings in the combinations involved in forming molecules, atoms, and ions. As the populations of these clusters are measures of contribution to concentration due to interactions among several particles, it is admitted that they can give contributions of reversed sign if exclusion effects exceed the effects of combination.

The calculation procedure presented is a treatment of a multicomponent system including the principal quantum effects remaining at ordinary or elevated temperatures. As such it is in some degree a generalization of the treatments for pure substances given by Kahn and Uhlenbeck [2], Kahn [3], and Kilpatrick [4], and for the nonquantum multicomponent treatments of McMillan and Mayer [5], Fuchs [6], and Muto [7]. A restricting assumption of additivity of pair energies, made in some of these treatments, has not been retained in the

[1] Figures in brackets indicate the literature references at the end of this paper.

present one. The assumption is considered to be a rather good approximation for mixtures of ordinary molecules but not universally for the many types of interaction occurring among the chemically unsaturated fragments of molecules existing at very high temperatures.

Though the cluster integral procedure provides a way of avoiding divergence difficulties associated with ordinary dissociation, there is a type of dissociation for which the separating parts of the molecule or cluster are oppositely charged. The distribution of rotational states for which such fragments occur as unexcited parts is similar to that existing when a single electron is nearly separated from a positive ion. In the latter case, just below the energy at which the continuum due to ionization begins, there is an infinity of discrete states, and each level of the outer electron specified by the principal quantum number n is actually a group of states whose number has $2n^2$ as a factor. In the method of Urey [8] and Fermi [9], discussed also by Fowler [10], the summation was halted at such electron orbits that at the given density an orbit based on one atomic ion would just "touch" an orbit of a neighboring atomic ion. Their method, which appears capable of extensive development and application, forms part of the basis for a treatment of high temperature thermodynamic properties of a gas given by Megreblian [11]. The method of Planck [12] involved the evaluation of a Gibbs phase integral with simplifying assumptions. The present treatment is somewhat related to that of Planck but takes some account of a known property of an ionic assembly in involving an exponential Debye shielding function multiplying the long range Coulombic ionic interaction, such as occurs in the Debye-Hückel theory of electrolytes. In their theory of a plasma, Bohm and Pines [13] made a canonical transformation to new coordinates of two kinds, one associated with pure translational motions, and one associated with a short-range interaction showing at least some resemblance to the Debye screened Coulomb potential. Of more immediate application, Mayer [14] derived thermodynamic quantities for ionic solutions including all ring-type graphs of interionic interaction, using an exponential shielding function multiplying the Coulombic ionic interaction as a tool in the mathematical analysis. In effect, as shown by Meeron [15], Mayer converted the calculated effect of interionic interactions as indicated by virial coefficients from a nonconvergent form for the unscreened Coulomb potential to a convergent form with the Debye screened potential and obtained also the well-known limiting law Debye-Hückel term. The avoiding of divergence in the integrals related to virial coefficients by using Debye screening corresponds in some degree with the avoiding of divergence by Ecker and Weizel [16] who noted that n, the principal quantum number for atomic states, must have an upper bound if the electron moves in a Debye screened potential field. The correspondence is not that of identity, however, since the virial-coefficient-type quantities receive part of their contribution from regions of phase space above the dissociation, or ionization energy.

As to the arrangement of the present paper, section 2, which follows, presents a number of items of cluster theory leading to the method of calculation used to treat chemical equilibrium and the virial coefficients related to further clustering of the aggregations considered as the chemical constituents. Many of the relations are so similar to those in earlier derivations of cluster theory as clearly to form obvious extensions from them. A somewhat extensive discussion pertaining to an analysis in rather elementary algebraic form has been included, however, which may serve to show the very simple physical meaning of the extended Ursell-type formulas and thereby permit an easy inference of the essential correctness of the treatment. The effect of quantization on the cluster integrals or effective partition functions for molecules is also treated.

In section 3, formulas are given for the Helmholtz free energy for the gaseous equilibrium mixture including molecules, atoms, and atomic ions, based in part on the ionic-solution theory of Mayer and in part on the equilibrium theory of clusters of section 2. Formulas for the equilibrium constants for chemical reactions which can occur among constituents are also given. Expressions for other themodynamic functions for the mixture in terms of functions for its constituents are given in the appendix.

Further discussion of the status of cluster theory, particularly in regard to its present application, will be found in section 4.

2. Application of Cluster Theory

Apart from effects associated with ionization, an accurate theory for the thermodynamic properties of equilibrium mixtures of chemically reacting substances at high temperatures may be directly formulated involving equilibrium constants identical with the quantum equivalent of the cluster integrals of gas theory. In the nonquantum treatment, the Gibbs phase integral

$$Q=\frac{1}{\prod_{s_i} N_{s_i}!}\int\cdots\int \exp\frac{-\epsilon}{kT}\prod_{s=1}^{N} h^{-3}d^3p_s d^3r_s \tag{2.1}$$

is analyzed according to the method of Ursell [1]. The extension to the exact quantum mechanical treatment involves the replacement of the Boltzmann factor by a Slater sum so as to provide an exact equivalent to

$$Q=\sum_n \exp\frac{-\epsilon_n}{kT}. \tag{2.2}$$

The treatment should give results similar to those obtained by Kahn and Uhlenbeck [2], and Kahn [3], for a pure gaseous substance.

The theoretical analysis is made in terms of cluster integrals $b_{(l_i)}$ defined by

$$Vb_{(l_i)}\prod_i l_i!=\int\cdots\int U_l\prod_i^t\prod_s^{l_i} d^3r_s, \tag{2.3}$$

with U_l to be defined in terms of products of quantities W_j to be described. The number of particles of type i within a given cluster is l_i, with the different types of particles extending to $i=t$. This general cluster will be said to have composition (l_i). The cluster is to be thought of as subdivided arbitrarily into fragments, including every possible way of subdividing the cluster. The number of particles of type i within a particular type j of fragment of the cluster is to be indicated as $(l_i)_j$ and the number of fragments of type j by k_j. Conservation of matter then indicates that

$$\sum_j k_j(l_i)_j=l_i \tag{2.4}$$

for each type of particle in the cluster. The total number of fragments according to a particular way of subdividing the cluster is

$$k=\sum k_j. \tag{2.5}$$

The quantity U_l may now be defined as the sum

$$U_l=\sum(-1)^{k-1}(k-1)!\prod_j\frac{1}{k_j!}\left(\frac{W_j q_j}{\prod_i (l_i)_j!}\right)^{k_j}\prod_{i=0}^{t} l_i!, \tag{2.6}$$

with the factor q_j arbitrarily separated to indicate an explicit counting of spin multiplicities for the fragments, if desired. The summation in eq (2.6) includes products formed according to every possible way of subdividing the cluster into fragments or groups of particles. Each product term involves different W_j's which together involve once and only once each particle of the cluster. W_j represents the probability of occurrence of an isolated fragment j of the cluster in a given geometric configuration as a relative probability compared with the occurrence of the fragment when there is no internal energy of interaction. Thus, W_j will represent a Boltzmann factor in a nonquantum treatment or a suitable Slater sum in a quantum treatment, such as is indicated by

$$W_j=\prod_s (h^2/2\pi m_s kT)^{3/2}\sum\psi_n\psi_n^*\exp[-\epsilon_n/kT]. \tag{2.7}$$

The integral of the Slater sum for each fragment or group of particles provides the sum over its quantized states, as far as quantized states exist, with the appropriate integral in the continuum for the remaining contribution. A number, q_j, of states of like spin may have essentially identical energy and then can naturally be counted together. The separation of this factor from eq (2.7) as written in eq (2.6) is clearly arbitrary. When completely separated, the spin factor $\prod_j q_j^{k_j}$ is the same as $\prod_{i=0}^{t} (2s_i+1)^i$, based on the individual spins of the constituent particles. The denominators $\prod_i (l_i)_j!$ under the W_j's in eq (2.6) occur as shown if the eigenfunctions in eq (2.7) are regarded as not restricted by the exclusion principle but instead as having the full number of states corresponding to the Boltzmann statistics as a limiting condition. If the Slater sum were obtained exactly according to the exclusion principle, then a compensatory multiplication by this factor would be required, as indicated in the theory for a pure gaseous substance as given by Kahn and Uhlenbeck and by Kahn.

With the preceding formulation, the cluster integrals are the equilibrium constants for cluster formation according to the equation

$$\frac{N_{(l_i)}}{V} = b_{(l_i)} \prod_i \left(\frac{N_{(i)}}{V} \right)^{l_i}, \tag{2.8}$$

where V is the volume accessible to the gas, where $N_{(l_i)}$ is the number of clusters of composition (l_i), and where $N_{(i)}$ is the number of separately occurring individual particles of type i, i. e., as "clusters" of one particle. This result can be inferred in accord with the analogy between the present case and the treatment for clusters for a single pure substance [2, 3]. Alternately, the result can similarly be easily inferred from the nonquantum formulation of Fuchs [6], on the grounds that the present formulation is equivalent except for its inclusion of quantum effects. Further indication of the correctness of these equations will be presented later in this section.

It is to be noted that the equilibrium constants of eq (2.8) are the theoretically exact ones for a treatment of the real gas as a mixture of ideal gas components. Hill [17] has pointed out that any modification of definition that would give clusters other than these (he terms the present ones "mathematical clusters"), would eliminate the ideal gas law dependence of each component cluster gas; this would not allow the simple mass action law of eq (2.8). Excluded volume effects are automatically included in our theoretical formulation at this stage and would not be added separately unless a compensating readjustment were introduced to remove an equivalent quantity from the cluster representation. It may be recognized that a cluster of a given composition can be called a molecule or free radical or ion, or a group of such entities, according to the normal custom for nomenclature. If a molecule happens to have various isomeric forms, the requirements of the particular application could determine whether the different forms would be treated together or separately according to a reasonable apportionment of accessible phase space.

The Helmholtz free energy for a mole of like clusters of type (l_i) in the absence of ionization may be represented as $A = kT \ln Q$ with

$$\begin{aligned} Q &= [Q_i^e]^N [Q_{tr}]^N / N! \\ &= \left[b_{(l_j)} \left(\frac{h^2}{2\pi \Sigma m_s kT} \right)^{3/2} \prod_s \left(\frac{2\pi m_s kT}{h^2} \right)^{3/2} \right]^N \left[\left(\frac{2\pi \Sigma m_s kT}{h^2} \right)^{3/2} V \right]^N / N!. \end{aligned} \tag{2.9}$$

The first bracket indicates Q_i^e, the effective internal partition function, and the second indicates Q_{tr}, the translational partition function for a single cluster.

From eq (2.9) with eq (2.3) and (2.6), one may infer that the effective partition function for the cluster may be represented formally as

$$Q^e = \sum (-1)^{k-1} (k-1)! \prod \frac{1}{k_j!} Q_j^{k_j}, \tag{2.10}$$

with Q_j taken as

$$Q_j=\frac{1}{\prod_s (l_s)_j!}\int\cdots\int W_j\prod_s\left(\frac{2\pi m_s kT}{h^2}\right)^{3/2} d^3r_s, \tag{2.11}$$

in accord with eq (2.1) and (2.7), since each W_j in eq (2.6) is a function of coordinates internal to the fragment j.

Even though the equations given follow plausibly from earlier investigations, it may be advantageous to examine some of the relations in greater detail. By such a procedure we may hope (1) to confirm definitely that the Ursell type formula is actually being extended correctly to mixtures with "non-additive" potentials, (2) to show that the structure of the correct Ursell-type formulas is simply that which provides the incremental contribution (per cluster) to the state sum, due to the particles being in the cluster rather than present in other, less combined forms, and further, (3) to obtain the result that the formation of a combined cluster from two component clusters is strictly analogous to the combination of two particles into a cluster of two, so that repeated application of a process analogous to calculating the second virial coefficient gives an analysis concerning clusters of any degree of complexity.

Thus it is informative to compare the effective partition functions for two cases differing in that in one case one additional particle is present within the cluster while in the other case it is counted as present in the assembly without interaction with other constituents of the cluster. The difference in magnitude between the state sum for the entire gas when the particle is combined and its value when the particle is uncombined includes the effect of inserting the particle into every subcluster or fragment of the cluster involved according to eq (2.6) or (2.10) for the effective partition function for the initial cluster. The numbers of subclusters after insertion of a single particle into one of them include k_{jr} of the type of the receptor subcluster (initially there were $k_{jr}+1$ of this type), k_{jp} of the type of the product subcluster (initially there were $k_{jp}-1$ of this type). The number of single particle subclusters for particles of type q after addition of the added particle of this type is to be indicated as k_{jq}. The increment in the total effective partition function for the system including the initial cluster and the added particle due to addition of the particle to the cluster will be indicated by

$$Q^e(l_1,l_2,\ldots l_q,\ldots)=\theta Q^e(l_1,l_2,\ldots l_q-1,\ldots), \tag{2.12}$$

where θ is an operator operating on $Q^e(l_1, l_2 \ldots l_q-1, \ldots)$, the effective partition function for the initial cluster. The total contribution to the effective partition function of the combined cluster formed by adding the new particle includes a contribution from each factor of each term of the partition function for the initial cluster. From this it can be seen that the numerical factors arising in use of the operator θ are identical with those occurring in a differentiation process. θ can be represented as $Q_1^*-Q_1$, in which Q_1^* is an operator which produces the ordinary partition function of a combined system when it operates on the ordinary partition function of the partial system, as $Q_1^*Q_b=\overline{Q_1Q_b}$, while Q_1 is an ordinary partition function of the added particle.

Making use of eq (2.10) for the effective partition function of the initial cluster, the effective partition function of the combined cluster obtained with this operator θ is indicated in accord with eq (2.6) and (2.11) using the corresponding $U_l/\prod_i l_i!$ in terms of the W's, now to be written omitting the spin factor $\prod_i(2s_i+1)$:

$$U_l/\prod l_i!=\sum(-1)^{k-1}(k-1)!\prod_j\frac{(W(l_1,l_2\ldots))^{k_j}}{(k_j)!(\prod_i(l_i)_j!)^{k_j}}\left[\sum_j\frac{(k_{jr}+1)}{(k_{jr}+1)}(l_q)_j k_{jp}+\sum_j{}'\frac{k_j k_{jq}}{k-1}+\frac{(k_{jq}-1)k_{jq}}{k-1}\right]\frac{1.}{(l_q)} \tag{2.13}$$

On the right-hand side of the equation, the expression before the bracket is the regular expression for the combined cluster. The expression within the bracket includes contributions of various kinds arising from the addition of the particle to various possible fragments of the

initial cluster. For the first term in the bracket, coming from the insertion of the added particle to a subcluster, the factor $k_{jr}+1$ in the numerator is due to there having been this number of subclusters to which the particle might be added to produce one particular type of product cluster. This modifies a particular product of the type preceding the bracket since there had been a factor $k_{jr}+1$ in the old factorial in the denominator and this factor now appears in the denominator of the term in the bracket. Similarly the new factor outside has a new factor k_{jp} in a factorial in its denominator (included in one of the $(k_j)!$ factors) which is balanced to the original by the k_{jp} in the numerator of the term in the bracket. Also, a new factor $(l_q)_j$ is in the denominator in front of the bracket (included as a net increase of one factor in the general $(l_i)_j!$) because of the k_j indicating k_{jp} instead of a former $k_{jp}-1$, and this is balanced in the term in the bracket by the $(l_q)_j$ in its numerator.

The other two terms in the bracket arise from the addition of the new particle as a separate subcluster arising in the $-Q_1$ term of the θ. For the initial cluster, the value of k was less by one than its value in such corresponding terms of the combined cluster, as are obtained using the Q_1 factor thus giving the opposite sign by $(-1)^k$, which, when combined with the minus sign on the $-Q_1$, gives positive contributions within the bracket for both terms. The occurrence of $k-1$ in their denominators is a compensation concerning the $(k-1)!$ factor and is also due to k for the terms for the initial cluster being one less than for the combined cluster. The first of these last two terms in the bracket has an origin somewhat analogous to that of its predecessor but with Q_1 involved rather than the combining Q_1^*. The prime on the summation sign is to indicate that the summation is to include only those j's for which the k's do not represent k_{jq}, so as to obtain the count of the number of terms which had been involved for the Q_1^*, except for those due to adding a single particle to a like particle. The effect of adding the separate single particle subcluster is to increase the exponent in front of the bracket for single particles q to k_{jq} from $k_{jq}-1$, its value in the initial cluster. To compensate for the matching extra factor in the factorial expression in the denominator preceding the bracket, the value k_{jq} occurs in the numerator of the present term in the bracket. The last term in the bracket is likewise analogous to the first term, with Q_1 involved rather than the combining Q_1^*. This term counts the number of separate occurrences in which the added particle enters into the formation of clusters of two like particles. This term appearing as a balancing quantity to which the effect of Q_1^* is compared, has the factor $k_{jq}-1$ for the number of initial subclusters in connection with which this final comparison process arises. In addition, the numerator contains the factor k_{jq}, as in the term preceding, to balance the augmented factorial in the denominator of the expression preceding the bracket.

The quantities in the bracket may now be combined. For the first term, k_{jp} occurs only for the subclusters produced by adding the new particle to a previously existing subcluster. Thus, it does not include j's for single particle subclusters, so that

$$\sum(l_q)_j k_{jp}=\sum(l_q)_j k_j-k_{jq}=l_q-k_{jq}. \tag{2.14}$$

For the second term, $\sum_j{}' k_j k_{jq}$, the summation is over j's for which the k_j's do not represent k_{jq}. As the full sum $\sum_j k_j$ would have been equal to k, $\sum_j{}' k_j$ is $k-k_{jq}$. The three terms are now readily combined as

$$l_q-k_{jq}+\frac{(k-k_{jq})k_{jq}}{k-1}+\frac{(k_{jq}-1)k_{jq}}{k-1}, \tag{2.15}$$

which reduces to l_q. This is cancelled by the l_q in the denominator after the bracket, representing an additional factor in the general factorial of the denominator needed to convert from phase integral to partition function as indicated in eq (2.1). From this demonstration eq (2.6), or its equivalent, eq (2.10), may be seen to be an appropriate extension of the ordinary Ursell-type formula to mixtures. Thus, an effective partition function agreeing with the Ursell-type formula may be generated relevant to the combined cluster, starting with an Ursell-type formula for the cluster of one less particle by simply evaluating the increase in the net state

sum due to counting an additional particle of the entire system as belonging to the cluster. On the one hand, one may see this as a logically correct process to build up the effective partition function, so that on the basis of the obvious correctness of the Ursell-type formula for small clusters of one or two particles, mathematical induction permits one to regard the present Ursell-type formula as clearly holding for clusters of arbitrary size and composition, but with due regard for details of particle statistics as required. Alternatively, for one who finds the present Ursell-type formula to be an obviously correct extension of the Ursell formulas previously known, the foregoing demonstration can show that the addition of a particle to a previous cluster can be treated formally in the simple form of a second virial coefficient as indicated, using the operator $\theta=Q_1^*-Q_1$ with eq (2.12). It may also be noted that the joining of one cluster with another to form a combined cluster may be treated similarly using an operator θ built from effective partition functions

$$\theta=Q_a^{e*}-Q_a^e, \tag{2.16}$$

since

$$Q_{ab}^e=\theta Q_b^e=\overline{Q_a^e Q_b^e}-Q_a^e Q_b^e \tag{2.17}$$

has a form identical with the pattern for obtaining the second virial coefficient for the effects of interaction between the two clusters. Thus, the calculation of the effective partition function for a diatomic molecule is directly related to and essentially identical with the calculation of the second virial coefficient for the interaction of its constituent atoms, no matter whether one regards the atoms as interacting particles or clusters of nuclei and electrons. Similarly, the treatment for a triatomic molecule is directly related to that for a cluster of three particles such as is involved in the cluster theory for the third virial coefficient. In all cases, states of higher electronic excitation should be allowed for if significantly present and should be understood as included in the present notation.

We now come to the particular advantage obtained by use of the effective partition functions as defined in the foregoing discussion. The partition function for the complete gas assembly can be written out readily when they are used in the analysis. Using total effective partition functions $\boldsymbol{Q}_j^e=Q_j^e(Q_{j\ \mathrm{trans}})$ for a cluster for which the number of particles of kind i is $(l_i)_j$, the partition function for an assembly involving N_i particles of each kind i is

$$Q_N=\sum_{(N)}\Big[\prod_j(\boldsymbol{Q}_j^e)^{m_j}/m_j!\Big], \tag{2.18}$$

with the sum including every kind of term consistent with the condition

$$\sum m_j(l_i)_j=N_i. \tag{2.19}$$

The most probable state may readily be found in the sense of determining the greatest term in the sum. This may be done on the basis that, in the immediate vicinity of the maximum, neighboring terms are almost exactly equal. If for a neighboring term, the number of clusters of type j is taken as m_j+n_j (where each n_j is a small integer) rather than the m_j of eq (2.18), then eq (2.19) takes the form $\sum(m_j+n_j)(l_i)_j=N_i$, and the difference between the two is the general conservation equation

$$\sum n_j(l_i)_j=0. \tag{2.20}$$

The requirement that neighboring terms near the maximum be approximately equal gives

$$\prod_j(\boldsymbol{Q}_j^e)^{m_j+n_j}/(m_j+n_j)!\approx\prod_j(\boldsymbol{Q}_j^e)^{m_j}/m_j!, \tag{2.21}$$

which reduces to

$$\prod_j(\boldsymbol{Q}_j^e)^{n_j}=\prod_j(m_j+n_j)!/m_j!, \tag{2.22}$$

or

$$\prod_j(\boldsymbol{Q}_j^e)^{n_j}\approx\prod_j m_j^{n_j}, \tag{2.23}$$

since $m_j \gg 1$ and n_j is a small integer. By substituting $Q_i^e Q_{j\ \mathrm{trans}}$ for Q_j^e and dividing by $\prod_{i=1} V^{n_j}$, the relation

$$\prod_j \left(\frac{m_j}{V}\right)^{n_j} = \prod_j (Q_j^e)^{n_j} \left(\frac{Q_{j\ \mathrm{trans}}}{V}\right)^{n_j} \tag{2.24}$$

is obtained. Since $Q_{j\mathrm{trans}}$ contains V as a factor as shown in eq (2.9), or according to

$$Q_{j\,\mathrm{trans}} = V\Lambda_{(l_i)j}^{-3}, \tag{2.25}$$

with

$$\Lambda_{(l_i)j} = h/(2\pi[\sum_i (l_i)_j m_i]kT)^{1/2}, \tag{2.26}$$

the right-hand side of eq (2.24) is independent of V, and by further reduction using items relevant to eq (2.9), is equal to $\prod_i (b_{(l_i)})_j^{n_j}$ and forms an equilibrium constant to which the product of concentrations on the left-hand side of the equation is equated. The reaction equation to which this law of mass action is relevant is

$$\sum n_j' Y_j \rightarrow \sum n_j'' Y_j$$

or

$$\sum n_j Y_j = 0, \tag{2.27}$$

where n_j represents both n_j'' and $-n_j'$, with Y_j representing the chemical symbol for the type of cluster (or molecule) referred to. For the reaction of formation of a single cluster (or molecule) from elementary particles or clusters, the mass action equation can be reduced to eq (2.8), with $N_{(l_i)}$ corresponding to the m_j of the equations just concluded.

If the representation of gas properties is carried out directly in terms of particular kinds of clusters, then these clusters may be considered afresh as the constituents of a gas mixture whose interactions lead to the virial coefficients for this mixture gas. These virial coefficients for the gas are of course related to the cluster integrals—or the effective partition functions—for the clusters formed among its constituents. An adequate theory representing their effects formally can be given using the grand partition function. Exactly the same results may be obtained in the present case, however, by noting that the gas acts as a mixture of ideal gases subject to chemical equilibrium, as shown by eq (2.24). Then, the pressure of the gas is the sum of the partial pressures of all kinds of clusters of the constituents. Similarly, the net concentration of any kind of constituent particle is proportional to an analogous sum in which each term of the pressure sum is multiplied by the number of that kind of constituent particle in the corresponding cluster. While the various terms of these two expressions are expressible using cluster-integral-type or effective-partition-function-type equilibrium constants, multiplied by products of powers of density-type fugacities of the various constituents, the ideal-gas-type relations which apply to each constituent permit the density-type relations which apply to each constituent permit the density-type fugacity to be equated to the quotient of the partial pressure of the constituent, divided by kT, so that

$$\frac{p}{kT} = \sum_j [b_{(l_i)}]_j \prod_j \left(\frac{p_i}{kT}\right)^{(l_i)_j} \tag{2.28}$$

and

$$\frac{N_i}{V} = \sum_j (l_i)_j [b_{(l_i)}]_j \prod_i \left(\frac{p_i}{kT}\right)^{(l_i)_j}, \tag{2.29}$$

giving

$$\frac{pV}{NkT} = \frac{\sum_j [b_{(l_i)}]_j \prod_i \left(\frac{p_i}{kT}\right)^{(l_i)_j}}{\sum_j [\sum_i (l_i)_j][b_{(l_i)}]_j \prod_i \left(\frac{p_i}{kT}\right)^{(l_i)_j}}. \tag{2.30}$$

The mole fraction of constituent i is $x_i = N_i/N$. The process of eliminating the fugacities (p_i/kT) from the expression for pV/NkT is more involved than that for a pure substance [18]. Using b_{ij} and b_{ijk} as the cluster integrals $b_{(i_l)}$ for two particles i and j and for three particles i, j, and k, respectively, the first two virial coefficients are obtained as

$$B = \sum\sum x_i x_j B_{ij} \tag{2.31}$$

and

$$C = \sum\sum\sum x_i x_j x_k C_{ijk}, \tag{2.32}$$

with

$$B_{ij} = -N b_{ij}, \tag{2.33}$$

and with

$$C_{ijk} = \frac{N^2}{3}\left[4b_{ij}b_{jk} + 4b_{ik}b_{kj} + 4b_{ki}b_{ij} - 6b_{ijk}\right]. \tag{2.34}$$

Higher virials may similarly be obtained, but much less readily due to the proliferation of algebriac expressions in the transformations. Even for the third virial, the problem of nonadditivity of pair potentials arises. For pure substances, Rosen [19] found nonadditive effects in the three helium atom interaction, Axilrod [20] has found such effects for the dispersion energies, and Jansen [21] has examined the entire problem at some length. Kihara [22] also has recognized the problem and has made use of Axilrod's results in estimating the effect on third virials for the pure noble gases. For gas mixtures, the problem is of added complexity as it involves the estimate of interaction between two unlike constituents as well as the nonadditivity among all the differing kinds of constituents considered three at a time, alike and unlike. In applications at elevated temperatures where the constituents may be other than ordinary stable substances, nonadditivity can be expected to have large effects. Where the prediction of properties of a gas mixture using rigorous theory is particularly impracticable, the use of empirical mixture rules becomes a natural expedient.

If one attempts to obtain the effective molecular partition functions from second virial or cluster integral calculations, a classical type calculation may be simplest and thus might most naturally be used, with potential functions based on empirical spectroscopic constants and other known facts. Corrections for quantization effects in such cases would also be needed. A study of the effects of the change of spacing of levels when the quantum of action, h, is considered as approaching zero, as discussed in Appendix 1 (section 5.1) shows that the quantum effective partition function (referred to the lowest quantized level) may be obtained approximately at high temperature by multiplying the classical effective partition function (referred to the classical zero energy) by the correction factor,

$$\left\{1 + \frac{1}{12}\frac{hc}{kT}\left[\sum_i d_i(d_i+1)x_{ii} + \sum_i\sum_{i<j} d_i d_j x_i\,(3 - \omega_i\omega_j^{-1} - \omega_j\omega_i^{-1}) + f\right] - \frac{1}{24}\left(\frac{hc}{kT}\right)^2 \sum_i d_i\omega_1^2 \right.$$
$$\left. + \frac{1}{5760}\left(\frac{hc}{kT}\right)^4\left[\sum_i (5d_i+2)d_i\omega_1^4 + 10\sum_i\sum_{i<j} d_i d_j \omega_i^2\omega_j^2\right]\right\} \exp\frac{hc}{kT}\sum\frac{\omega_i d_i}{2}, \tag{2.35}$$

where for nonlinear polyatomic molecules

$$f = 2\sum_i g_{ii} + \tfrac{1}{2}\sum_i d_i\omega_i(A_e^{-1}\alpha_1^A + B_e^{-1}\alpha_1^B + C_e^{-1}\alpha_1^C) + (2A_e + 2B_e + 2C_e - A_eB_eC_e^{-1} - B_eC_eA_e^{-1}),$$

while for linear molecules

$$f = 2\sum_i g_{ii} + \sum_i d_i\omega_i B_e^{-1}\alpha_i + 4B_e.$$

The constants in these expressions follow the usual spectroscopic notation with vibrational energy given by

$$\sum_i \omega_i\left(v_i + \frac{d_i}{2}\right) + \sum_i x_{ii}\left(v_i + \frac{d_i}{2}\right)^2 + \sum_i\sum_{i<j} x_{ij}\left(v_i + \frac{d_i}{2}\right)\left(v_j + \frac{d_i}{2}\right) + \sum_i g_{ii}l_i^2,$$

with rotational constants

$$A_v = A_e - \sum_i \alpha_i^A \left(v_i + \frac{d_i}{2} \right),$$

$$B_v = B_e - \sum_i \alpha_i^B \left(v_i + \frac{d_i}{2} \right),$$

$$C_v = C_e - \sum_i \alpha_i^C \left(v_i + \frac{d_i}{2} \right),$$

for the nonlinear molecule, and

$$B_v = B_e - \sum_i \alpha_i \left(v_i + \frac{d_i}{2} \right)$$

for the linear molecule. The diatomic molecule may be regarded as a special case of the linear molecule. The terms purely in ω_i in the bracket in eq (2.35) amount to a simple extension of a result which Herzfeld and Teller [23] obtained by the method of Wigner and Kirkwood, and which others have used in other forms [24, 25]. Except for form, the terms linear in hc/kT agree exactly with the result of Mayer and Mayer [26] for diatomic molecules. It will be noticed that if the two kinds of partition functions, quantum and classical, are to be referred to the same zero of energy, say the classical zero or the zero of the potential energy function, then the additional required factor $\exp [(-hc/kT)G_0]$, where G_0 is the zero point energy, removes the factor of $\exp [(hc/kT)\Sigma(\omega^1 d_1/2)]$ of eq (2.35) and replaces it with an exponential factor based on the much smaller anharmonicity constants. Thus, for such a quantization correction, the zero point energy might be considered as not being involved. The detailed procedure of taking a calculation with the zero of energy with the cluster particles dispersed and adjusting to a zero of energy at the lowest quantized level for the cluster to conform with custom in the tabulation of molecular thermal functions involves, in addition to eq (2.35), the use of the factor $\exp [(-hc/kT)D_e] = \exp [(hc/kT)(D_0 + G_0)]$. This gives as the combined correction the expression in the bracket in eq (2.35), multiplied by $\exp [(-hc/kT)D_0]$ $\exp [(hc/kT)(\Sigma\{\omega_i d_i/2\} - G_0)]$. In the adoption of eq (2.35) as the approximate quantization correction, not only has the existence of other than Boltzmann statistics been ignored as of no importance in calculations at high temperature and up to moderate densities, but also the quantization correction contributions associated with fragments of the cluster have also been disregarded, since at moderate temperatures the net quantization effects due to the fragments would be very small because of reduction due to powerful Boltzmann factors.

The molar thermal functions for molecular-like clusters according to this formulation are to be consistent with

$$A = -kT \ln Q \tag{2.36}$$

as in eq (2.9), but with each effective internal partition function Q_i^e including its appropriate quantization effect given by eq (2.35) and also multiplied by $\exp (-hc/kT)D_e$ so as to be based on the usual molecular zero of energy.

In eq (2.17) it is indicated that the effects of interactions between two different clusters or between a cluster and a particle may be indicated formally as a cluster integral for the joining of the two parts into a combined cluster. In making use of this principle as a guide in obtaining approximate thermodynamic functions for a gas mixture, it seems appropriate to emphasize its indication of the permissible arbitrariness of assignment of regions of phase space either completely to the formation of the combined cluster (in the style of the so-called mathematical cluster), or partly to the combined cluster (now possibly called a physical cluster), and partly to a second virial type interaction between the two parts of the cluster.

One application of this principle is in regard to the effective internal partition function for the interaction of two atoms forming a diatomic molecule. One alternative is to use the entire effect in this partition function and the corresponding thermodynamic functions. On

the other hand, any part of this partition function may be used in obtaining the thermodynamic functions for the constituent, provided that the remainder of the effective partition function is retained as contributing in its appropriate way to the second virial type interaction between the corresponding atomic constituents.

Somewhat similarly, the combination of an added outer electron with a positive atomic ion to form an atom or a positive atomic ion with one unit less of charge may also be treated in good approximation using an arbitrary subdivision of phase space. In a gas in which considerable excitation of levels near ionization occurs, there is also considerable formation of free ions, for which the effective interaction potential in the assembly as a whole may be taken as the Debye screened Coulomb form. Meeron [15] has shown that the nonquantum-mechanical treatment of Mayer [14] for ionic solutions can be given this simple interpretation, using quantities corresponding to second virial coefficients, even though expansion of higher order terms would not be the equivalent of a higher virial evaluation using the Debye screened Coulomb potential. Application to a high-temperature gas involves details of quantized states of the combined atom with ionic screening to which the approximate treatment by Ecker and Weizel [16] is relevant. Further discussion of this subject may be presented in a later paper. It would appear that a conventional sum of states for the atom up to some moderate principal quantum number of the outer electron should be acceptable provided that the remainder of the effective partition function be used in obtaining corrections for equation of state quantities. A very different division of phase space has been used in the treatment which will be presented in the following section and in the next paper of the present series.

As the virial coefficients based on additive pair interactions as used by Mayer [14] in deriving quantities for his theory of ionic solutions are consistent with the cluster integrals for the Coulombic interaction, since this is additive, it is possible to treat the effect of ionization using Mayer's classical ion-solution theory, which he arranged primarily for an assembly of ions with each pair separated by a distance greater than its particular sphere radius. The interior of each ion sphere is a region actually accessible to the electrons of the system, as they can enter and become energetically attached so as to form ions of various numbers of electrons. As each such group is a cluster of particles, one would wish to evaluate contributions to the Ursell integrals for electrons within the sphere but with such quantization corrections as would be needed to approximate the effects due to the discrete states of the ions. Unfortunately for purposes of evaluation, the integrand of the general integral for the many-particle case is of such complexity and the integrals are so highly multiple that precise direct evaluation according to this procedure appears impossible. It is therefore appropriate to make use of convenient approximations. The effective partition function may be estimated approximately using the observed and estimated low lying quantized states with classically estimated contributions from higher energy regions of phase space within the assigned radii. These may depend on the representation of effective potential-energy functions, with simplifying approximations made possible by partial compensation for cognate fragment terms in the cluster integrals.

Because the thermodynamic functions obtained are specifically arranged for use with an ionic-gas treatment based on Mayer's development of ion-solution theory with specific values for the ion radii, it seems appropriate now to summarize the results of his approximate treatment when applied to such an ionic-gas mixture in chemical equilibrium.

3. Ionized Gas as an Ionic Solution

The nonquantum-mechanical theory of ionic solutions given by Mayer [14] retains terms applying to ions free to move to any accessible pair separation greater than their collision radius. By also including the contribution of Mayer's eq (46) due to the departure of the non-Coulombic pair potential from rigid-sphere form, an approximate expression consistent with the terms retained in his original derivation may be obtained. On this basis, the

Helmholtz free energy for the gaseous assembly of molecules, atoms, atomic ions, and electrons with the accompanying thermal radiation may be taken approximately as

$$-A/RT=(V/V_0)\left\{\sum_s C_s[(-A^0/RT)_s-\ln C_s-\ln T/T_0]+\frac{2}{3}\pi^{1/2}(\sum Z_s^2C_s)^{3/2}\epsilon^3(DkT)^{-3/2}(N_0/V_0)^{1/2}\right.$$

$$+\frac{1}{2(\sum Z_s^2C_s)}\sum_{s=1}\sum_{r=1}\sum_{\nu=\nu_{sr}^0}(-1)^\nu C_sC_rZ_s^\nu Z_r^\nu\alpha_{sr}^{1-\nu}[b_\nu(\varphi_{sr})+g_\nu(\varphi_{sr})]+\sum_s\sum_r C_sC_r\frac{N_0}{V_0}\int_0^\infty h_{sr}2\pi R_{sr}^2dR_{sr}$$

$$\left.+\left[\frac{1}{12\pi}\frac{h^2\epsilon^2}{mk^2T^2}\frac{N_0}{V_0}-\frac{1}{32}\left(\frac{h^2}{\pi mkT}\right)^{3/2}\frac{N_0}{V_0}\right]C_e^2+\frac{8\pi^5}{45}\frac{k^3T^3}{h^3c^3}\frac{V_0}{N_0}\right\}+\Delta(-A/RT), \quad (3.1)$$

where C_e is the C_s representing electron concentration and where terms are given for the first-order quantum corrections for an electron gas including Fermi-Dirac statistics [27, 28] for electrons.

The symbols used in the present ion-solution equations have the following meanings:

C_s=concentration relative to that of a pure ideal gas at standard conditions, i. e., $C_s=N_sV_0/N_0V$,

Z_s=ionic charge of each ion of type s, in protonic units,

ϵ=electronic charge,

D=effective dielectric constant, $\sim$ unity for low density,

k=Boltzmann constant,

$\alpha_{sr}=a_{sr}DkT/\epsilon^2$,

a_{sr}=collision radius for ion s and ion r.

$b_\nu(\varphi)$, $g_\nu(\varphi)$, and $h_\nu(\varphi)$ are functions defined and tabulated by Poirier [29]. The argument of these functions is defined by

$$\varphi_{sr}=\frac{2\pi^{1/2}\alpha_{sr}(\sum Z_s^2C_s)^{1/2}\epsilon^3}{(DkT)^{3/2}}\left(\frac{N_0}{V_0}\right)^{1/2}=\kappa a_{sr},$$

where $\kappa^2=4\pi\epsilon^2\sum Z_s^2C_s/DkT$, as known from the Debye-Hückel theory.

The omission of b_1, g_1, and h_1 (h_ν appears in appendix 2) on the basis of net electrical neutrality for the complete assembly is acceptable in case there is but one value of a_{sr}, the case for which Poirier's tables were prepared. If there are several values of a_{sr}, then cancellation does not occur in general for ion separations between the least and greatest a_{sr}. Evaluation of the net contribution may then be based on the explicit expressions

$$b_1(\varphi)=\tfrac{1}{2}e^{-\varphi}[1+\varphi-\tfrac{1}{2}\varphi^2]-\tfrac{1}{2},$$

$$q_1(\varphi)=\tfrac{1}{2}e^{-\varphi}[1+\varphi+\tfrac{1}{2}\varphi^2]-\tfrac{1}{2},$$

and

$$h_1(\varphi)=\tfrac{1}{2}-\tfrac{1}{2}e^{-\varphi}[1+\varphi+\tfrac{1}{2}\varphi^2-\tfrac{1}{2}\varphi^3].$$

$\Delta(-A/RT)$ has been included to account for any further corrections omitted from the equation of state. As pointed out in the preceding section, nonionic equation-of-state effects at low and moderate density may be treated by cluster theory and could be accounted for by including all clusters as separate new constituents in the first term in the brackets in eq (3.1). Alternatively, the effects may be indicated in accord with the usual procedure employed to obtain thermodynamic corrections for nonideality. Thus, one might use

$$\Delta\left(-\frac{A}{RT}\right)=-\frac{V}{V_0}\left[\frac{(B-B_0)}{V_0}(\sum C_s)^2+\frac{(C-C_0)}{2V_0^2}(\sum C_s)^3+\frac{(D-D_0)}{3V_0^3}(\sum C_s)^4\cdots\right], \quad (3.2)$$

where $B-B_0$, $C-C_0$, and $D-D_0$ represent additional parts of the virial coefficients required over and above the zeroth order values implied by the remainder of the ion-solution-cluster treatment being used. Corrections to a nonvirial type representation could similarly be provided.

The quantity h_{sr} in eq (3.1) has the value

$$\exp\left\{\left[-U_{sr}+\frac{Z_sZ_r\epsilon^2}{DR_{sr}}\left(1-e^{-\kappa R_{sr}}\right)\right]\Big/kT\right\},$$

for $0<R_{sr}<a_{sr}$ and the value

$$\exp\left\{\left[-U_{sr}+\frac{Z_sZ_r\epsilon^2}{DR_{sr}}\left(1-e^{-\kappa R_{sr}}\right)\right]\Big/kT\right\}-\exp\left[-\frac{Z_sZ_r\epsilon^2}{DR_{sr}kT}e^{-\kappa R_{sr}}\right]$$

for $a_{sr}<R_{sr}<\infty$. In the present method of describing effects between ion cores and an outer electron, h_{sr} will be taken as zero in the range $0<R_{sr}<a_{sr}$, since this is a region which contributes to the internal sum of states determining the function $(-A^\circ/RT)_s$ for the corresponding constituent of ion core with outer electron, and the effect is taken into account by that means. If a_{sr} is well chosen for the approach of two atomic ions, h_{sr} can be small in almost all of both regions, as pointed out by Mayer for his closely related k_{sr}. Thus for $R<a_{sr}$, h_{sr} is small because the pair potential U_{sr} is very large; while for $R>a_{sr}$, it is small because U_{sr} is almost identical with $Z_sZ_r\epsilon^2/DR_{sr}$.

If the contribution within the braces of eq (3.1) due to h_{sr} for the interaction of ions of like charge is to be based on the use of a Debye screened Coulomb repulsion for $R_{sr}<a_{sr}$ as well as for $R_{sr}>a_{sr}$, it may be given as

$$\frac{2\pi}{3}a_{sr}^3\frac{N_0}{V_0}\sum_s\sum_r C_sC_r\sum_{n=0}q_n(x_{sr})\varphi_{sr}^n,$$

with

$$x_{sr}=Z_sZ_r\epsilon^2/Da_{sr}kT=Z_sZ_r/\alpha_{sr}.$$

Formulas for $q_n(x)$ are given in Appendix 3 (section 5.3).

Equation (3.1) has been written in rather general form which allows it to be used in more than one way. An approximate treatment for an assembly including atomic ions under conditions of high-ion density may be obtained by choosing a single a_{sr} to apply throughout or a very small number of different a_{sr}'s, with suitably limited sums to represent the internal partition functions. For conditions of relatively low density, however, it may be desirable to use internal partition functions for the atomic ions based on an extensive set of levels extending to moderately large electron separations. The so-called "collision radius" between an electron and an atomic ion could in principle be taken correspondingly large in this case, but with the added detail that the ν_{sr}^0 or initial index in the summation in eq (3.1) and in similar expressions in Appendix 2 (section 5.3) would be greater than zero, signifying free entry into the ion sphere for this one case rather than having a zero value signifying the exclusion from the ion sphere such as is used in regard to the close approach of two atomic ions.

Calculations concerning the concentration of the various constituents of the gas mixture under conditions of equilibrium can be made based on this ion-solution treatment according to well known principles. Thus, we may consider a stoichiometric chemical reaction among substances Y_s with stoichiometric coefficients $n_{ks'}$ and $n_{ks''}$ in the reaction equation (c.f., eq (2.27))

$$\sum n_{ks'}Y_{s'}\rightarrow\sum n_{ks''}Y_{s''},$$

which may be written as

$$\sum n_{ks}Y_s=0, \tag{3.3}$$

with n_{ks} representing both $n_{ks''}$ and $-n_{ks'}$. The equation for chemical equilibrium for this kth reaction equation is

$$\sum n_{ks}\mu_s=0 \tag{3.4}$$

in terms of the chemical potentials μ_s, with

$$\mu_s=(\partial A/\partial N_s)_{T,V}. \tag{3.5}$$

This gives

$$K_k=\prod_s C_s^{n_{ks}}=\left(\frac{T_0}{T}\right)^{\sum n_{ks}}\exp\left[\sum n_{ks}\left(-\frac{F^\circ-H_0^\circ}{RT}\right)_s-\frac{\Delta H_0^\circ}{RT}\right]\prod_i\gamma_i=K_k^{(0)}\prod_s\gamma_i \tag{3.6}$$

where ΔH_0° is $\sum n_{ks}\, H_0^\circ$ for the reaction with

$$\gamma_1=\exp\left[\frac{\pi^{1/2}(\sum Z_s^2C_s)^{1/2}(\sum n_{ks}Z_s^2)\,\epsilon^3N_0^{1/2}}{V_0^{1/2}(DkT)^{3/2}}\right] \tag{3.7}$$

according to the Debye-Hückel theory, and with

$$\gamma_2=\exp\left\{\frac{1}{(\sum Z_s^2C_s)}\sum_s\sum_r\sum_\nu{}_0(-1)^\nu C_rZ_r^\nu Z_s^\nu\alpha_{sr}^{1-\nu}n_{ks}[b_\nu(\varphi_{sr})+g_\nu(\varphi_{sr})]\right.$$
$$\left.-\frac{(\sum Z_s^2n_{ks})}{(\sum Z_s^2C_s)^2}\sum_s\sum_r\sum_\nu{}_{0\atop sr}(-1)^\nu C_sC_rZ_s^\nu Z_r^\nu\alpha_{sr}^{1-\nu}g_\nu(\varphi_{sr})\right\} \tag{3.8}$$

as the principal correction based on the tabulated functions representing Mayer's extension of the theory. A correction for the effect of the h_{sr} terms may be expressed by

$$\gamma_3=\exp\left\{2\sum_s\sum_r n_{ks}C_r\frac{N_0}{V_0}\int_0^\infty h_{sr}2\pi R_{sr}^2dR_{sr}+\frac{\left(\sum_s Z_s^2n_{ks}\right)}{2\left(\sum_s Z_s^2C_s\right)}\sum_s\sum_r C_sC_r\frac{N_0}{V_0}\int_0^\infty\kappa\frac{\partial h_{sr}}{\partial\kappa}\cdot 2\pi R_{sr}^2dR_{sr}\right\}, \tag{3.9}$$

which for Debye screened Coulomb repulsion between ions takes the form

$$\gamma_3=\exp\left\{\frac{2\pi}{3}a_{sr}^3\frac{N_0}{V_0}\left[2\sum_s\sum_r C_r\sum_{n=0}q_n(x_{sr})\varphi_{sr}^n n_{ks}\right.\right.$$
$$\left.\left.+2\left[\frac{1}{12\pi}\frac{h^2\epsilon^2}{mk^2T^2}\frac{N_0}{V_0}-\frac{1}{32}\left(\frac{h^2}{\pi mkT}\right)^{3/2}\frac{N_0}{V_0}\right]C_0\tilde{n}_{k0}+\left[\frac{\sum_s\sum_r C_sC_r}{2(\sum Z_s^2C_s)}\sum_n nq_n(x_{sr})\varphi_{sr}^n\right]Z_s^2n_{ks}\right]\right\}. \tag{3.9a}$$

An estimate for effect of dependence of dielectric constant D on composition may be made using

$$\gamma_4=\exp\left\{\left[-\frac{\pi^{1/2}(\sum Z_s^2C_s)^{3/2}\epsilon^3}{(DkT)^{3/2}}\left(\frac{N_0}{V_0}\right)^{1/2}-\frac{1}{2(\sum Z_s^2C_s)}\sum_{\nu\geq 0}(-1)^\nu C_sC_rZ_s^\nu Z_r^\nu\alpha_{sr}^{1-\nu}\right.\right.$$
$$\left.\left.[\nu b_\nu(\varphi_{sr})+(\nu-2)g_\nu(\varphi_{sr})]\right]\left[\sum n_{ks}\frac{d\ln D}{dC_s}\right]\right\}, \tag{3.10}$$

although a more detailed microscopic analysis of the kinds of screening affecting both γ_3 and γ_4 should be made. In fact, the rapid increase of atomic polarizability with principal quantum number poses another convergence problem unless each atomic state be taken as defining an independent constituent. Additional effects related to the equation of state may be estimated from

$$\gamma_5=\exp\{-\sum n_{ks}(\partial/\partial C_s)[(B-B_0)(\sum C_s)^2/V_0$$
$$+(C-C_0)(\sum C_s)^3/2V_0^2+(D-D_0)(\sum C_s)^4/3V_0^3+\ \ldots]\} \tag{3.11}$$

It is also necessary to take into account the dependence of energies of states and the heats of formation and reaction on the ion density. Some indication of the dependence for atomic ions may be obtained from a study of atomic levels for a Debye screened atomic ion. Discussion of these effects will be deferred until a later publication.

The equations for "mass" and charge balance are well known and obvious but may be represented here for completeness. Thus if the number of atoms of element $X^{(i)}$ in a molecule of constituent Y_s is l_{is}, then

$$\sum_s C_sl_{is}=C^{(i)} \tag{3.12}$$

is the local average concentration of this element, usable either directly or in ratio to other similar quantities in the expression of conservation of each chemical element. Similarly, if the electric charge on each molecule of constituent Y_s is Z_s in protonic units, then

$$\sum_s C_s Z_s = 0 \tag{3.13}$$

states that, on the average the gas is electrically neutral.

The concentrations of constituents as given by these equations may be termed nominal concentrations of clusters considered as molecules. To obtain the actual molecular concentrations $C_s^{(m)}$ from the corresponding nominal cluster concentrations C_s, one may make use of the ratio

$$C_s^{(m)}/C_s = Q_s^{(m)}/Q_s^{\text{eff}} = \sum_i g_i \exp\ (-\epsilon_i/kT)/Q_s^{\text{eff}}, \tag{3.14}$$

with the partition function

$$Q_s^{(m)} = \sum_i g_i \exp\ (-\epsilon_i/kT), \tag{3.15}$$

formed by a sum over whatever group of states is deemed to comprise the specification of the molecular form (or similarly for atoms and atomic ions). The concentration of molecules in their ground states is given by

$$C_s g_0 \exp\ (-\epsilon_0/kT)/Q_s^{eff}, \tag{3.16}$$

where g_0 is the *a priori* weight of the ground-state level and ϵ_0 is its energy relative to the energy zero used in obtaining Q_s^{eff}.

It is to be emphasized that nominal concentrations of clusters are in general not identical with concentrations of molecules or ions bearing the equivalent name. If accurate estimates for concentrations of these species are required, then (3.14) and (3.15) must be used.

4. Discussion

The calculation of thermodynamic properties of gas mixtures in chemical equilibrium at high temperature and moderate density, with each molecule, atom, or ion considered as a cluster of its constituent particles, has been discussed. The method of calculation may be used for very high temperatures at which the number density of ions is high, using ion-solution theory in Mayer's formulation.

The detailed discussion of the method of calculation of thermodynamic functions for the atoms and atomic ions that form the principal constituents of the gas mixture at high temperature is reserved for paper II of this series. Under conditions of considerably elevated density, the proportion of small molecules may be enough to make accurately descriptive functions desirable, even at rather high temperatures. Methods of calculating such functions for diatomic molecules may be discussed further in paper III of this series, including both conventional partition functions and the effective partition functions provided by cluster integrals. Molecular cluster integrals automatically include distortion and stretching effects due to centrifugal forces and so are especially suited to calculation at high temperature. The effect of quantization on the molecular cluster integrals has been included in considerable detail, yielding estimated "effective partition functions." Ratios between these functions give proper equilibrium constants for the treatment of a gas mixture as a mixture of ideal gases in the absence of ionization for the purpose of representing the over-all thermodynamic properties of the mixture.

Special emphasis can be given to the concept of the "effective partition function" considered as a convenient function for expressing the increase of the partition function of the entire gas due to the joining together of the parts of the cluster. It is thought that this concept is useful in clarifying the physical meaning of the kind of cluster which has sometimes been called a "mathematical cluster."

The analysis of the gas-mixture properties by means of equilibrium constants for cluster formation, or the cluster integrals for clusters of all compositions for small numbers of particles is formally no less complete than the representation of the gas properties according to a virial series expansion carried through virials of an equivalent order, or involving interactions of an identical number of particles as in the highest virial coefficient included. Indeed, in the low density region the cluster integral representation as a treatment of chemical equilibria is considerably the more complete when applied to effects of chemical bond formation under conditions that favor the formation of small clusters (molecules) only. This detail of good representation may be touched on again in connection with paper III of this series, dealing with diatomic molecules. If triatomic molecules were the largest molecules formed, then a cluster treatment including all clusters of three atoms would include all chemical bonding effects varying directly exactly as the third power of the free atom concentration and would include higher order virial type effects due to chemical bonds in pairs and triples of atoms. In the high-density region, however, the higher virial coefficients have large excluded volume effects which are not included in a treatment covering only pairs and triples of atom particles as clusters. For these, the cluster treatment would need to be carried through for clusters of the same number of particles as the numerical order of the virial coefficient in order to give a complete representation for the given coefficient. Application in the high-density region is complicated further by the detail that for an ordinary chemically inert gas, the virial expansion itself, to which the cluster treatment is formally equivalent, is found to be progressively poorer as a representation when extended to higher and higher density. This might suggest that the virial expansion itself may be correct only asymptotically in the limit of low density. Nevertheless, the virial expansion is to be regarded as a useful approximation capable in principle of giving good estimates up into regions of considerable density. As the equivalent cluster treatment gives a still less suitable extension to high density, the problem of practical estimation of properties of chemically reacting gas mixtures at high density and temperature calls for further estimates of volume effects beyond accessible cluster evaluation, so as to be either in accord with empirical and relevant theoretical knowledge of higher virial coefficients or in accord with gas theory of still broader application.

5. Appendices

5.1. Appendix 1

For high temperature calculations of thermodynamic functions for molecules according to the present cluster approach, one might first obtain the ordinary nonquantum cluster integrals based on potential functions agreeing with empirical spectroscopic constants and other known facts, following which, one would wish to combine quantum corrections based on known molecular spectroscopic constants. By taking the ratio between the ordinary partition function for the molecule and a limiting partition function consistent with it, obtained by reducing the spacing between levels uniformly to zero with a proportionate reduction in weight per level, one may readily obtain a principal correcting factor for the effect of quantization. Since the fragment submolecules implied in the cluster integral occur at much higher energy than the combined molecule, only a small error is introduced by ignoring the quantization corrections for these fragments.

In a well-known system of notation, the logarithm of the ordinary partition function, with energy referred to the ground-state level of a molecule, may be written as

$$\ln Q=\ln Q_R+\frac{\theta_1}{T}-\sum_i d_i \ln(1-e^{-u_i})-\left(\frac{hc}{kT}\right)\left\{\sum_i x_{ii}d_i(d_i+1)e^{-2u_i}(1-e^{-u_i})^{-2}\right.$$
$$\left.+\sum_{i<j}\sum x_{ij}d_id_je^{-u_i}e^{-u_j}(1-e^{-u_i})^{-1}(1-e^{-u_j})^{-1}+2\sum g_{ii}e^{-u_i}(1-e^{-u_i})^{-2}\right\}+\sum_i a_i d_i e^{-u_i}(1-e^{-u_i})^{-1}. \tag{A1.1}$$

Here Q_R is the rotational partition function for the ground vibrational state in classical approximation, θ_1 represents the Stripp-Kirkwood [30] correction for nonlinear molecules or

the Mulholland correction for linear molecules due to the finite spacing of the rotational levels. The variable u_i may be expressed in terms of the usual vibrational constants of

$$G=\sum_i \omega_i(v_i+d_i/2)+\sum_i x_{ii}(v_i+d_i/2)^2+\sum_{i<j}\sum x_{ij}(v_i+d_i/2)(v_j+d_j/2)+\sum g_{ii}l_i^2 \qquad \text{(A1.2)}$$

according to

$$u_i=\frac{hc}{kT}\left[\omega_i+(d_i+1)x_{ii}+\tfrac{1}{2}\sum_{j\neq i} d_j x_{ij}\right]. \qquad \text{(A1.3)}$$

In view of the principal vibrational dependence of the rotational partition function, representable by a factor exp $\sum a_i v_i$, $\ln Q_R$ may be replaced by $\ln Q_{Re}+\frac{1}{2}\sum_i d_i a_i$, where Q_{Re} refers to the equilibrium configuration. The derivation of the main part of the vibrational effect proceeds as already stated with a factor λ for the level spacing appearing wherever a quantum number factor $(v_i+d_i/2)$ appears in the fundamental expressions:

$$\ln Q(\lambda)=\sum_i d_i\ln\lambda-\sum d_i\ln[1-e^{-u_i(\lambda)}]-\left(\frac{hc}{kT}\right)\lambda^2\Bigg\{\sum_i x_{ii}d_i(d_i+1)e^{-2u_i(\lambda)}(1-e^{-u_i(\lambda)})^{-2}$$
$$+\sum_{i<j}\sum x_{ij}d_i d_j e^{-u_i(\lambda)}e^{-u_j(\lambda)}(1-e^{-u_i(\lambda)})^{-1}(1-e^{-u_j(\lambda)})^{-1}+2\sum_i g_{ii}e^{-u_i(\lambda)}(1-e^{-u_i(\lambda)})^{-2}\Bigg\}$$
$$+\lambda\sum_i g_i d_i[e^{-u_i(\lambda)}(1-e^{-u_i(\lambda)})^{-1}+\tfrac{1}{2}] \qquad \text{(A1.4)}$$

with

$$u_i(\lambda)=\frac{hc}{kT}[\lambda\omega_i+\lambda^2(d_i+1)x_{ii}+\tfrac{1}{2}\lambda^2\sum_{j\neq i} d_j x_{ij}]. \qquad \text{(A1.5)}$$

The quantity $\ln Q(\lambda=1)-\ln Q(\lambda=0)$ gives the vibrational quantization correction, to be put in suitable form by expansion of the various functions, either directly or giving the form

$$Q(\lambda=1)/Q(\lambda=0)=\Bigg\{1+\frac{1}{12}\frac{hc}{kT}[\sum d_i(d_i+1)x_{ii}+\sum_{i<j}\sum d_i d_j x_{ij}(3-\omega_i\omega_j^{-1}-\omega_j\omega_i^{-1})$$
$$+\sum_i d_i a_i+2\sum_i g_{ii}]-\frac{1}{24}\left(\frac{hc}{kT}\right)^2\sum_i d_i\omega_i^2+\frac{1}{5760}\left(\frac{hc}{kT}\right)^4[\sum_i(5d_i+2)d_i\omega_i^4$$
$$+10\sum_{i<j}\sum d_i d_j\omega_i^2\omega_j^2]\Bigg\}\exp\frac{hc}{kT}\sum_i\frac{\omega_i d_i}{2}. \qquad \text{(A1.6)}$$

The rotational quantization correction is already known, being given by the factor $1+\theta_1/T$ as indicated earlier above.

It may be noted that the expression is in such form as to change from a classical treatment with energy measured from the classical $v_i=0$ or potential minimum value to a quantum treatment with energy measured from the quantum $v_i=0$ or ground-state energy.

5.2. Appendix 2.

Additional thermodynamic functions and relations for the equilibrium gas mixture as derived from eq (3.1) are:

$$\frac{PV}{RT}=\frac{V}{V_0}\Bigg\{\sum C_s-\frac{1}{3}\frac{\pi^{1/2}(\sum Z_s^2C_s)^{3/2}\epsilon^3}{(DkT)^{3/2}}\left(\frac{N_0}{V_0}\right)^{1/2}-\frac{1}{2(\sum Z_s^2C_s)}\sum_s\sum_r\sum_{\nu=\nu_{sr}^0}(-1)^\nu C_sC_rZ_s^\nu Z_r^\nu\alpha_{sr}^{1-\nu}[b_\nu(\varphi_{sr})-g_\nu(\varphi_{sr})]$$
$$-\sum_s\sum_r C_sC_r\frac{N_0}{V_0}\int_0^\infty\left(h_{sr}+\frac{\kappa}{2}\frac{\partial h_{sr}}{\partial\kappa}\right)\cdot 2\pi R_{sr}^2dR_{sr}-\left[\frac{1}{12\pi}\frac{h^2\epsilon^2}{mk^2T^2}\frac{N_0}{V_0}-\frac{1}{32}\left(\frac{h^2}{\pi mkT}\right)^{3/2}\frac{N_0}{V_0}\right]C_0^2$$
$$+\frac{8}{45}\pi^5\frac{k^3T^3}{h^3c^3}\frac{V_0}{N_0}\Bigg\}+\Delta\frac{PV}{RT}, \qquad \text{(A2.1)}$$

with

$$\frac{\Delta PV}{RT}=\frac{V}{V_0}\left[\frac{(B-B_0)}{V_0}(\sum C_s)^2+\frac{(C-C_0)}{V_0^2}(\sum C_s)^3+\frac{(D-D_0)}{V_0^3}(\sum C_s)^4+\dots\right].$$

The dependence of the dielectric constant D on the gas density using the Clausius-Mosotti relation provides as a further contribution[2] to PV/RT, the quantity

$$-\frac{(D+2)(D-1)}{D}\left(\frac{\delta E}{RT}\right)_{\text{ionic}},$$

where $(\delta E/RT)_{\text{ionic}}$ includes the ordinary ionic terms in eq (A2.2), i. e., the limiting law Debye-Hückel term and the Mayer-Poirier terms for which the dependence on D is of the same form as for T.

$$\frac{E}{RT}=\frac{V}{V_0}\Bigg\{\sum C_s\left(\frac{E^0}{RT}\right)_s-\frac{\pi^{1/2}(\sum Z_s^2C_s)^{3/2}\epsilon^3}{(DkT)^{3/2}}\left(\frac{N_0}{V_0}\right)^{1/2}$$
$$-\frac{1}{2(\sum Z_s^2C_s)}\sum_s\sum_r\sum_{\nu=\nu_{sr}^0}(-1)^\nu C_sC_rZ_s^\nu Z_r^\nu\alpha_{sr}^{1-\nu}[\nu b_\nu(\varphi_{sr})+(\nu-2)g_\nu(\varphi_{sr})]$$
$$+\sum_s\sum_r C_sC_r\frac{N_0}{V_0}\int_0^\infty\frac{Tdh_{sr}}{dT}\cdot 2\pi R_{sr}^2dR_{sr}-\left[\frac{1}{6\pi}\frac{h^2\epsilon^2}{mk^2T^2}\frac{N_0}{V_0}-\frac{3}{64}\left(\frac{h^2}{\pi mkT}\right)^{3/2}\frac{N_0}{V_0}\right]C_0^2$$
$$+\frac{8}{15}\pi^5\frac{k^3T^3}{h^3c^3}\frac{V_0}{N_0}\Bigg\}+\frac{\Delta E}{RT}, \qquad \text{(A2.2)}$$

with

$$\frac{\Delta E}{RT}=-\frac{V}{V_0}\left[\frac{T(dB/dT-dB_0/dT)}{V_0}(\sum C_s)^2+\frac{T(dC/dT-dC_0/dT)}{2V_0^2}(\sum C_s)^3\right.$$
$$\left.+\frac{T(dD/dT-dD_0/dT)}{3V_0^3}(\sum C_s)^4+\dots\right]$$

$$\frac{H}{RT}=\frac{V}{V_0}\Bigg\{\sum C_s\left(\frac{H^0}{RT}\right)_s-\frac{4}{3}\frac{\pi^{1/2}(\sum Z_s^2C_s)^{3/2}\epsilon^3}{(DkT)^{3/2}}\left(\frac{N_0}{V_0}\right)^{1/2}$$
$$-\frac{1}{2(\sum Z_s^2C_s)}\sum_s\sum_r\sum_{\nu=\nu_{sr}^0}(-1)^\nu C_sC_rZ_s^\nu Z_r^\nu\alpha_{sr}^{1-\nu}[(1+\nu)b_\nu(\varphi_{sr})-(3-\nu)g_\nu(\varphi_{sr})]$$
$$+\sum_s\sum_r C_sC_r\frac{N_0}{V_0}\int_0^\infty\left(T\frac{dh_{sr}}{dT}-\frac{\kappa}{2}\frac{\partial h_{sr}}{\partial\kappa}-h_{sr}\right)\cdot 2\pi R_{sr}^2dR_{sr}-\left[\frac{1}{4\pi}\frac{h^2\epsilon^2}{mk^2T^2}\frac{N_0}{V_0}-\frac{5}{64}\left(\frac{h^2}{\pi mkT}\right)^{3/2}\frac{N_0}{V_0}\right]C_0^2$$
$$+\frac{32}{45}\pi^5\frac{k^3T^3}{h^3c^3}\frac{V_0}{N_0}\Bigg\}+\frac{\Delta H}{RT}, \qquad \text{(A2.3)}$$

with

$$\frac{\Delta H}{RT}=\frac{V}{V_0}\Bigg\{\frac{B-B_0-T(dB/dT-dB_0/dT)}{V_0}(\sum C_s)^2$$
$$+\frac{2(C-C_0)-T(dC/dT-dC_0/dT)}{2V_0^2}(\sum C_s)^3+\frac{3(D-D_0)-T(dD/dT-dD_0/dT)}{3V_0^3}(\sum C_s)^4\dots\Bigg\}$$

$$\frac{S}{R}=\frac{V}{V_0}\Bigg\{\sum C_s\left[\left(\frac{S_0}{R}\right)_s-\ln C_s-\ln\frac{T}{T_0}\right]-\frac{1}{3}\frac{\pi^{1/2}(\sum Z_s^2C_s)^{3/2}\epsilon^3}{(DkT)^{3/2}}\left(\frac{N_0}{V_0}\right)^{1/2}$$
$$+\frac{1}{2(\sum Z_s^2C_s)}\sum_s\sum_r\sum_{\nu=\nu_{sr}^0}(-1)^\nu C_sC_rZ_s^\nu Z_r^\nu\alpha_{sr}^{1-\nu}[(1-\nu)b_\nu(\varphi_{sr})+(3-\nu)g_\nu(\varphi_{sr})$$
$$+\sum_r\sum C_sC_r\frac{N_0}{V_0}\int_0^\infty\left(T\frac{dh_{sr}}{dT}+h_{sr}\right)2\pi R_{sr}^2dR_{sr}-\left[\frac{1}{12\pi}\frac{h^2\epsilon^2}{mk^2T^2}\frac{N_0}{V_0}-\frac{1}{64}\left(\frac{h^2}{\pi mkT}\right)^{3/2}\frac{N_0}{V_0}\right]C_0^2$$
$$+\frac{32}{45}\pi^5\frac{k^3T^3}{h^3c^3}\frac{V_0}{N_0}\Bigg\}+\frac{\Delta S}{R}, \qquad \text{(A2.4)}$$

[2] The approximate contribution to PV/RT due to the effect of the dielectric constant should apply also to the closely related H/RT and F/RT of (A2.3) and (A2.5). F/RT and H/RT are also subject to a small contribution not given here due to the dependence of specific polarizabilities on the temperature. This will also affect C_v/R of eq (A2.6).

with

$$\frac{\Delta S}{R}=-\frac{V}{V_0}\Big\{\frac{(d/dT)[T(B-B_0)]}{V_0}(\sum C_s)^2+\frac{(d/dT)[T(C-C_0)]}{2V_0^2}(\sum C_s)^3+\frac{(d/dT)[T(D-D_0)]}{3V_0^3}(\sum C_s)^4$$
$$+\cdots\Big\},\quad -\frac{F}{RT}=\frac{V}{V_0}\Big\{\sum C_s\Big[\Big(-\frac{F^0}{RT}\Big)_s-\ln C_s-\ln T/T_0\Big]+\frac{\pi^{1/2}(\sum Z_s^2C_s)^{3/2}\epsilon^3}{(DkT)^{3/2}}\Big(\frac{N_0}{V_0}\Big)^{1/2}$$
$$+\frac{1}{(\sum Z_s^2C_s)}\sum_s\sum_r\sum_{\nu=\nu_{sr}^0}(-1)^\nu C_sC_rZ_s^\nu Z_r^\nu\alpha_{sr}^{1-\nu}b_\nu(\varphi_{sr})+\sum_s\sum_r C_sC_r\frac{N_0}{V_0}\int_0^\infty\Big(2h_{sr}+\frac{\kappa}{2}\frac{\partial h_{sr}}{\partial\kappa}\Big)$$
$$\cdot 2\pi R_{sr}^2dR_{sr}+\Big[\frac{1}{6\pi}\frac{h^2\epsilon^2}{mk^2T^2}\frac{N_0}{V_0}-\frac{1}{16}\Big(\frac{h^2}{\pi mkT}\Big)^{3/2}\frac{N_0}{V_0}\Big]C_0^2\Big\}+\Delta\Big(-\frac{F}{RT}\Big),\qquad\text{(A2.5)}$$

where

$$\Delta\Big(-\frac{F}{RT}\Big)=-\frac{V}{V_0}\Big\{2\frac{(B-B_0)}{V_0}(\sum C_s)^2+\frac{3}{2}\frac{(C-C_0)}{V_0^2}(\sum C_s)^3+\frac{4}{3}\frac{(D-D_0)}{V_0^3}(\sum C_s)^4+\cdots\Big\}.$$

$$\frac{C_v}{R}=\frac{V}{V_0}\Big\{\sum C_s\Big(\frac{C_v^0}{R}\Big)_s+\sum C_s\frac{d\ln C_s}{d\ln T}\Big(\frac{E^0}{RT}\Big)_s+\frac{1}{2}\frac{\pi^{1/2}(\sum Z_s^2C_s)^{3/2}\epsilon^3}{(DkT)^{3/2}}\Big(\frac{N_0}{V_0}\Big)^{1/2}$$
$$-\frac{3}{2}\frac{\pi^{1/2}(\sum Z_s^2C_s)^{1/2}\epsilon^3}{(DkT)^{3/2}}\Big(\sum Z_s^2C_s\frac{d\ln C_s}{d\ln T}\Big)\Big(\frac{N_0}{V_0}\Big)^{1/2}+\frac{1}{2(\sum Z_s^2C_s)}\sum_s\sum_r\sum_{\nu=\nu_{sr}^0}(-1)^\nu C_sC_rZ_s^\nu Z_r^\nu\alpha_{sr}^{1-\nu}[\nu^2b_\nu(\varphi_{sr})$$
$$+(\nu-1)(\nu-3)g_\nu(\varphi_{sr})+h_\nu(\varphi_{sr})]+\frac{1}{2(\sum Z_s^2C_s)^2}\sum_s\sum_r\sum_{\nu=\nu_{sr}^0}(-1)^\nu C_sC_rZ_s^\nu Z_r^\nu\alpha_{sr}^{1-\nu}\Big[\sum Z_{s'}^2C_{s'}\frac{d\ln C_{s'}}{d\ln T}$$
$$-\frac{2d\ln C_r}{d\ln T}(\sum Z_{s'}^2C_{s'})\Big]\cdot[\nu b_\nu(\varphi_{sr})+(\nu-2)g_\nu(\varphi_{sr})]+\sum_s\sum_r C_sC_r\frac{N_0}{V_0}\int_0^\infty\Big[2T\frac{dh_{sr}}{dT}\Big(1+\frac{d\ln C_s}{d\ln T}\Big)$$
$$+\frac{T^2d^2h_{sr}}{dT^2}\Big]2\pi R_{sr}^2dR_{sr}+\Big[\frac{1}{6\pi}\frac{h^2\epsilon^2}{mk^2T^2}\frac{N_0}{V_0}-\frac{3}{128}\Big(\frac{h^2}{\pi mkT}\Big)^{3/2}\frac{N_0}{V_0}\Big]C_0^2+\frac{32}{15}\pi^5\frac{k^3T^3}{h^3c^3}\frac{V_0}{N_0}\Big\}+\Delta\frac{C_v}{R},\qquad\text{(A2.6)}$$

with

$$\Delta\frac{C_v}{R}=-\frac{V}{V_0}\frac{d}{dT}\Big\{\frac{T^2}{V_0}\frac{d(B-B_0)}{dT}(\sum C_s)^2+\frac{T^2}{2V_0^2}\frac{d(C-C_0)}{dT}(\sum C_s)^3+\frac{T^2}{3V_0^3}\frac{d(D-D_0)}{dT}(\sum C_s)^4+\cdots\Big\}.$$

For such ion interactions as are taken to have identical radii α_{sr}, the factors $\sum_s\sum_r C_sC_rZ_s^\nu Z_r^\nu$ in (3.1) and (A2.1) to (A2.6) can be grouped together as $\Big(\sum_s C_sZ_s^\nu\Big)\Big(\sum_r C_rZ_r^\nu\Big)$, reducing further to the form used by Poirier if all are identical.

5.3. Appendix 3

Functions relevant to the Coulombic interaction in the close approach region for ions of like sign include a contribution to $-A/RT$ due to h_{sr} given by

$$\frac{V}{V_0}\frac{2\pi}{3}\frac{N_0}{V_0}\sum_s\sum_r C_sC_ra_{sr}^3\sum_{n=0}q_n(x_{sr})\varphi_{sr}^n,\qquad\text{(A3.1)}$$

with

$$x_{sr}=Z_sZ_r/\alpha_{sr},$$

where

$$q_0(x)=\left(1-\frac{1}{2}x+\frac{1}{2}x^2\right)e^{-x}+\frac{1}{2}x^3\,\mathrm{Ei}\,(-x),$$

$$q_1(x)=xq_0(x),$$

$$q_2(x)=-\frac{3}{8}xe^{-x}+\frac{5}{8}x^2q_0(x),$$

$$q_3(x)=\frac{1}{10}(x-4x^2)e^{-x}+\frac{3}{10}x^3q_0(x),$$

$$q_4(x)=-\frac{1}{48}\left(x-\frac{43}{5}x^2+\frac{223}{20}x^3\right)e^{-x}+\frac{343}{2880}x^4q_0(x),$$

$$q_5(x)=\frac{1}{280}\left(x-\frac{53}{3}x^2+\frac{578}{15}x^3-\frac{407}{15}x^4\right)e^{-x}+\frac{64}{1575}x^5q_0(x),$$

$$q_6(x)=-\frac{1}{1920}\left(x-\frac{249}{7}x^2+\frac{1763}{14}x^3-\frac{9043}{70}x^4+\frac{17443}{280}x^5\right)e^{-x}+\frac{2187}{179200}x^6q_0(x).$$

The related contribution to PV/RT is

$$-\left(\frac{V}{V_0}\right)\cdot\frac{2\pi}{3}\frac{N_0}{V_0}\sum_s\sum_r C_sC_ra_{sr}^3\sum_{n=0}\left(1+\frac{n}{2}\right)q_n(x_{sr})\varphi_{sr}^n. \tag{A3.2}$$

A similar contribution to E/RT is given by

$$\left(\frac{V}{V_0}\right)\frac{2\pi}{3}\frac{N_0}{V_0}\sum_s\sum_r C_sC_ra_{sr}^3\sum_{n=0}e_n(x_{sr})\varphi_{sr}^n, \tag{A3.3}$$

with

$$e_n(x_{sr})=-\frac{n}{2}q_n(x_{sr})-x_{sr}\frac{d}{dx_{sr}}q_n(x_{sr}),$$

giving

$$e_0=-3q_0+3e^{-x},$$

$$e_1=-\frac{9}{2}xq_0+3xe^{-x},$$

$$e_2=-\frac{15}{4}x^2q_0+\left(\frac{3}{4}x+\frac{3}{2}x^2\right)e^{-x},$$

$$e_3=-\frac{9}{4}x^3q_0-\left(\frac{1}{4}x-\frac{3}{2}x^2-\frac{1}{2}x^3\right)e^{-x},$$

$$e_4=-\frac{343}{320}x^4q_0+\left(\frac{1}{16}x-\frac{59}{80}x^2+\frac{429}{320}x^3+\frac{1}{8}x^4\right)e^{-x},$$

$$e_5=-\frac{224}{525}x^5q_0-\left(\frac{1}{80}x-\frac{23}{80}x^2+\frac{41}{50}x^3-\frac{307}{400}x^4-\frac{1}{40}x^5\right)e^{-x},$$

$$e_6=-\frac{6561}{44800}x^6q_0+\left(\frac{1}{480}x-\frac{313}{3360}x^2+\frac{923}{2240}x^3-\frac{18029}{33600}x^4+\frac{14643}{44800}x^5+\frac{1}{240}x^6\right)e^{-x}.$$

The contribution to H/RT is given by

$$\left(\frac{V}{V_0}\right)\frac{2\pi}{3}\frac{N_0}{V_0}\sum_s\sum_r C_s C_r a_{sr}^3 \sum_{n=0} h_n(x_{sr})\varphi_{sr}^n, \tag{A3.4}$$

with

$$h_n(x_{sr}) = e_n(x_{sr}) - \left(1+\frac{n}{2}\right) q_n(x_{sr}),$$

or

$$h_0 = -4q_0 + e^{-x},$$

$$h_1 = -6xq_0 + 3xe^{-x},$$

$$h_2 = -5x^2 q_0 + \left(\frac{3}{2}x + \frac{3}{2}x^2\right)e^{-x},$$

$$h_3 = -3x^3 q_0 - \left(\frac{1}{2}x - \frac{5}{2}x^2 - \frac{1}{2}x^3\right)e^{-x},$$

$$h_4 = -\frac{343}{240}x^4 q_0 + \left(\frac{1}{8}x - \frac{51}{40}x^2 + \frac{163}{80}x^3 + \frac{1}{8}x^4\right)e^{-x}.$$

The contribution to S/R is

$$\left(\frac{V}{V_0}\right)\frac{2\pi}{3}\frac{N_0}{V_0}\sum_s\sum_r C_s C_r a_{sr}^3 \sum s_n(x_{sr})\varphi_{sr}^n, \tag{A3.5}$$

with

$$s_n = q_n + e_n,$$

or

$$s_0 = -2q_0 + 3e^{-x},$$

$$s_1 = -\frac{7}{2}xq_0 + 3xe^{-x},$$

$$s_2 = -\frac{25}{8}x^2 q_0 + \left(\frac{3}{8}x + \frac{3}{2}x^2\right)e^{-x},$$

$$s_3 = -\frac{39}{20}x^3 q_0 - \left(\frac{3}{20}x - \frac{11}{10}x^2 - \frac{1}{2}x^3\right)e^{-x},$$

$$s_4 = -\frac{343}{360}x^4 q_0 + \left(\frac{1}{24}x - \frac{67}{120}x^2 + \frac{133}{120}x^3 + \frac{1}{8}x^4\right)e^{-x}.$$

The contribution to $-F/RT$ is

$$\left(\frac{V}{V_0}\right)\frac{2\pi}{3}\frac{N_0}{V_0}\sum_s\sum_r C_s C_r a_{sr}^3 \sum_{n=0}\left(\frac{n+4}{2}\right) q_n(x_{sr})\varphi_{sr}^n. \tag{A3.6}$$

The contribution of this kind to C_v/R is

$$\left(\frac{V}{V_0}\right)\frac{2\pi}{3}\frac{N_0}{V_0}\sum_s\sum_r C_s C_r a_{sr}^3 \left\{\sum_n\left[\left(1-\frac{n}{2}\right) - \frac{n}{2}\left(\frac{d\ln D}{d\ln T}\right)_V + 2\left(\frac{d\ln C_s}{d\ln T}\right)_V + \frac{n}{2}\sum Z_{s'}^2 C_{s'}\left(\frac{d\ln C_{s'}}{d\ln T}\right)_V\right] e_n(x_{sr})\varphi_{sr}^n - \sum_n\left[1+\left(\frac{d\ln D}{d\ln T}\right)_V\right]\left(x_{sr}\frac{de_n}{dx_{sr}}(x_{sr})\right)\varphi_{sr}^n\right\} \tag{A3.7}$$

with the e_n as given above, and with xde_n/dx obtainable by differentiation, giving relations such as

$$xde_0/dx = -9q_0 + (9-3x)e^{-x},$$

$$xde_1/dx = -18xq_0 + \left(\frac{33}{2}x - 3x^2\right)e^{-x},$$

$$xde_2/dx = -\frac{75}{4}x^2q_0 + \left(\frac{3}{4}x + \frac{27}{2}x^2 - \frac{3}{2}x^3\right)e^{-x},$$

$$xde_3/dx = -\frac{27}{2}x^3q_0 - \left(\frac{1}{4}x - \frac{13}{4}x^2 - \frac{27}{4}x^3 + \frac{1}{2}x^4\right)e^{-x},$$

$$xde_4/dx = -\frac{343}{20}x^4q_0 + \left(\frac{1}{16}x - \frac{123}{80}x^2 + \frac{1523}{320}x^3 + \frac{19}{8}x^4 - \frac{1}{8}x^5\right)e^{-x}.$$

6. References

[1] H. D. Ursell, Proc. Cambridge Phil. Soc. **23,** 685 (1927).
[2] B. Kahn and G. E. Uhlenbeck, Physica **5,** 399 (1938).
[3] B. Kahn, Thesis, Utrecht (1938).
[4] J. E. Kilpatrick, J. Chem. Phys. **21,** 274 (1953).
[5] W. G. McMillan and J. E. Mayer, J. Chem. Phys. **13,** 276 (1945).
[6] K. Fuchs, Proc. Roy. Soc. (London) [A] **179,** 408 (1942).
[7] Y. Muto, J. Phys. Soc. Japan **4,** 233, 238, 242 (1949).
[8] H. C. Urey, Astrophys. J. **59,** 1 (1924).
[9] E. Fermi, Z. Physik **26,** 54 (1924).
[10] R. H. Fowler, Statistical Mechanics, 2d Edition (The Macmillan Co., London, Engl., 1936).
[11] R. V. Megreblian, Dissertation, (Calif. Inst. Technol., 1953); or Guggenheim Jet Propulsion Center Tech. Report No. 7, (Calif. Inst. Technol., Nov. 1952).
[12] M. Planck, Ann. Phys. [4] **75,** 673 (1924).
[13] D. Bohn and D. Pines, Phys. Rev. **85,** 338 (1952); **92,** 609 (1953).
[14] J. E. Mayer, J. Chem. Phys. **18,** 1426 (1950).
[15] E. Meeron, J. Chem. Phys. **26,** 804 (1957).
[16] G. Ecker and W. Weizel, Ann. Phys. [6] **17,** 126 (1956).
[17] T. L. Hill, J. Chem. Phys. **23,** 617 (1955).
[18] H. W. Woolley, J. Chem. Phys. **21,** 236 (1953).
[19] P. Rosen, J. Chem. Phys. **21,** 1007 (1953).
[20] B. M. Axilrod, J. Chem. Phys. **19,** 719 (1951).
[21] L. Jansen, Dissertation (Leiden, 1955); see also, L. Jansen and Z. I. Slawsky, J. Chem. Phys. **22,** 1701 (1954).
[22] T. Kihara, Rev. Mod. Phys. **27,** 412 (1955); Y. Midzuno and T. Kihara, J. Phys. Soc. Japan **11,** 1045 (1956); S. Koba, S. Kaneko, and T. Kihara, J. Phys. Soc. Japan **11,** 1050 (1956).
[23] K. F. Herzfeld and E. Teller, Phys. Rev. **54,** 912 (1938).
[24] J. Bigeleisen and M. G. Mayer, J. Chem. Phys. **15,** 261 (1947).
[25] J. Bigeleisen, J. Chem. Phys. **23,** 2264 (1955).
[26] J. E. Mayer and M. G. Mayer, Statistical Mechanics (John Wiley & Sons, Inc., New York, N. Y., 1940).
[27] R. J. Plock, Dissertation, Yale (1957).
[28] E. C. Stoner, Phil. Mag. [7] **21,** 145 (1936); [7] **28,** 257 (1939).
[29] J. C. Poirier, J. Chem. Phys. **21,** 965, 972 (1953).
[30] K. F. Stripp and J. G. Kirkwood, J. Chem. Phys. **19,** 1131 (1951).

WASHINGTON, July 18, 1958.

Parallel Testing Interferometer

James B. Saunders

The conventional methods of testing the parallelism of opaque bodies, such as gage blocks, by interferometry require wringing of the body to an optical flat. This operation disturbs the temperature equilibrium, necessitating long periods between tests, especially for long blocks. It often injures the surfaces of both the optical flat and the test body. Also, if the body is a standard gage block, repeated wringings during use ultimately change the dimension. This paper describes an interferometer for measuring the parallelism of gage blocks and other bodies of any reasonable length without the necessity of the wringing operation. Two forms of this instrument are used—one for testing long blocks and another for testing short blocks. Either form can be constructed for testing blocks of any length, but two forms are found to be more practical.

1. Introduction

The conventional procedures for measuring the parallelism of gage blocks [1, 2] require the wringing of the blocks onto an optical flat. The wringing operation often injures the contacted surfaces and repeated wringings necessitate frequent refinishing of the optical flat that is used as a base. A method for measuring parallelism, without the wringing operation, has significant advantages because the danger of injury to the contacted surfaces is eliminated. Accordingly, two instruments that utilize this method are described: one is for testing very long blocks and similar bodies, whereas the other is designed for short blocks. Both instruments use low orders of interference and neither requires the use of a standard.

2. Optics of the Interferometer

A description of the optics for either form of this instrument covers a large portion of that for the other. For distinction we will designate them as "the long-block interferometer" and "the short-block interferometer". The double-image prism used in these instruments is adjusted during construction [3] so that a ray of light, shown in the plane of figure 1A, after division into two component rays, 1 and 2, at P_0 will, on reflection at P_1 and P_2, lie in planes that are parallel to the semireflecting plane of the prism but deviate equally toward or from opposite sides of the plane of figure 1A. The projection of the light rays on the dividing plane is shown in figure 1B, which is perpendicular to the plane of figure 1A. This deviation is effected by rotating one component of the prism relative to the other about an axis normal to the dividing plane of the prism. If this deviation is held constant, the width of the interference fringes in the direction normal to the plane of figure 1A is fixed. This component of fringe width is, therefore, frozen into the system [4] when the cement between the component prisms becomes hard by cooling after adjustments are complete. Furthermore, the tilting of any plane surface outside the prism that affects the two component beams between division and recombination, will produce equal effects in this direction and, consequently, will not affect the fringe width. However, the rotation of plane surfaces about an axis normal to the plane of figure 1A will produce equal effects on the two component beams but in opposite directions, thus producing a proportionate effect on the fringe width in the direction parallel to this plane.

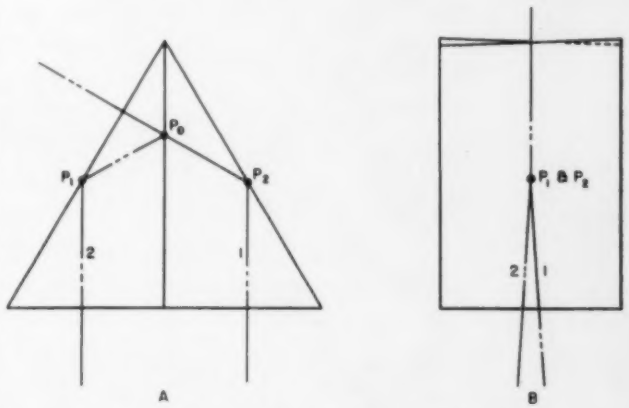

FIGURE 1. *Kösters double-image prism.*

A small angle is formed by the two 30° edges shown exaggerated in B.

Because of the above-described properties of this prism, adjustments of the instrument in which it is used affect the fringe width in one direction only. Consequently, when measuring the parallelism of gage blocks the test can be applied to parallelism in only one direction at a time. To test for parallelism in other directions the block must be rotated.

2.1. Long-Block Interferometer

Figure 2A is a horizontal section through the optical elements of this instrument. The light from a source at $S_1(S_2)$ is collimated by lens $L_1(L_2)$ and divided into two equal components by the beam-dividing plane $B_1(B_2)$. Each component suffers total internal reflection in the prism and emerges in planes

[1] Gauges and fine measurements, by F. H. Rolt, **I**, p. 204 (Macmillan and Co., Ltd., London 1929).
[2] The science of precision measurement, by The DoAll Co., p. 143 (1953).
[3] Construction of a Kösters double-image prism, by J. B. Saunders, J. Research NBS **58**, 21 (1957) RP2729.
[4] NBS Tech. News Bul. **42**, 30 (1958).

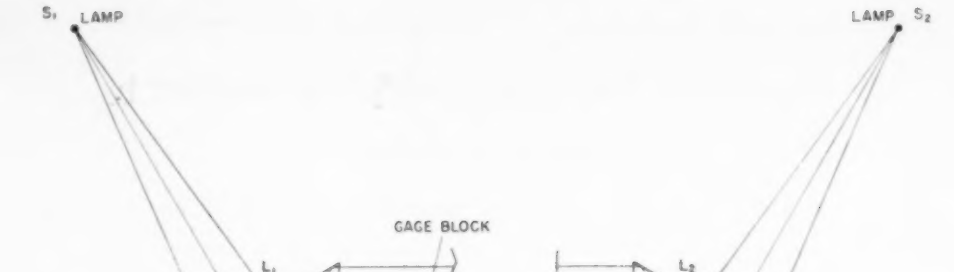

FIGURE 2. *Optics of interferometer for testing parallelism of long blocks.*

Figures B through G represent observed interference fringes.

parallel to $B_1(B_2)$, but at a small angle to the base surface $C_1(C_2)$. The latter condition is obtained by a slight rotation of $P_1(P_2)$ about an axis normal to the dividing plane $B_1(B_2)$. This serves to permit the elimination of light reflected from $C_1(C_2)$.

The two prisms, P_1 and P_2, are separated by a distance exceeding the length of the longest block to be tested. If desired, this distance may be made adjustable. The two dividing planes, B_1 and B_2, are adjusted to be coplanar and the two base faces, C_1 and C_2, are adjusted parallel to each other. A line joining the centers of P_1 and P_2 is adjusted to form a small angle with the normal to faces C_1 and C_2.

The light emerges from prism $P_1(P_2)$ as two separated components, one on each side of the dividing plane. It enters prism $P_2(P_1)$, again suffers total internal reflection, and each pair of component rays recombines in the plane of $B_2(B_1)$. One-half of each beam proceeds to the neighborhood of source $S_2(S_1)$ and the other half to $S_2'(S_1')$. An observer at $S_2'(S_1')$ sees a set of interference fringes that cover the entire aperture.

If a gage block, G, is inserted in the position shown with its end face, G_1, adjusted normal to the light beams, it will reflect equal and corresponding parts of the two component light beams from S_1 back through P_1 to S_1'. Accordingly, the observer at S_1' sees a background set of fringes, produced by light from S_2 and another set on the face of G_1, that is produced by light from S_1. Since G_1 is normal to the light beams these two sets of fringes will be parallel to each other and to the plane of figure 2A. If the other end, G_2, of the gage block is parallel to G_1, the fringes seen at S_2' will likewise be parallel to each other and to the plane of figure 2A. If, however, G_2 is not parallel to G_1, in the plane of figure 2A, it will not be normal to the light beams, and the sets of fringes seen at S_2' will not be parallel to each other. The angle between these two sets of fringes is a measure of the angle between G_1 and G_2 in the plane of figure 2A. The component of the angle between G_1 and G_2 that is perpendicular to the plane of figure 2A (or horizontally in figs. 2B to 2G) does not affect the fringes because it affects all pairs of component beams equally. If the component of the angle between the gage-block surfaces that is normal to the plane of figure 2A (or vertically in figs. 2B to 2G) is desired, the block must be rotated 90° and the operation repeated.

Since each prism is adjusted for complete compensation in the plane of figure 2A, white light can be used. A measure of the vertical width of the fringes (perpendicular to fig. 2A) for a known monochromatic light, with a micrometer eyepiece at S_2', gives a calibration of the micrometer scale in units (microns, millionths of an inch, etc.) of length for measuring the displacement of white-light fringes from a chosen reference point on the gage-block surface.

The procedure for adjusting a gage block is explained with the aid of inserts in figure 2. In general, when the block is placed on its supports, the light reflected from its end will not reach the observer because of excessive angular deviation from the

eyepiece. The block will appear in silhouette, as indicated in figure 2B. When the surface G_1 is adjusted approximately normal to the light, fine fringes will usually be visible in the area covered by both images of it, as shown in figure 2C. The images of the two parts of G_1 are made to coincide by rotating G about the center line of figure 2A, causing the image to change from that of figure 2C to figure 2D. A lateral motion, without rotation, will then change the image from that shown in figure 2D to figure 2E. A further small rotation of G about an axis normal to figure 2A brings G_1 normal to the light and the fringes on G_1 will appear horizontal and parallel to the background fringes as shown in figure 2F. The observer then moves to position S_2' and observes the set of fringes shown in figure 2G. The angle between these two sets of fringes corresponds to the angle between surfaces G_1 and G_2.

A photograph of the long-block interferometer is shown in figure 3. The base of the instrument is designed for rigidity so as to avoid flexure. Rigidity is quite important. The two prisms are mounted on rigid tables at each end of the base. Three screws (D_1 and two others not shown) permit raising and lowering of prism P_2. They also permit rotation or tilting of this prism about any chosen horizontal axis. The prism housings are fastened to the table tops by means of large-headed screws, in oversize holes, that permit lateral adjustments of the prisms relative to each other. Two screws, D_2 and another concealed by the housing of prism P_2, permit small rotations of this prism about a vertical axis by applying lateral torques to the legs of the table. Similarly, screws D_3 and D_4 permit rotary adjustments of the other prism housing.

The adjustments described above permit the alinement of the two prisms. This adjustment is critical, rather difficult to attain, but when once obtained is very stable. The final adjustments are executed while observing interference fringes produced by lens L'_2, in one of the many images of the source S_2. This author uses a pinhole source of approximately 1-mm diam and a short-focus lens to observe its image at S_2'. There are two sets of fringes, superimposed upon each other, in the proper image to be used. When these two sets of fringes are horizontal and very broad, fringes can be seen with the two eyepieces when focused on the pinhole. These fringes, in white light, are horizontal with the zero order in the center of the field.

The supports on which the long blocks rest are located at the Airy points so as to reduce changes in the angle between G_1 and G_2 due to gravitational distortion.[5] These supports rest on an adjustable plate which, in turn, is supported at one end by two points and at the other by one point. This plate is adjustable at one end, laterally with screw D_5 and vertically with another screw D_6 which is concealed in figure 3.

2.2. Short-Block Interferometer

The optics of the short-block interferometer are shown in figure 4. The double-image prism, lenses light source, and viewing position in figure 4B are identical to that of either end of the long-block instrument described above. A reflecting prism, P_R in figure 4, replaces one of the prism assemblies of the long-block instrument. Also, the optical axis of the instrument is vertical instead of horizontal. Figure 5 is a photograph of the short-block interferometer. Figure 4A may be considered a section through the center of 4B, coincident with the dividing plane of prism P. The indicated rays, 1 and 2 in figure 4A, however, do not lie in this plane. Their positions relative to it are indicated in 4E, which is a vertical view through 4B. The two surfaces, G_1 and G_2, of the gage block (figs. 4A and 4D) appear as G and G′ in figure 4E. G'_2 in figure 4A is an image of G_2 as seen by light reflected from the right-angle prism, P_R.

[5] F. H. Rolt, Gauges and fine measurements **II**, 340 (Macmillan and Co., 1929).

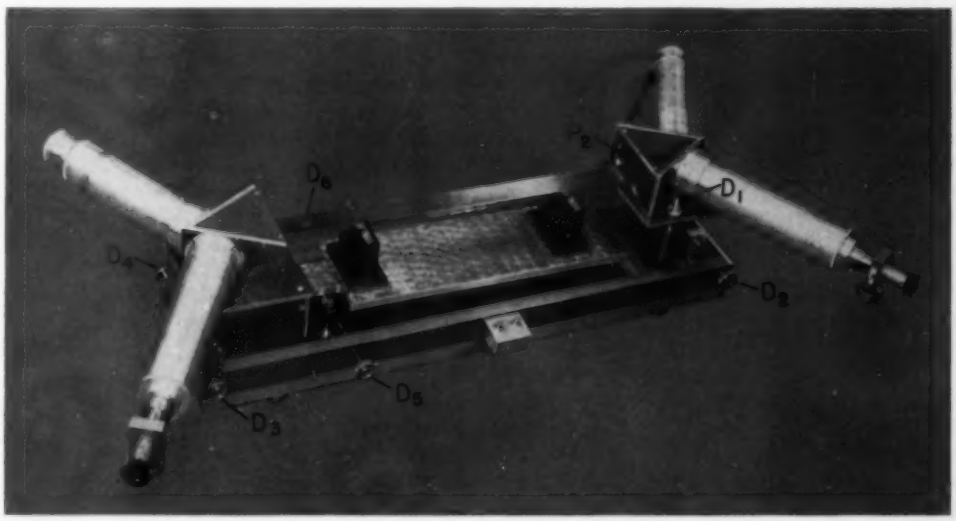

FIGURE 3. *Photograph of the long-block interferometer.*

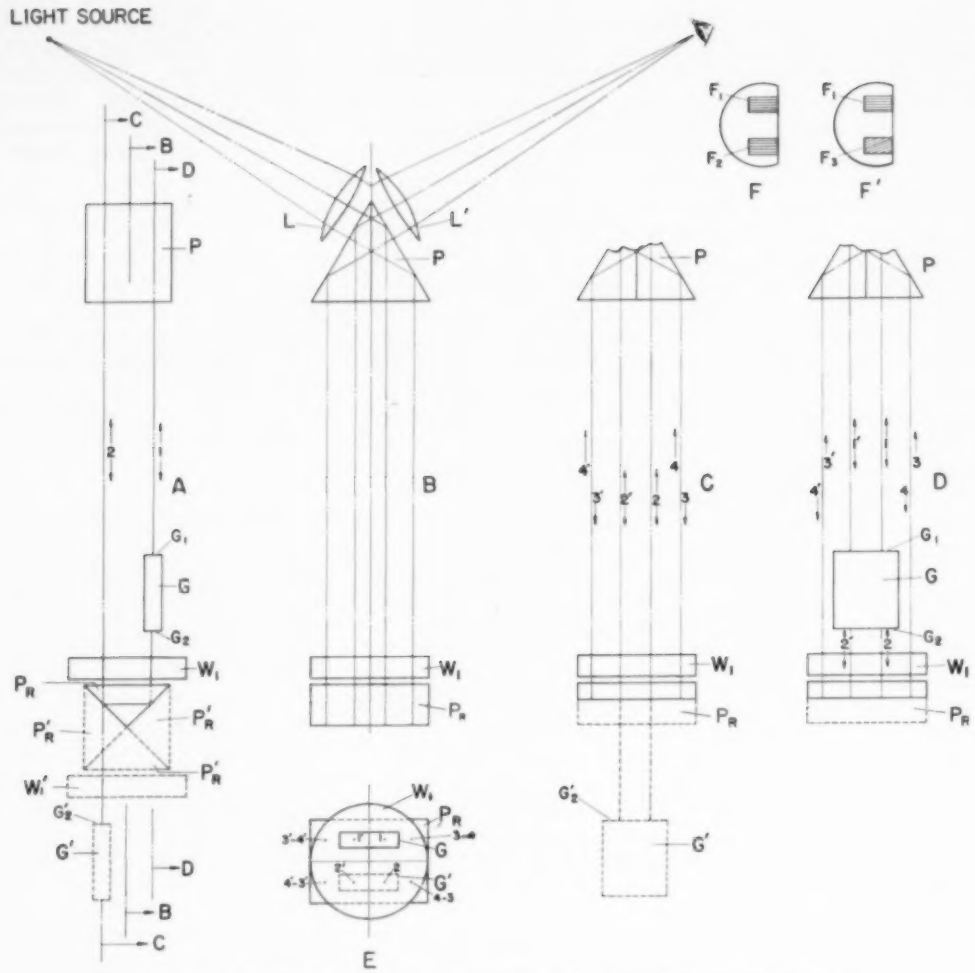

FIGURE 4. *Optics of the interferometer for testing parallelism of short blocks.*

Figures B, C, and D are sections through A. Figure E is a vertical view. Figures F and F′ represent interference fringes for a parallel and a nonparallel block, respectively.

A plane optical wedge, W_1, and its image, W'_1, (in figure 4A) are shown between G and its image G′. Figures 4B, 4C, and 4D are sections through 4A, along the lines indicated. The gage block is not located in the center as was the case in the instrument described above.

The two component rays of light, 1 and 1′ (figs. 4A and 4D), are caused to reflect normally from G_1 by adjusting G with a leveling screw. They return into P where they recombine to produce the interference fringes, F_1, shown in figure 4F. The two component rays, 2 and 2′ (figs. 4A and 4C) are transmitted downward through the optical wedge, W_1, suffer two internal reflections in P_R, and if P_R is properly adjusted, return upward and parallel to their directions of incidence through W_1 to G_2.

The wedge, W_1, is adjusted initially by rotation so that its thickness is constant at all points in either of the planes B, C, and D. When in this neutral position it does not affect the interference fringes because of compensation in each pair of component beams that pass through it. The function of W_1 will be explained later.

In order to measure the angle between G_1 and G_2, the deviation of the light by P_R toward or from the dividing plane of P must either be reduced to zero or its effect eliminated by measuring the observed angle for two orientations of G, which are 180° apart. The light that is not intercepted by G forms an interference pattern of uniform tint (or color) that fills the background about and between the two images of the gage block, shown in figure 4F or 4F′. Figures 4F and 4F′ represent the conditions observed when the ends of the block are parallel and nonparallel, respectively. A typical pair of component rays, which form this interference pattern, is indicated by 3 and 3′. They travel downward in figure 4C and upward in figure 4D. If the right-angle edge of P_R is normal to the dividing plane of P, the pair of rays 3 and 3′ in figure 4C can be made to return in planes that are parallel to the dividing plane, by rotating P_R about an axis parallel to the plane of 4A and normal to the incident light. This condition is attained when the background fringe is infinitely broad. The direction of the background fringes, when not infinitely broad,

FIGURE 5. *Photograph of the short-block interferometer.*

remain parallel to the dividing plane, because for each pair of component rays, such as 3 and 3′, there is a corresponding pair, 4 and 4′, that travel identical paths but in opposite directions. The optical path differences are, therefore, equal to each other and also equal to that for any other pair of component rays in the plane of 4C and 4D. The order of interference along the dividing plane corresponds to the optical path difference that was introduced into the double-image prism by the built-in wedges at the point that corresponds to the point of intersection of the right-angle edge of P_R and the dividing plane of P. This point is located in the center of figure 4E.

In general, due to the inherent error of judging when the background fringes are infinitely broad and to imperfections in the optical elements, a more precise method of evaluating the wedge between G_1 and G_2 is to measure the wedge for two positions that differ by 180°. If the background fringes are unaltered, the instrumental errors will be equal for the two positions and the value of the wedge unchanged except in sign. Consequently, the albebraic difference yields twice the value of the wedge.

There are three ways that one might evaluate the wedge between G_1 and G_2. The first is to rotate P_R until the order of interference at points C and E (fig. 6A) are equal; then rotate the gage block until the orders at A and B are equal; and finally, observe the difference in order of interference at points F and H. The second method is: After performing the above operations, instead of reading the order difference between F and H, reduce this order difference to zero by rotating W_1 and read the resultant change on a scale attached to W_1, figure 4E. This scale may be calibrated with monochromatic light and the units may be radians, degrees, or the corresponding variation in height of the block. A third method is to leave the wedge in its neutral position, adjust G so that the orders of interference of A and B are equal, and change the order at H to equal that at F by rotating P_R about an axis normal to the incident light and parallel to the plane of figure 4A. The order of interference between two points such as C and D (fig. 6A) after rotating P_R will be equal to one-half of that between F and H before this rotation was performed. By choosing a point, such as E in figure 6, such that CE equals K times CD, the order difference between C and E will be K times that between C and D.

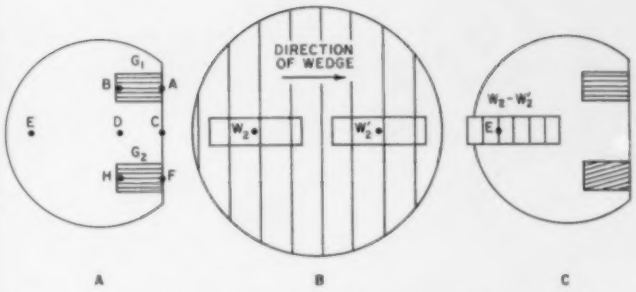

FIGURE 6. *Figures A and C represent the positions of reference points relative to the different sets of interference fringes.*

Figure B shows the wedge from which the two smaller wedges, W^2 and $W^{2'}$, were cut and the difference in optical thickness between them.

When using this last method for testing gages that are almost parallel, the angle between G_1 and G_2 will be small and the background fringes will be too broad for reading fractions of fringes. To eliminate this difficulty, an optical wedge, illustrated in figure 6B, is constructed and from it two sections W_2 and W_2' are cut and placed on P_R as shown in figure 7. The wedges W_2 and W_2' are equal, but when placed in the position shown, the effect is to narrow the background fringes seen through them. The results are illustrated in figure 6C. The difference in thickness of W_2 and W_2' at a selected reference point E (fig. 6C) is determined by the choice of the corresponding positions on the plate from which they were cut. This difference in thickness is chosen so as to cause the zero order of interference to pass through the chosen point when the background fringes about W_2–W_2' are infinitely broad.

If the angles of wedges W_2 and W_2' are properly chosen, the width of the fringes seen through them will be most favorable for measuring the fractional parts of fringes. Also, the position of the zero-order fringe, relative to point E, may be calibrated to read directly the angle between the ends of the gage blocks.

The recommended procedure for measuring a block is: (1) Adjust the two sets of fringes seen on the ends of the block so that they are perpendicular to the dividing plane, as in figure 4F; (2) note the position

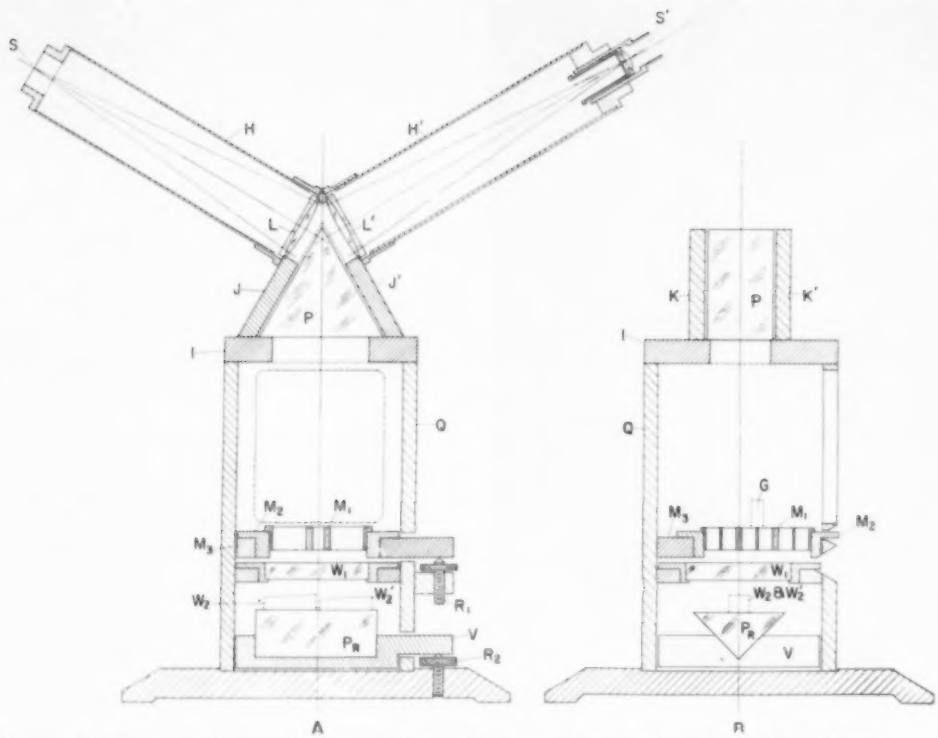

FIGURE 7. *Two vertical sections, at right angles to each other, through the short-block interferometer.*

of the zero-order fringe (or absolute order at E, fig. 6C); (3) rotate the block 180° about a vertical axis through its center; (4) readjust the fringes to restore the condition of (1) above; (5) again note the position of the zero-order fringe (or absolute order at E); (6) the difference in the two observed orders at E, or positions of the zero-order fringe, multiplied by the constant K, described above, is a measure of the angle between the ends of the block.

Figure 7 shows two vertical sections through the center of the short-block interferometer that are mutually perpendicular to and through the centers of each other. A pinhole, S, illuminated either with monochromatic or polychromatic light from outside the tube H, serves as source. The position of the pinhole is adjustable in the focal plane of the collimator lens, L, and the collimator tube is adjustable in length. The prism, P, rests on a thick plate, I, to which is fastened the lens-holding plates, J and J′. The plates, K and K′, which cover the ends of P, are not fastened to J or J′. Consequently, small stresses applied to tube H′ while adjusting the eye-piece or manipulating a micrometer in it, are not transmitted to P.

The material of the instrument, except for the collimator, the eye-piece tubes and optical elements, is made of steel. Steel was chosen because its expansivity approximates that of the glass elements more nearly than other usable materials.

The gage block, G, rests on a rotatable plate, M_1, that is perforated so as to transmit the required parts of the light beams used for making measurements. See also figure 8 for a vertical view of M_1 and its supporting parts. The plate, M_1, rotates in an annulus ring, M_2, which in turn is rotatable, from outside the instrument, in another annulus, M_3. The aperture in M_3 has its center displaced from the center of the instrument in a direction parallel to the dividing plane of P and by an amount equal to one-half the horizontal separation between the centers of the gage block, G_1, and its image, G′. The gage block rests on the center of M_1 (see fig. 6B). Accurate placement of the block is facilitated by stops.

The eccentric annulus, M_3, has an arm that projects through the wall, Q, of the instrument and is supported by this arm at one of its three supporting points by an adjusting screw, R_1. The other two supports for M_3 are steel balls, T_1 and T_2, (fig. 8B), which are held in conical holes by means of two screws, U_1 and U_2, respectively. The ends of these screws have eccentric conical depressions that permit a limited amount of rotation of M_3 about an axis normal to the dividing plane of P. The screw R_1 permits fine adjustment of M_2, and consequently the gage block, which it supports, about a horizontal axis parallel to the dividing plane of P. A similar pair of balls, screws, and the adjustable screw R_2 permits rotation of P_R about two axes parallel to those used for adjusting M_3.

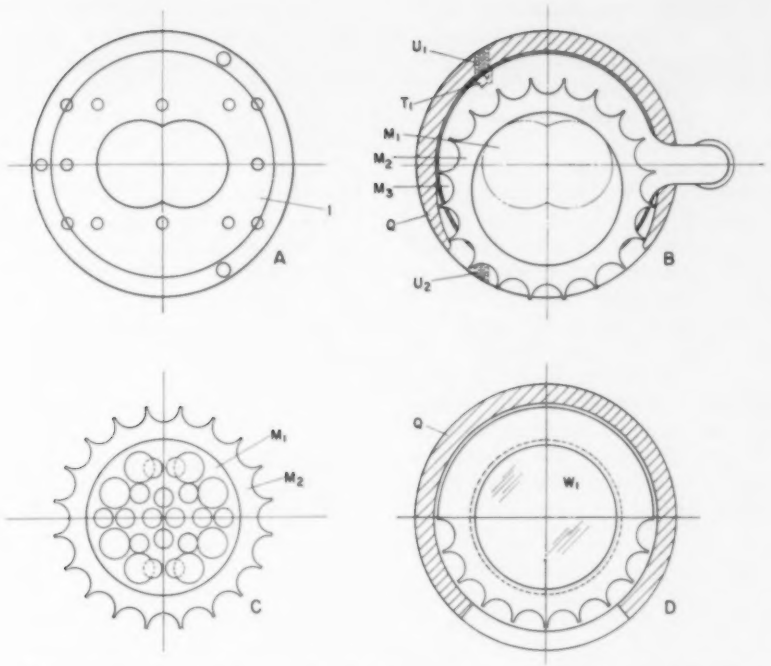

FIGURE 8. *Several views showing individual parts of the short-block interferometer.*

If the refracting edge of the optical wedge, W_1, is made perpendicular to the dividing plane of P (i. e., parallel to the plane of fig. 7B), each pair of component rays will traverse this plate at points of equal thickness. Consequently, W_1 in this orientation, does not affect the fringes of interference. It does, however, serve as a window, protecting the prism P_R from the accumulation of dust. Other functions of W_1 will be discussed later.

The prism, P, is centered over the aperture in plate I (figs. 7A and 8A) with its ends parallel to plates K and K′ (fig. 7B). Using the base surface of P as a plane mirror, the pinhole aperture S is located in the focal plane of lens L by varying the length of tube H and at a point in this plane where the light will form an image of the pinhole upon itself. This places the light beams, after division at the dividing plane, normal to the prism base and, consequently, parallel to each other.

A gage block, whose end faces are parallel to each other, is placed on the center of plate M_1 with its lower surface parallel to the top surface of M_1. When the surface of the block is adjusted parallel to the base of P by means of screws R_1, U_1, and U_2, the light from S is reflected normally from the top surface of the block and observed at the eyepiece as interference fringes.

The parts of the light beams that are not intercepted by the block and its support M_1, traverse the optical wedge W_1, and enter the right-angle prism P_R. After two internal reflections in P_R, the light returns along a path that is symmetrical to its incident path with respect to the 90° edge of P_R. The 90° edge of P_R is made normal to the dividing plane of P by means of screws in its support similar to U_1 and U_2 and the fine-adjusting screw R_2 (fig. 7A). This light forms the background fringes used in the test, but no interference is observed until this prism edge is nearly normal to the dividing plane. When it is not normal the two images of this edge, formed by the two component light beams, intersect in the extension of the beam dividing plane. The prism P_R is rotated until the two images coincide—perfection being attained when the background fringes have maximum contrast.

The above-mentioned contrast in the background fringes is not affected by screw, R_2, since it has no vertical rotational effect on the prism. Its effect is to change the width of the background fringes only. When the background fringes are made infinitely broad, the collimated beam of light returns toward P parallel to the incident beam—all rays having suffered a horizontal shift in P_R, as illustrated in figure 4A.

The holes in the gage-block support, M_1 (fig. 8C), are so spaced that when M_1 is rotated to one of the four positions for which the rectangular sides of the block are either parallel or perpendicular to the dividing plane, all light that goes through M_1 returns again through it. That is, the apertures in M_1 are symmetrical both with respect to the dividing plane and to the 90° edge of P_R. Parts of the beam (rays 3, 3′, 4, and 4′ in fig. 4) will pass downward through M_1 to P_R, shift horizontally in P_R, and pass upward through other apertures in M_1 to P. Other parts of the beam (rays 2 and 2′ in fig. 4) will pass downward through M_1, shift horizontally in P_R, pass

upward through M_1 to the lower surface of the gage block, return through M_1 to P_R and again upward through M_1 to P. If the two end faces, G_1 and G_2, are parallel, the light will be incident on G_1 and G_2 at equal angles. When G_1 is adjusted normal to the light, G_2 will also be normal to it.

We have three sets of fringes, shown in figure 4F′, to consider: (1) The set F_1 is formed by light reflected from the top surface, G_1, of the gage block; (2) the background fringe between and about F_1 and F_3, formed by light reflected from P_R but not incident on the gage block; and (3) the set F_3 formed by light reflected from P_R to G_2 and back through P_R. The direction or orientation of F_1 determines the angle between G_1 and the incident wavefront; the width of the background fringes determine the direction between the incident and reflected beams to and from P_R; and the orientation of F_3 determines the angle between G_2 and the wavefront that is reflected from it.

The set of fringes, F_1, is adjusted by means of P_R normal to the dividing plane of P, for which condition G_1 is normal to the incident light. The background fringe is made infinitely broad, for which condition the light beams returning from P_R are parallel to the incident beams. If the two surfaces of G are parallel, the set of fringes appearing on G_2 will be parallel to those on G_1 and indicated as the set F_2 in figure 4F. If G_1 and G_2 are not parallel, the fringes seen on them and indicated as F_1 and F_3 in figure 4F′ will not be parallel to each other. The angle between these two sets of fringes is a measure of the angle between the two ends of the gage block.

WASHINGTON, May 5, 1958.

Journal of Research of the National Bureau of Standards Vol. 61, No. 6, December 1958 Research Paper 2918

Correction for Instrumental Drift in Flame Photometry

Barry W. Mulligan and Alan F. Haught

The application of the principles of experimental design to correct for drift in instrumental measurements, specifically in flame photometry, is described. Based on the procedure proposed by Youden, samples and reference standards may be measured in combinations of pairs in a manner such that errors caused by drift can be minimized and the actual amount of drift can be determined. Where the drift is dependent on the magnitude of the quantity measured, grouping by magnitude prior to final measurement is necessary. Application of the procedure to flame photometric determination of alkali elements, under conditions of severe drift, resulted in improving coefficients of variation from an original range of 2.0 to 3.5 to a range of 0.6 to 1.2.

1. Introduction

In any series of measurements, drift in the response of the measuring instrument may introduce appreciable errors. Although the errors may be reduced by improved adjustment or design of the instrument, some drift may be inevitable.

An unusual example of drift was encountered in measurements with a flame photometer. Replacement of the detector, a photomultiplier tube, was later found to overcome most of the drift; however, the possibility of compensating for drift by appropriate design of the experiment in this and similar cases was explored.

Youden[1] proposed a design and statistical treatment of data using a method of incomplete blocks to minimize errors caused by instrumental drift, and at the same time, to measure the magnitude of this effect. The applicability of his procedure to this drift problem was examined.

2. Experimental Procedures

During the development of a method for determining the alkali metals with a Beckman model DU[2] flame photometer with photomultiplier attachment, it was noted that the readings of the instrument were shifting with time. The determinations were being made on a long series of solutions, so that a shift in readings would seriously affect the results.

In Youden's method to compensate for drift,[1] the objects to be measured (here the sample and standard solutions) are arranged in an appropriate sequence. Specifically, the objects are grouped in pairs, so that each object appears in a pair with every other object. For example, 5 objects are grouped in 10 pairs, as shown in table 1, the sequence of the pairs being immaterial. The objects are then measured on the instrument in a manner such that the time between measurements on the objects in a pair is small in comparison to the time between pairs.

The rigorous method of Youden for computing the drift involves long arithmetic calculations. A simplified, yet accurate, alternate method, suggested later by Youden, will be described here. No difference was found in the values computed by the two methods, within the accuracy of the data. The method involves, first, the determination of calculated, or corrected, values for the measurements on the objects, A, B, C, etc., and second, the computation of drift using the observed values and calculated values of the objects.

TABLE 1. *Design of experiment*

Pair	1	2	3	4	5
Object	AB	DE	BC	EA	CD
Pair	6	7	8	9	10
Object	EB	AC	BD	CE	DA

A calculated value for each object is determined as is shown by the steps in table 2. In the table, A_1 represents the measured value of object A in pair 1, C_7 the measured value of object C in pair 7, etc. The differences between A and the object with which it appears are summed, $+A$ and $-A$ are added to the left side of the equation, the equation is divided by five, and everything but A is transposed to the right side. Since the expression $(A+B_1+C_7+D_{10}+E_4)/5$ will be approximately equal to the average of the 20 measurements, (that is, four each on A, B, C, D, and E, divided by 20), the last equation is obtained. A similar computation is performed to obtain the calculated values for the other objects, B, C, D, and E.

In addition to correction for drift, the method also provides a measure of the drift. Table 3 shows the method of computing the average drift for each pair. The differences between the observed values and the calculated values of the two objects in the pair are averaged, and the result represents the average drift for the pair. The drift for the pairs is then plotted as the deviation from the mean drift. It should be noted that the validity of the statistical method rests on the assumptions that the objects do not change in the course of the measurements and that the drift is independent of the magnitude of the measurements made.

TABLE 2. *Calculated value for object A*

$$A_1 - B_1 = X_1$$
$$A_7 - C_7 = X_2$$
$$A_{10} - D_{10} = X_3$$
$$A_4 - E_4 = X_4$$

$$4A - (B_1 + C_7 + D_{10} + E_4) = \Sigma_1^4 X_i$$

$$\therefore A = \text{Average of all measurements} + \frac{\Sigma_1^4 X_i}{5}$$

[1] W. J. Youden, Science **120**, No. 3121, 627 (1954).
[2] H. H. Carey and A. O. Beckman, J. Opt. Soc. Am. **31**, 682 (1941).

TABLE 3. *Computation of drift in pair 1*

Value observed	Value calculated	Difference
A_1	A	X
B_1	B	Y
Average drift $= \frac{X+Y}{2}$		

Figure 1 shows an instrumental-drift curve obtained by this method for a series of readings on sodium. This is a normal type of curve with narrow limits. The abscissa is the number rather than the time of the reading, since the only time requirement is that the 2 objects in any 1 pair are immediately consecutive. Thus, for example, the third point on the graph is plotted midway between readings 5 and 6, since these 2 readings were used to compute the point. The ordinate is the deviation from mean drift in terms of instrument readings and in this particular case one instrument unit represents approximately 2 percent of the amount of sodium present.

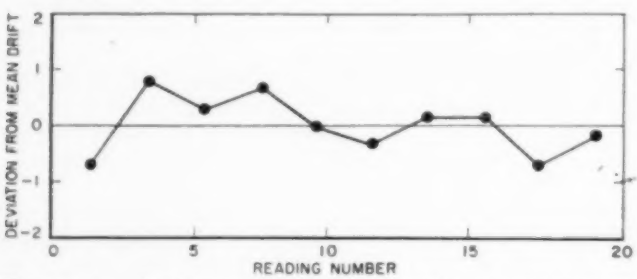

FIGURE 1. *Instrument drift during a series of measurements on sodium.*

One ordinate unit equals approximately 2 percent of the amount of sodium present.

The value of this method became immediately evident upon examination of the curve shown in figure 2. This represents a series of readings on potassium in which, unexpectedly, the range of the instrument had to be changed from low to high during the measurement of the series. The instrument response was evidently slow.

The original method employed in these determinations consisted of making measurements on a series of unknown solutions with standard solutions measured periodically during the series. A large change in readings on an object during any series of readings with other objects is, of course, evident to the observer. Instead of having to discard data and begin over, as was done in the original method, the information obtained when using a drift correction is perfectly valid. Similarly, any small instrumental drift, unnoticed by the observer, is corrected for in the calculations. Another advantage of the method is that the experimenter may interrupt a series of readings at any point between pairs, and upon return may resume at the point of interruption, rather than start over again.

The coefficients of variation obtained when using

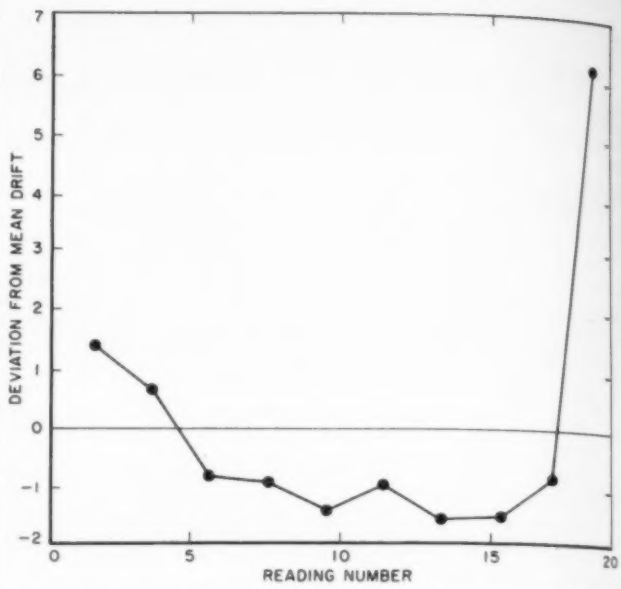

FIGURE 2. *Instrument drift during a series of measurements on potassium.*

The range of the instrument was changed between readings 18 and 19.

this refinement show a marked improvement over those obtained with the previously mentioned original method, in which no instrumental drift correction was applied. Coefficients (obtained from 10 determinations on each of 2 samples of lithium solutions and 2 of potassium) which were in the range of 2.0 to 3.5 were improved to fall in a range of 0.6 to 1.2 by the new method.

In an effort to determine the nature and cause of the drift, the statistical method of incomplete blocks was again employed. A sodium determination was made on 10 solutions of widely different concentrations under standard-operating conditions in a statistically designed sequence during a 2¼ hr time interval. From the observed readings, the drift was computed and was plotted as a function of time. The curve obtained (fig. 3) indicated an initially rapid but continually decreasing drift with an irregular drift superimposed on it. Because the "reality" of the superimposed drift was doubted, additional measurements were made on a solution containing 3 ppm of lithium and on a solution containing 20 ppm of potassium. Experiment had shown that determinations of these elements are less subject to random fluctuations than those for sodium and they are less liable to error because of contamination by contact with dust in the air. The runs in each case were made on a single solution and the drift was computed as the deviation of the observed readings from their mean. With both the potassium and the lithium solutions only the initially rapid but continually decreasing drift was obtained, and none of the superimposed, irregular drift was present. This would indicate that the drift may be dependent on the magnitude of the measurement being made, contrary to one of the assumptions of the statistical method.

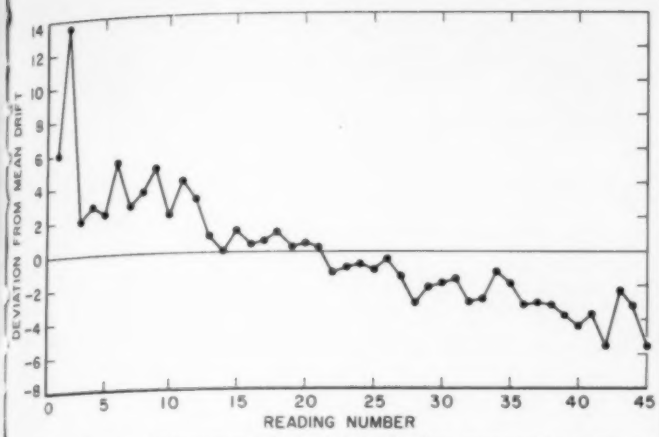

FIGURE 3. *Instrument drift obtained when measuring a series of 10 sodium solutions having widely different concentrations.*

To test the effect of a wide range of concentrations on the drift, runs were made on 2 lithium solutions, 1 twice the concentration of the other. The drift in each case was computed as the difference between the observed readings and their mean and was plotted as a function of time as shown in figure 4. The ordinates of the two curves are in a constant ratio at all points along the abscissa, within the accuracy of the readings, showing the drift is dependent upon the intensity of the light being measured.

The variation of the drift with the incident light intensity explains the irregular character of the drift obtained previously (fig. 3) on the group of sodium solutions having different sodium concentrations. The larger deviations were caused by the large drift of the readings for the highly concentrated solutions and the points closer to the average drift curve by the small drift for the less concentrated solutions. The particular sequence of solutions of high and low concentrations resulted in the irregular drift.

The cause of the drift was finally ascertained to be due to fatigue of the photomultiplier tube, a phenomenon usually associated with these tubes [3] but only at much higher phototube current levels than those encountered here. This effect may be in either a positive or negative direction, although it is most commonly negative.

The phenomenon of fatigue is not a strictly reversible process, that is, the recovery curve is much less steep than the fatigue curve. However, the statistical method described here is based in part on the assumption that the drift is independent of the measurements made; accordingly, a modification was made in the procedure to ensure accurate results. When a particular element in a group of unknown solutions is to be determined, a quick initial run is made without the use of any statistical sequence or repetition of readings. This gives a good approximation of the concentrations of all the unknown solutions. The solutions are then grouped according to these preliminary results so that the concentrations of all the solutions within one group are very near one another. Standard solutions for each group are selected to approximate the concentrations of the group. The group of samples and standard solutions is then measured using the method of incomplete blocks, the normal drift curves are computed, and the results are corrected for drift. There is no irregular trend of the curves, since all the readings in a group are close together. This grouping is also advantageous from the standpoint that smaller errors in interpolation are introduced when readings on standards and unknowns are close together.

[3] R. W. Engstrom, J. Opt. Soc. Am. **37**, 420 (1947).

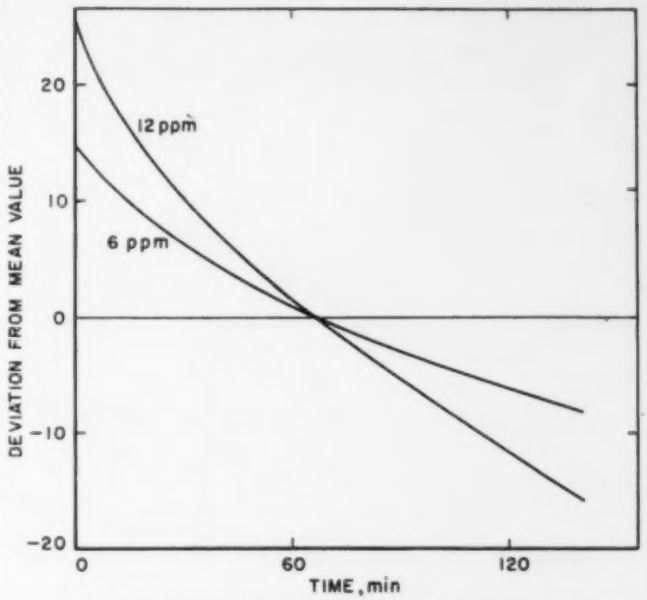

FIGURE 4. *Instrumental-drift curves of 6 ppm and 12 ppm lithium solutions.*

Instrument sensitivity is approximately 0.04 ppm per unit.

3. Conclusion

This paper has discussed a problem of instrumental drift in the laboratory to which a statistical solution involving incomplete blocks has been applied. While the magnitude of the drift encountered was not characteristic of the instrument, it served as a good example of a complicated drift problem. The statistical method improved the precision and provided a measure of the drift, except when quantities of widely different magnitudes were intercompared. Investigation showed that the drift resulted from fatigue of the photoelectric tube involved in the measurement, and that the drift was dependent upon the intensity of the light to which the tube was exposed. When drift is dependent on the magnitude of the measurement, it appears necessary to group the quantities according to order of magnitude before final measurements are made and the drift correction is applied.

Suggestions received from W. J. Youden during the course of this work are gratefully acknowledged.

WASHINGTON, August 15, 1958.

Journal of Research of the National Bureau of Standards Vol. 61, No. 6, December 1958 Research Paper 2919

Mechanism of Stress-Corrosion Cracking in the AZ31B Magnesium Alloy

Hugh L. Logan

The mechanism of stress-corrosion cracking of annealed AZ31B magnesium alloy in an aqueous $NaCl$-K_2CrO_4 solution was investigated. Cracking was predominantly an electrochemical process and was shown to be dependent on the rate of strain in the specimen following loading in tension. It is postulated that cracks develop if the protective film on the metal surface is ruptured (over narrow segments of the specimen) at a greater rate than it is repaired in the corroding medium. This would expose film-free metal that is anodic to the filmed metal.

1. Introduction

An investigation of the mechanism of stress-corrosion cracking of metals, sponsored jointly by the Corrosion Research Council and the National Bureau of Standards, is in progress. Certain of the magnesium alloys are admirably suited for such an investigation. While reports of failure in service are extremely rare, laboratory techniques that will produce stress-corrosion cracking in minutes are well known. As a result, extensive series of experiments can be performed in a conveniently short time.

In earlier work on the AZ31B magnesium alloy in this laboratory [1] [1] and elsewhere [2, 3], it was shown that in certain corrodents a threshold stress could be obtained below which cracking would not occur in 1,000 hr. Above this stress level, specimens would generally fail in less than 5 min. Furthermore, it was found, both in this laboratory and elsewhere, that the threshold stress was procedure sensitive [4]. It was appreciably higher if the specimens were loaded in tension before the corrodent was added than if the specimens were already immersed in the corrodent when the stress was applied. While a threshold stress was readily obtained in laboratory experiments, such threshold stress has not been observed in weather-exposure tests, most probably because these specimens were also subject to general corrosion. Furthermore, there was little difference in average times to failure, at a given stress, whether the specimens were exposed in a marine atmosphere at Hampton Roads, Va., or in an urban atmosphere at the Bureau. It was noted that, in both environments, most failures occurred during or following rain.

Two excellent motion pictures [5, 6] showing the stress-corrosion cracking of magnesium alloys have been prepared. Both showed plastic deformation preceding fractures, and Harwood [7] has suggested that some plastic extension must precede stress-corrosion cracking in all materials.

Priest [8] reported that cracking of the AZ61 alloy, once started, could be stopped by the application of cathodic protection. It was considered important to determine whether or not this was also possible with the AZ31B alloy and if so, to see what information the application of cathodic protection might give as to the mechanism of stress-corrosion cracking. The results of these investigations are reported in this paper.

[1] Figures in brackets indicate the literature references at the end of this paper.

2. Materials and Experimental Procedure

Four lots of the annealed AZ31B alloy material, in two gages, were used in the investigation. The chemical compositions of these materials, as reported by the manufacturers, did not differ appreciably from the nominal composition of aluminum 3.0 percent, zinc 1.0 percent, manganese 0.3 percent, with the impurities iron, nickel, and copper below the maxima permitted in ASTM Specification B90–57T. Both 0.064- and 0.125-in.-gage materials were used; however, most of the work was done with the thicker gage. The materials were machined into ½-in. reduced-section tensile specimens. In order to remove any impurities that may have been present on the surface of the sheet as a result of rolling, most specimens were immersed in an aqueous solution containing 30 ml of HNO_3 and 10 ml of H_2SO_4 per liter until approximately 0.001 in. of material had been removed from each face. A few specimens machined from sheet that had been chrome pickled were used with the original surface intact. The specimens were mounted into cells similar to those used in the earlier work [1] and were stressed in tension using lever systems. The corrodent [9] was an aqueous solution containing 3.5 percent of $NaCl$ plus 2.0 percent of K_2CrO_4 used at 30° ±2° C.

The threshold stress was determined at 30° C for the 0.125-in.-thick materials, in terms of the percent of yield strength of the individual lots of material. These yield strengths (0.2% offset) ranged from 21,900 to 23,100 lb/in^2.

In stressing the specimens, they were first subjected to the load of the lever alone, the equivalent stress being 2,000 to 4,000 lb/in.^{2}, depending on the specimen thickness. The full load was then added as a unit without impact in 1 to 3 sec, thus increasing the stress to the desired value[2] of 21,500 to 23,000 lb/in.^{2} Wire strain gages attached to opposite faces of specimens, read individually, were used to determine the strain produced in specimens by the addition of both the

[2] The lever system used in stressing the specimens had a ratio of 25 to 1. It was easily possible for one person to apply the full load to the lever without overload or impact.

minor and major stresses. As was to be expected, the major strain accompanied the application of the major load. It was noted, however, that specimens exposed in air at 30° C continued to extend after loading as long as the stress was applied. For the first few minutes, at any rate, the logarithm of the strain rate decreased linearly with the logarithm of the time.

Wire strain gages, of course, could not be used to determine the strain rate of specimens immersed in the corrodent. It was found, however, that in the strain-rate range that was to prove most important in the investigation (namely less than 500×10^{-6}/min) a relationship could be obtained between the strain rate determined using wire strain gages and that computed from dial-gage readings, the dial gage being actuated by the lever system. Thus, it was possible to follow the strain rate of a specimen stressed either in the corrodent or in air (beginning approximately 30 sec after stressing) from periodic readings of a dial gage. It was also possible to follow the strain rate of a specimen to some preselected value, using wire-strain gages, and then rapidly strip off the gages and add the corrodent. The extension at the moment the corrodent was added could be estimated very closely from the extrapolated strain rate-time curve.

3. Results and Discussion

3.1. Specimens Immersed in Corrodent Before Application of Stress

The strain rate increased markedly as the stress was increased above the threshold value (approximately 95½% of the yield strength). After tabulating the data from many specimens it was evident that if the corrodent was added before the major stress was applied and the strain rate exceeded $500 \pm 100 \times 10^{-6}$/min 1 min after the stress was applied, early failure by stress-corrosion cracking was to be expected. If the strain rate had fallen below this value, specimens generally did not fail in 1,000 min and were then removed from the corrodent; the earlier work had shown that if a specimen did not fail in this period it probably would not fail in 10,000 min. The times for failure for the various specimens are plotted against the percents of their respective yield strengths in figure 1.

In an earlier investigation [10] it was shown that straining of a magnesium alloy above its yield strength ruptured the protective surface film and exposed film-free metal that was approximately 240 mv anodic to the filmed surface. If the stress was held constant so that the strain rate fell off rapidly, the protective film re-formed on the surface where it had been ruptured.

It is postulated that above the threshold stress and at very high strain rates the protective film is ruptured on most of the surface of the specimen and corrosive attack is of a general nature. As the rate decreases, certain crystals work harden rapidly, the strain rate on them decreases to the point where, with the aid of the K_2CrO_4 inhibitor, a stable film is formed. With the average strain rate above

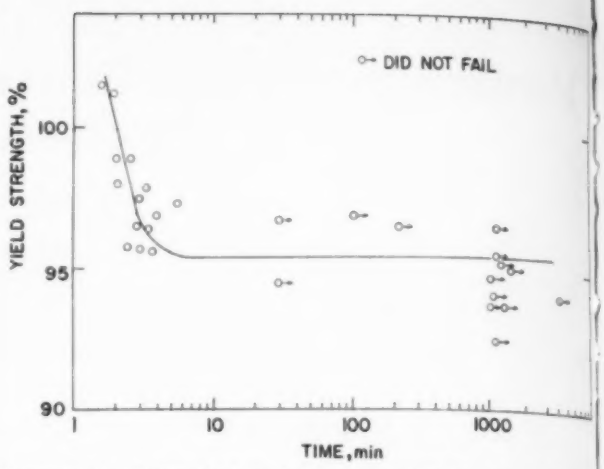

FIGURE 1. *Stress-time to failure curve for two lots of 0.125-in.-thick annealed specimens of AZ31B magnesium alloy.*

The corrodent was a 3.5 percent NaCl plus 2.0 percent K_2CrO_4 aqueous solution at 30°±2° C. Threshold stress was 95.5 percent of yield strength.

500×10^{-6}/min, however, the strain rate will be sufficiently high on other crystals so that the ruptured film over narrow areas perpendicular to the direction of strain will not be repaired. These film-free areas will be anodic to the filmed areas in the $NaCl$-K_2CrO_4 solution and most probably will be very small compared to the cathodic areas. Electrochemical corrosion will result and unless the strain rate decreases to such an extent that the protective film can re-form, stress cracks will be initiated and rapid failure of the specimen may follow.

If no cracks are formed before the average strain rate falls below 500×10^{-6}/min it is believed that film repair generally is as rapid as film rupture so that stress-corrosion cracking does not occur.

3.2. Specimens Stressed Before Immersion in Corrodent

It would be expected, then, that the specimen would not fail if it had been loaded in air and the corrodent was not added until the strain rate had fallen below 500×10^{-6}/min. Data indicated, however, that if the specimen had been given the nitric acid-sulfuric acid pickle prior to use, it would fail unless the strain rate had decreased to less than 100×10^{-6}/min before the addition of the corrodent. A typical strain rate-time curve for one of the specimens is shown in figure 2. It is seen that the strain rate increases very rapidly with the addition of the corrodent. The maximum strain rate reached was of course the average over the whole specimen. The subsequent behavior of the specimen indicated that the measured strain was most probably concentrated in short segments. Following this rapid increase in the strain rate, it decreased over most of the specimen length. However, the extension rate was still so high over several short lengths of the specimen that the protective film was not able to re-form and stress-corrosion cracks developed, probably between the 6th and 7th min. They had

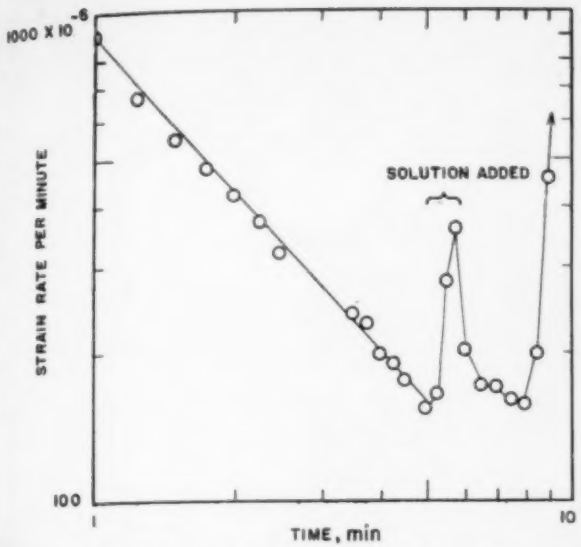

FIGURE 2. *Strain rate-time curve for specimen stressed for 5 min prior to addition of solution.*

*The first increase in strain rate, upon addition of corrodent, is believed to result from escape of dislocations previously blocked by oxide film.

penetrated so deeply by the 8th min that the average strain rate for the specimen was increasing rapidly and early failure would have occurred had not the stress been removed. Subsequent examination of the specimen showed that the cracks were segregated in several short lengths of the specimen and not more or less uniformly distributed as was the usual case. An anomalous change in strain rate has been reported for polycrystalline iron [11] and for single crystals of cadmium [12] under somewhat similar experimental conditions. No report of such behavior in magnesium alloys has come to the author's attention. If explanations given for other materials are also applicable to this alloy, it is suggested that the escape of dislocations from the metal was blocked by the film formed by pickling in the H_2SO_4-HNO_3 solution. Contact of specimens with the corrodent momentarily dissolved this film permitting the escape of trapped dislocations and the subsequent slip of individual crystals with the resulting marked change noted in the rate of extension of the specimen.

The corrodent was added to specimens, machined from a chrome pickled sheet, that were extending at a strain rate as high as 280×10^{-6}/min without subsequent failure. There was no measurable increase in the average strain rate with these specimens when the corrodent was added. At higher strain rates there was apparent dislocation escape at the machined edges with high local strain rates but not appreciable over-all increase in the strain rate. Failures resulted in these instances from cracks penetrating into the metal from the unprotected edges.

From these data, a tentative explanation can be made of the fact that most failures of weather-exposure specimens occurred following rain. It is suggested that solutions formed by water collecting on the specimens would dissolve the oxide film over some areas on the metal sufficiently to permit the escape of block dislocations. This would allow slip on certain microscopic areas and microscopic extension at a sufficiently high rate to initiate stress-corrosion cracking in the rainwater solution. Propagation of the cracks was sometimes stopped by evaporation of the solution before fracture was complete, as is shown in figure 3 taken from the earlier

FIGURE 3. *Specimen exposed to weather at NBS. Note stress-corrosion crack extending about ⅛ through specimen.*

Cracks of this type, found after rain, are believed to have been initiated by microscopic strain after dissolution of the oxide film by the rainwater-corrosion product solution which permitted the escape of blocked dislocations. Propagation of the cracks continued in this solution until failure occurred or evaporation of the solution stopped the reaction.

486859—59——5

paper [1]. In many cases, however, specimens were found to have failed completely after a rain.

3.3. Effects of Cathodic Protection

The effects of the application of cathodic protection to a specimen in which stress-corrosion cracks are developing offers much information as to the mechanism of the corrosive process. It was determined that 0.125-in.-thick specimens stressed to 98.6±0.4 percent of their yield strength would fail in an average period of 152 sec (standard deviation 39 sec). Cathodic protection [3] was applied to other specimens subjected to the same stress after exposure periods of 90 and 105 sec. A typical strain rate-time curve for these specimens is shown in figure 4. Examinations, using a binocular microscope, of specimens that had been removed from the corrodent after 35 to 40 sec exposure (stressed to 98.5 to 99% of the yield strength) indicated that cracking began during this interval. Hence, it is logical to assume that stress-corrosion cracking is an important factor in the increase in the extension rate as shown in figure 4 after 1 min of exposure. The marked change in extension rate with the application of cathodic protection (at a current density of 0.5 ma/cm^2 over the exposed area) indicated that cracking was almost if not completely stopped. This is substantiated by the fact that a specimen subjected to the conditions described above had not failed in 20 hr although it had extended about 0.04 in. Figure 5 shows the total extension and potential curves, for this specimen, plotted against the time just before and immediately following removal of the cathodic protection. It is seen that the specimen began to extend rapidly within 2 min after the protection was removed. It would have failed within another minute had not the stress been removed. There was no lasting polarization of the specimen as the result of cathodic protection. With its removal, the potential of the specimen immediately became approximately 400 mv more positive than it had been before protection was applied. The potential soon changed to the nominal value of −1.5 v and as the extension of the specimen opened up stress-corrosion cracks and exposed unfilmed metal, became still more negative.

[3] A cylindrical anode of stainless steel was placed around the inside of the cell. The ends of the specimen were masked off with "Duco Cement" so that only 15 cm^2 of the reduced area of the specimen was exposed to the corrodent.

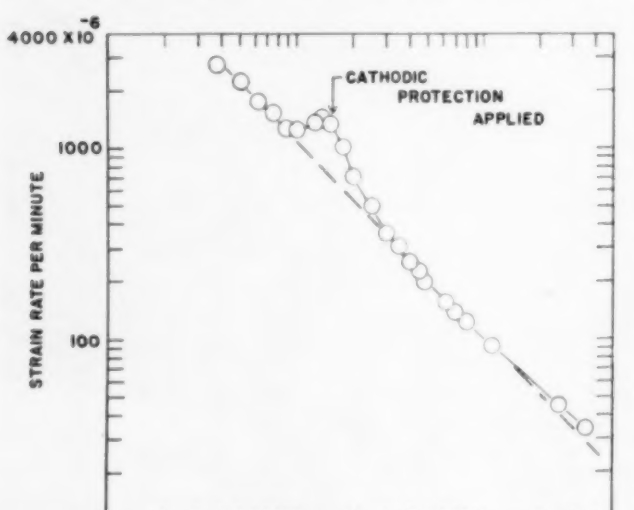

FIGURE 4. *Extension rate-time curve for specimen stressed to approximately 99 percent of its yield strength.*

Deviation of the curve from a straight line (after 1 min) was due to development of stress-corrosion cracks. (First cracks develop in 0.6 to 0.67 min). The application of cathodic protection stops the crack propagation; after 3 min the extension rate was approximately that to be expected had no cracking occurred.

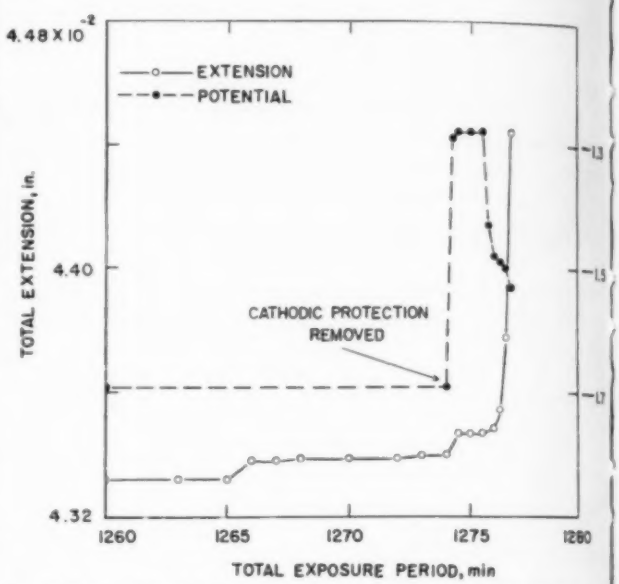

FIGURE 5. *Total extension-time and potential-time curves for specimen after immersion for 1,260 min in the corrodent.*

Note the change in potential with the removal of cathodic protection. Nominal potential of material with respect to a saturated calomel electrode was −1.50 v. The increase in extension rate after the removal of cathodic protection indicated that early failure of the specimen would have occurred had the stress not been removed.

The fact that stress-corrosion cracking can be stopped by the application of cathodic protection and that it will start again after the removal of this protection indicates that, in this alloy at least, it is primarily electrochemical. Specimens removed from the solution after the application of cathodic protection, contained cracks as is shown in figure 6. The depths to which cracks penetrated into the metal were determined on longitudinal metallographic sections taken well away from the edges. Maximum crack depths were determined in 0.125-in.-thick specimens to which protection was applied after 90 sec and in 0.064-in. specimens to which the protection was added after 60 to 65 sec. Cracking was assumed to have started in each case after 35 sec exposure. Penetration rates for some of the deeper cracks amounted to 4×10^{-4} in./sec. In the average exposure periods to failure for the two thicknesses of specimens, the penetrations would be approximately 0.02 and 0.047

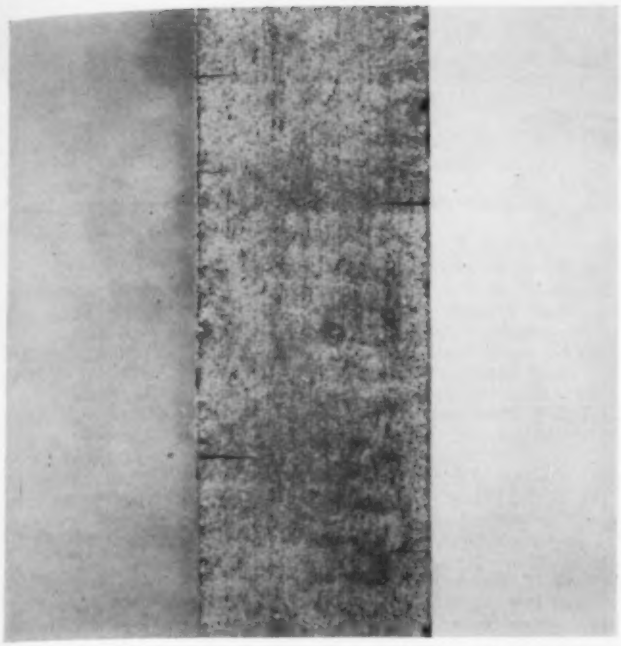

FIGURE 6. *Edge of specimen given cathodic protection 80 sec after application of major load.*

Cracks extending into specimen from edges are believed to have developed in period between 35th and 80th sec after loading. Specimen was removed from corrodent after approximately 18 hr exposure. × 10.

in. for the 0.064- and 0.125- in. specimens, respectively, i. e., 30 to 37 percent of the thickness of the specimens. Satisfactory measurements of the depth of penetration of the stress cracks at the point of failure are difficult to make, in that failures frequently result from a crack or cracks that penetrated into the specimen simultaneously from an edge and the opposite faces. It is believed that the weakening of the specimen by stress-corrosion cracks, to the point where it will fail by tensile fracture, resulted from penetration of the cracks at the rate indicated above, and was therefore primarily electrochemical.

3.4. Current Density Associated With Stress-Corrosion Cracking

If it can be assumed that Faraday's law applies to the dissolution of a metal as well as to its deposition, and if the electrochemical equivalent of the alloy is then taken to be the same as that for magnesium, the current density necessary to produce a crack penetration of 4.0×10^{-4} in./sec may be easily shown to be approximately 14 amp/cm^2. It should be noted that this calculation assumes only that the anodic reaction is 100 percent efficient; it requires no assumptions as to the width of the anodic area at the tip of the crack. If the anodic reaction is even in part,

$$Mg=Mg^{+}+e,$$

as has been suggested by Hoey and Cohen [13] and others instead of the conventional

$$Mg=Mg^{++}+2e,$$

the current density requirements are materially reduced. They are, however, much higher than any that have come to the author's attention for other materials. Hoar and Hines [14] estimated that a current density of 1.5 amp/cm^2 would account for the rate of crack penetration (2.2×10^{-5} in./sec) that they found in austenitic stainless steel in a boiling 42 percent $MgCl_2$ solution. They further report that under certain conditions, iron can be anodically dissolved at five times the rate of propagation of the cracks in the austenitic stainless steel reported above.

It is the author's experience that the stress-corrosion cracking of austenitic stainless steels in a boiling 42 percent $MgCl_2$ solution is a very much slower process than that of the AZ31B alloy in the NaCl-K_2CrO_4 solution. No failures of 0.064-in.-thick stock of type 304 stainless steel have occurred in this laboratory in less than 1 hr, although cracking is believed to have been initiated in less than 30 min.

The NaCl-K_2CrO_4 corrodent had a specific resistance of 11 ohm cm; with a difference in potential between the cathodes and anodes of less than ½ v, it is seen that the cathode areas must be largely within the cracks if a current of the magnitude indicated above is to flow. The motion pictures mentioned above showed copious quantities of gas (probably hydrogen) escaping from the stress-corrosion cracks which would also indicate that the cathodes were located primarily on the sides of the cracks.

4. Summary

1. A study has been made of the mechanism of stress-corrosion cracking of the AZ31B magnesium alloy in an aqueous solution containing 3.5 percent of NaCl plus 2.0 percent of K_2CrO_4.

2. Specimens dead loaded in tension by means of lever systems continued to extend for an appreciable time following stressing. Specimens stressed in the corrodent and extending at an average strain rate in excess of $500\pm100\times10^{-6}$/min, 1 min after the stress was applied, generally failed in less than 5 min by stress-corrosion cracking. Specimens extending at a slower rate, in most instances, did not fail in 1,000 min.

3. The strain rate for specimens stressed above the threshold stress prior to immersion in the corrodent must fall appreciably below 500×10^{-6}/min or the specimens will fail. The strain rate on addition of the corrodent depended on the surface condition of the specimen. It was suggested that the addition of the corrodent to specimens, pickled in the H_2SO_4-HNO_3 solution, permitted the escape of blocked dislocations and an appreciable increase in the average strain rate. Escape of dislocations from abraded or chrome pickled surfaces was prevented (except in some highly localized areas) and no increase in the average strain rate was noted.

4. The advancement of stress-corrosion cracks was halted for at least 20 hr by the application of a cathodic current of 0.5 ma/cm^2 of exposed area. With the removal of cathodic protection, stress-corrosion cracking continued so that the total time to failure (without protection) was little, if any more, than would have been required had the process not been interrupted by the application of cathodic protection.

5. The evidence indicates that stress-corrosion cracking of the AZ31B alloy is primarily an electrochemical process. Segments of a stressed specimen are strained at a higher-than-the-average rate so that the protective film on these crystal surfaces ruptured by the first strain is not repaired. These film-free surfaces are anodic to surfaces on which film repair has taken place. An electrochemical reaction occurs with very rapid attack at the anodes. This forms a groove or notch at the anode and acts as a region of stress concentration so that the material at the tip of the notch can continue to extend at stresses lower than the initial stress. The protective film does not re-form on these areas and the crack propagates primarily by the electrochemical action until failure occurs.

6. If it is assumed that the alloy has the same electrochemical weight as magnesium, it is calculated from crack-penetration rates that there is an effective current density of 14 amp/cm^2 at the crack tips.

7. It is suggested that the effect of rain on weather-exposure specimens was to form a solution with the corrosion products that would permit the escape of dislocations and hence the rapid extension of micro-segments of the specimen as described in 3 above. This would result in partial or complete failure in the rainwater solution by the process postulated in 5 above.

5. References

[1] H. L. Logan and H. Hessing, Stress corrosion of wrought magnesium base alloys, J. Research NBS **44,** 233 (1950) RP2074.

[2] W. S. Loose and H. A. Barbian, Stress corrosion testing of magnesium alloys, Symposium on Stress Corrosion Cracking of Metals, ASTM, AIME, p. 273, 1944.

[3] R. B. Mears, R. H. Brown, and E. H. Dix, Jr, A generalized theory of stress corrosion of alloys, Symposium on Stress Corrosion Cracking of Metals, ASTM, AIME, p. 323, 1944.

[4] W. S. Loose, private communication.

[5] D. K. Priest, Motion picture of stress corrosion cracking of magnesium alloy; D. K. Priest, F. H. Beck and M. G. Fontana, Trans. ASM **47,** 473 (1955).

[6] R. D. Williams, Film produced by Aluminum Company of America Research Laboratories. Shown NACE Conference March 16, 1954 (Kansas City, Mo.).

[7] J. J. Harwood, The phenomena and mechanism of stress corrosion cracking, Stress corrosion cracking and embrittlement, p. 1 (edited by W. D. Robertson, John Wiley & Sons, Inc., 1956).

[8] D. K. Priest, The mechanism of stress corrosion cracking observed in a magnesium alloy, Stress corrosion cracking and embrittlement, p. 81 (edited by W. D. Robertson, John Wiley & Sons, Inc., 1956).

[9] G. F. Sager, R. H. Brown, and R. B. Mears, Tests for determining susceptibility to stress corrosion cracking, Symposium on Stress Corrosion Cracking of Metals, ASTM, AIME, p. 255, 1944.

[10] H. L. Logan, Film-rupture mechanism of stress corrosion, J. Research NBS, **48,** 99 (1952) RP2291.

[11] C. S. Barrett, An abnormal after-effect in metals, Acta Met., **1,** 2 (1953).

[12] C. S. Barrett, After-effects in polycrystalline cadmium. Trans. AIME **197,** 1652 (1953).

[13] G. R. Hoey and M. Cohen, Corrosion of anodically and cathodically polarized magnesium in aqueous media, J. Electrochem. Soc. **105,** 245 (May 1958).

[14] T. P. Hoar and J. G. Hines, The stress corrosion cracking of austenitic stainless steels, J. Iron Steel Inst., **182,** 124 (1956).

Washington, August 20, 1958.

Journal of Research of the National Bureau of Standards Vol. 61, No. 6, December 1958 Research Paper 2920

Evaluation of Lens Distortion by Visual and Photographic Methods[1]

Francis E. Washer, William P. Tayman, and Walter R. Darling

The evaluation of lens distortion by photographic and visual methods is discussed. Measurements made on a single lens using the two methods are reported. The precision of measurement of each method is determined which shows that the observed differences must be attributed to systematic error. Various sources of systematic error are considered. Uncompensated differential plate tipping is identified as the most probable cause of the observed differences. A method of correction is developed. It is concluded that when work is done with extreme care and with due account taken of various insidious sources of error, it is possible to achieve comparable results with either method.

1. Introduction

The measurement of radial distortion in the focal plane of photographic objectives has been the subject of intensive study since the advent of aerial mapping from photographs. This particular aberration is of prime interest as its magnitude determines the accuracy with which the final negative maintains the correct relationships among the array of point images making up the photograph of the corresponding array of points in the area photographed. It was early realized that the reliability of the quantitative information obtained from a photograph increased as the distortion in the taking lens decreased. Consequently, the development of improved lenses was encouraged with the result that succeeding series of new lenses were characterized by ever lower values of distortion.

During this period of change, diverse methods of evaluating the distortion of lenses came into use at various laboratories. The reason for such diversity was primarily the availability of given types of measuring instruments in various laboratories. There are now three principal methods of measuring distortion plus numerous additional methods that are either the inverse of one of the principal methods or a variation thereof. The nodal slide bench is one of the oldest methods; this is a visual method capable of high accuracy and is perhaps the most widely used. The photographic method is more recent and arose out of the desire to make measurements under conditions approximating that of use. The third principal method is the goniometric method which is used to considerable extent in Europe.

Because of the diversity of methods being used in the evaluation of distortion, it seems worthwhile to investigate the results of measurement made in a single laboratory on a number of lenses by a variety of methods to determine whether or not the values so obtained varied appreciably with method. This is being done for several different methods and some preliminary results are reported herein for two methods.

The two methods are as follows:

A. Photographic, precision lens testing camera,
B. Visual, nodal slide optical bench.

[1] This work was performed in connection with the research project sponsored by the U. S. Air Force.

2. Methods of Measurement

Methods A and B have been described at some length in the literature. However, for purposes of clarity, in the following section, a brief description of these methods is given.

2.1. Precision Lens Testing Camera. Method A

The precision lens testing camera [1][2] shown in figure 1 was developed at the Bureau by I. C. Gardner and F. A. Case. It is one of the earliest successful devices developed to measure the performance of lenses by photographic means. It consists of a bank of collimators spaced at 5-deg intervals having resolution test charts as reticles. The lens under test is mounted at the center of convergence of the collimator fan and can be aimed at any one of them by rotation of a carriage which carries the lens holder and camera back whereon the photographic recording plate is mounted. As presently constituted, the lens testing camera has 10 collimators covering a total angle of 45 deg. When used to test wide angle lenses, the camera is aimed at one of the extreme collimators (position I) and the test made. In order to cover a complete diameter, a second test is made with the camera aimed at the collimator at the opposite ex-

[2] Figures in brackets indicate the literature references at the end of this paper.

FIGURE 1. *Precision lens testing camera (Method A).*

This photograph shows the camera back with a light metering device in place on the plate holder. The values of illumination in the focal plane are read from the large meter above the collimator. Use of this device enables the operator to adjust for uniform exposure in making the test negatives from which the values of distortion, D_A, are obtained.

treme (position II). It has been found by experience that the results obtained from two negatives made in this manner are quite reliable.

To determine the value of the distortion, the best row of images is selected on the negative made in position I. The separation of all images on this row from the image formed by light from the 0° collimator is measured. The equivalent focal length (*EFL*) is then determined from the relations

$$f_1 = d_5 \cot \beta_5, \tag{1}$$

$$f_2 = d_{10} \cot \beta_{10}, \tag{2}$$

$$EFL = \frac{f_1 + f_2}{2}. \tag{3}$$

Where d_5 and d_{10} are the measured distances on the negative separating the images formed by the lens for the target in the 0° collimator from the corresponding images formed by the lens for the targets in the collimators located at $\beta = 5°$ and 10° respectively from the 0° collimator. One then determines the distances from the 0° image to the other images using the relation

$$d_\beta = EFL \tan \beta. \tag{4}$$

The difference between the distances found with the aid of eq (4) and the corresponding measured distance for a given value of β is the value of the distortion at that point. It is positive if the measured location of the image is farther from the central image than the computed location. Similar computations are made for the negative obtained for position II and the results averaged and accepted as final.

It has always been maintained that the probable error of values of distortion obtained by this method did not exceed ±0.020 mm. The sources of error arising from error in angle in plate measurement are discussed in an earlier publication [2] where it was established that errors from this source should not exceed ±0.013 mm.

In making the negatives, the collimator targets are illuminated by light from a tungsten source after passing through a K–3 filter. Eastman Kodak Spectroscopic plates, emulsion Type V–F, are used to record the image formed by the lens under test. The exposed plates are processed in trays containing Eastman Developer D–19 and 68° F for 3 min with continuous agitation.

2.2. Visual Optical Bench, Direct Nodal Slide. Method B

The visual optical bench has long been the basic tool for evaluating the optical constants of lenses. The one used at the Bureau has been in existence for approximately 30 yr and can still be regarded as a precision instrument [3]. For measuring distortion, one uses a collimator, nodal slide lens holder shown in figure 2, and micrometer microscope. The lens is carefully alined in the holder and the axial image formed by the lens under test of the illuminated

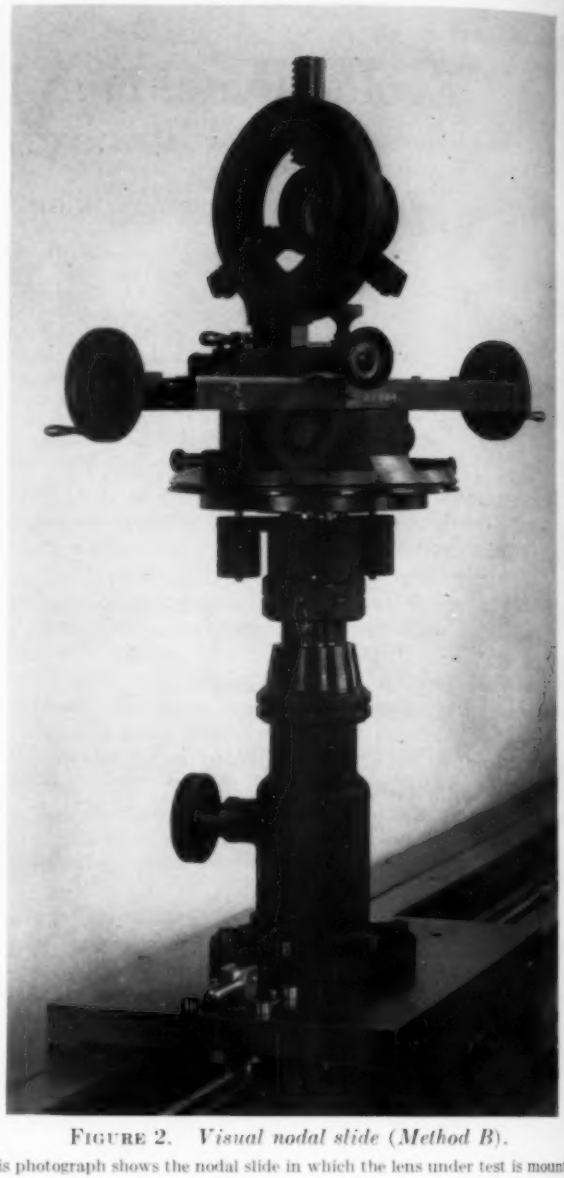

FIGURE 2. *Visual nodal slide (Method B).*
This photograph shows the nodal slide in which the lens under test is mounted.

reticle of the target is brought into coincidence with the object plane of the viewing microscope. The reticle is illuminated by filtered light from a tungsten source. The effective wavelength is approximately 575 mμ. By a series of successive adjustments, a condition is found for which a small rotation of the lens about a vertical axis does not produce a displacement of the axial image viewed. The rear nodal point of the lens is then considered to coincide with the center of vertical rotation of the nodal slide.

Assuming the equivalent focal length, f, to be known, the nodal slide is rotated by amount β about the vertical axis using the calibrated circle of the nodal slide to position it exactly. The entire saddle carrying the nodal slide and lens is then moved away from the microscope toward the collimator by an amount, $f(\sec \beta - 1)$. The viewing microscope is shifted laterally to the new position of the image

and its dial read and recorded as reading R. The nodal slide is then rotated to position $-\beta$ and a second setting of the microscope, L, is made. The distortion, D_β, is then obtained from the relation

$$D_\beta = \frac{(R-L)}{2} \sec \beta. \quad (5)$$

3. Results of Measurement

At the time this study was initiated, it was planned to make measurements of distortion on a series of seven or more lenses by different methods and to compare the results. Measurements have been made on seven lenses by two different methods and comparative tables of results prepared. All values of distortion are referred to the calibrated focal length [4] for ease of comparison. In general the results are comparable and all values fall within the range of ± 0.02 mm which has been established here as the accepted maximum value of the probable error for distortion measurements. However, the agreement fell somewhat short of that expected in that systematic differences were observed. Because of these systematic differences, it was deemed wise to concentrate on the analysis of the results of measurement made on a single lens by the two methods, in the belief that more information on the causes of lack of agreement could be gained thereby. This has proved to be the case, and in the following pages some of the steps in this investigation and analysis are reported.

3.1. Values of the Distortion by Methods A and B for Wide Angle Lens No. 3

The values of the distortion referred to the calibrated focal length obtained photographically with the precision lens testing camera (D_A) and visually with the nodal slide optical bench (D_B) are shown in table 1. These values are based on a single run by each method. For method A, a single run provides two negatives, one each for positions I and II; each negative is measured 5 times and the results are averaged. For method B, a single run consists of two independent sets of measurements; the accepted values of distortion are based on the average of two sets. It is clear from table 1, that the values of D_A and D_B do not depart from their average by more than 12 μ at most and accordingly either set of values can be regarded as accurate within the usual tolerance of ± 20 μ. However, the differences in the values obtained by the two methods $D_B - D_A$ which are also shown in table 1 do not appear to be random but rather appear to indicate the presence of systematic error. This is shown more strikingly in figure 3 where $D_B - D_A$ is plotted as a function of β.

TABLE 1. *Measured values of the distortion versus angular separation β from the axis for wide angle lens No. 3*

The values obtained with the precision lens testing camera are designated D_A while those obtained on the nodal slide optical bench are designated D_B. All values are referred to the calibrated focal length and are given in microns.

β	D_A	D_B	$D_B - D_A$
deg			
0	0	0	0
5	−11	−6	5
10	−18	−8	10
15	−17	1	18
20	−2	19	21
25	32	50	18
30	65	89	24
35	97	104	7
40	76	80	4
45	−97	−104	−7

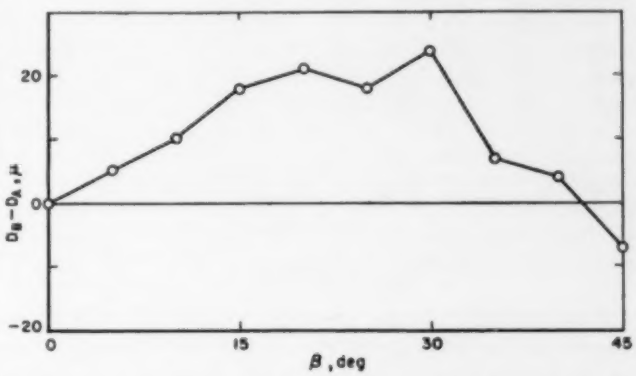

FIGURE 3. *Variation of distortion difference, $D_B - D_A$, with angular separation from the axis β.*

3.2. Precision of Measurement for Visual Nodal Slide

One's first thought when confronted with discrepancies in the results of measurement obtained by two different methods is to make additional measurements using the method most likely to be suspected. The visual nodal slide optical bench in use at the time of these measurements was somewhat antiquated so it seemed proper to check its performance first. Five additional independent sets of measurements were made. A pinhole reticle was used initially, but a transparent crossline was substituted for it during two sets of measurements. Some time elapsed between the first two sets of measurements and the 3d, 4th, 5th, and 6th calibration. During this time, the lens cells were removed from the test barrel and replaced. A similar operation occurred between calibrations 6 and 7. Additional care was taken in checking alinement in the course of calibration 3 and 7. Each set of data was carefully processed and the values of distortion adjusted to a calibrated focal length with maximum plus at 35° and maximum minus at 45°. The results are shown in table 2. Cursory examination of these values indicates quite good agreement, so an average for all seven including the first two calibrations was made. The table also shows the probable error of a single determination, and the value of PE_s. The values of PE_s are so low that it seems there is no cause to question the precision of method B. While there may be a systematic error present that impairs the accuracy, none comes to mind at the present writing.

TABLE 2. *Values of the distortion, D_B, versus β for seven sets of measurement using method B*

These values of D_B were obtained for wide angle lens No. 3 with the visual nodal slide bench. All values are referred to the calibrated focal length and are given in microns. The values of PE_s are also shown.

β	Values of D_B obtained from calibration							Average value of D_B	PE_s
	1	2	3	4	5	6	7		
deg									
0	0	0	0	0	0	0	0	0	±0
5	−6	−6	−7	−7	−7	−8	−8	−7	1
10	−7	−8	−9	−8	−6	−6	−11	−8	1
15	1	1	1	4	3	3	−7	1	2
20	19	19	21	24	23	27	13	21	3
25	48	52	52	53	60	53	45	52	3
30	88	89	85	88	85	87	84	87	1
35	103	104	105	107	104	105	111	106	2
40	83	78	86	82	80	69	77	79	4
45	−103	−104	−105	−107	−104	−105	−111	−106	2

3.3. Precision of Measurement for Lens Testing Camera

a. First Trial

Comparison of the average values of distortion based on the seven separate determinations shown in table 2 with the values of D_B for the first two determinations shown in table 1 indicates that the difference between D_B and D_A can not be explained by lack of precision in method B. The average value of D_B for the seven calibrations differ at most by 2 μ from the average of the first two calibrations. Accordingly further tests by method A were made. Five new negatives were made in position I on the precision lens testing camera and five new negatives were made in position II. Test negatives 1 to 4 were made under identical conditions in position I so also were test negatives 5 to 8 in position II. The lens was removed, replaced, and realined for test before making negatives 9 and 10. Each negative was measured and the distortion evaluated separately and the results are shown in table 3. Part (a) of table 3 shows the results for position I, and part (b) shows the results for position II. In part (c), the results shown in parts (a) and (b) are combined by pairs and results of this combination are shown. The values of the precision index, PE_s, are somewhat higher in parts (a) and (b) than those shown in part (c) where the results are averaged in the usual manner. The differences in the average value of D_A for positions I and II are not regarded as serious as it is presumed to arise from a small amount of plate tipping of a nature that becomes negligible on averaging. The final values of the average, D_A, shown in part (c) of table 3, differ by a few microns from the values of D_A shown in table 1, but have not changed in a manner that appreciably reduces the values of $D_B - D_A$. The values of the precision index PE_s shown in part (c) compare favorably with the similar values shown in table 2 for method B. However, the magnitudes of PE_s for both methods are too small to justify the existence of differences in the values of the distortion as great as are found.

TABLE 3. *Values of the distortion, D_A, versus β for the first trial using method A*

These values of distortion were obtained for Wide Angle Lens No. 3 with the precision lens testing camera. All values are referred to the calibrated focal length and are given in microns. In part (a) values are given for position I for five negatives, together with the average value of D_A and the value of PE_s. In part (b), similar results are given for position II, and in part (c) average values for paired negatives for position I and II are given.

(a)

β	Values of D_A obtained in position I from negatives					Average value of D_A	PE_s
	1	2	3	4	10		
deg							
0	0	0	0	0	0	0	±0
5	−13	−13	−13	−11	−9	−12	1
10	−21	−18	−22	−18	−15	−19	2
15	−16	−12	−15	−9	−5	−11	3
20	2	1	1	3	7	3	2
25	20	24	28	26	32	26	3
30	53	60	63	58	64	60	3
35	87	91	96	86	83	89	4
40	81	75	84	77	83	80	3
45	−87	−91	−96	−86	−83	−89	4

(b)

	Values of D_A obtained in position II for negatives					Average value of D_A	PE_s
	5	6	7	8	9		
deg							
0	0	0	0	0	0	0	±0
5	−10	−12	−16	−12	−12	−12	1
10	−15	−22	−22	−19	−18	−19	2
15	−10	−23	−20	−16	−18	−17	3
20	6	−9	−6	−4	2	−2	5
25	34	22	22	22	33	26	5
30	72	50	63	56	75	63	8
35	108	102	100	101	117	106	5
40	88	86	82	84	95	87	3
45	−107	−103	−101	−100	−117	−106	5

(c)

	Values of D_A obtained in position I and II for negative pairs					Average value of D_A	PE_s
	1 and 5	2 and 6	3 and 7	4 and 8	10 and 9		
deg							
0	0	0	0	0	0	0	±0
5	−12	−12	−14	−12	−10	−12	1
10	−18	−20	−22	−18	−16	−19	2
15	−13	−18	−18	−12	−12	−15	3
20	4	−4	−4	0	4	0	3
25	27	23	25	24	32	26	2
30	62	55	63	57	68	61	4
35	98	96	98	94	100	97	2
40	84	80	83	80	89	83	2
45	−97	−97	−98	−93	−100	−97	2

b. Second Trial

While the first values of the distortion obtained in section 3.3a compare favorably with the values shown in table 1 for method A, it is disquieting to see the large discrepancies that exist between values obtained in positions I and II. While it is probable that these discrepancies arise from actual differences in performance along the opposing radii, nonetheless it seemed worthwhile to determine whether or not any maladjustment of the lens testing camera could produce this effect. Careful analysis showed that when the camera was properly alined

so as to point properly at the center of the collimator reticle for position I that it did not so point when swung into position II. Instead there was an error of 36 sec in the pointing for position II. Computation indicated that this defect in alinement in position II could produce small errors in the distortion although the indicated magnitude was too small to change the values of D_A by more than a few microns. This alinement error was corrected, the angles were recalibrated, 10 additional negatives were made, and the measurements described in section 3.3a were repeated. The new results are shown in table 4.

TABLE 4. *Values of the distortion, D_A, versus β for the second trial using method A*

These values of the distortion were obtained for Wide Angle Lens No. 3 with precision lens testing camera following its recalibration. All values are referred to the calibrated focal length and are given in microns. In part (a) values are given for position I for five negatives together with the average value of D_A and the value of PE_v. In part (b) similar results are given for position II, and in part (c), averaged values for paired negatives for positions I and II are given.

β	(a) Values of D_A obtained in position I for negatives					Average value of D_A	PE_v
	11	12	13	14	20		
deg							
0	0	0	0	0	0	0	±0
5	−10	−12	−12	−16	−15	−13	2
10	−18	−23	−21	−19	−19	−20	2
15	−12	−20	−18	−15	−16	−16	2
20	1	−9	−7	0	−2	−3	3
25	27	16	19	25	22	22	3
30	64	57	57	68	62	62	3
35	95	91	94	94	98	94	2
40	86	82	86	83	87	85	2
45	−95	−91	−94	−94	−98	−94	2

β	(b) Values of D_A obtained in position II for negatives					Average value of D_A	PE_v
	15	16	17	18	19		
deg							
0	0	0	0	0	0	0	±0
5	−19	−19	−19	−19	−17	−19	0
10	−28	−26	−25	−26	−26	−26	1
15	−27	−23	−23	−21	−23	−23	1
20	−11	−8	−9	−5	−9	−8	2
25	17	18	21	25	21	20	2
30	58	56	55	62	54	57	2
35	99	102	100	104	96	100	2
40	77	80	84	85	78	81	3
45	−99	−102	−100	−104	−96	−100	2

β	(c) Values of D_A obtained in positions I and II for negative pairs					Average values of D_A	PE_v
	11 and 15	12 and 16	13 and 17	14 and 18	20 and 19		
deg							
0	0	0	0	0	0	0	±0
5	−14	−16	−16	−18	−16	−16	1
10	−23	−24	−23	−22	−22	−23	1
15	−20	−22	−20	−18	−20	−20	1
20	−5	−8	−8	−2	−6	−6	2
25	22	17	20	25	22	21	2
30	61	56	56	65	58	59	3
35	97	96	97	99	97	97	1
40	82	81	85	84	82	83	1
45	−97	−96	−97	−99	−97	−97	1

When the final results obtained from negatives 11 to 20 are compared with those obtained from negatives 1 to 10, it is clear that while there is slightly better agreement at the large angles than before, the agreement is somewhat worsened at the small angles. Finally, the average values for the second trial, shown in part (c) of table 4, are substantially the same as those obtained from the first trial, shown in table 3.

C. Summation

The final accepted values obtained by methods A and B are brought together for comparison in table 5. The values of D_A and D_B differ slightly from the values shown in table 1 but are believed to be more reliable as each value is the average of many more determinations. It is noteworthy that the magnitude of ΔD has increased slightly. This table also shows the probable error of the mean for the values of D_A, D_B, and ΔD. Consideration of these various values indicates that the systematic error still exists and has not been reduced by the multiplication of measurements.

TABLE 5. *Comparison of the average values of distortion, D_A, derived from 20 negatives using method A and the average values of distortion, D_B, derived from sevenc alibrations using method B.*

The difference is shown as $\Delta D = D_B - D_A$. Values of the probable error of the mean for each set of determinations are also shown. All values are expressed in microns.

β	D_A	D_B	$\Delta D = D_B - D_A$	PE_m for		
				D_A	D_B	ΔD
0	0	0	0	±0.0	±0.0	±0.0
5	−14	−7	7	.6	.4	.7
10	−21	−8	13	.6	.4	.7
15	−17	1	18	.9	.8	1.2
20	−3	21	24	1.0	1.1	1.5
25	24	52	28	0.8	1.1	1.4
30	60	87	27	1.0	0.4	1.1
35	97	106	9	0.3	.8	0.9
40	83	79	−4	.6	1.5	1.6
45	−97	−106	−9	.3	0.8	0.9

3.4. Effect of Plate Curvature

In view of the known effects of plate curvature on the values of distortion, [2] it seemed worthwhile to examine the emulsion surfaces of the negatives used in method A. This was done and a small amount of plate curvature was found. However, in no instance was curvature present in sufficient amount to produce more than one-fourth of the measured differences in distortion values. The average departure from flatness for the 20 negatives could not produce differences in distortion in excess of one-tenth of that found. It may therefore be stated that plate curvature is not a prime cause of the differences in values of distortion found by the two methods.

3.5. Effect of Plate Tipping

The plate holder in the precision lens testing camera is so constructed that the emulsion surfaces are coplanar for positions I and II. For the coplanar

or parallel plane condition, small departures of the plane from true normality to the optical axis of the system under test would not produce variations in the average value of distortion even though the measured distortion on either side of center would be different. However, if a slight warpage of the holder has occurred, the plate in position II would not be coplanar with that in position I and a small amount of asymmetric distortion would persist and adversely affect the final average. Accordingly a procedure was developed for checking this possibility based on the plate tipping analysis described in an earlier paper [5]. The final product of this analysis is shown in table 6. When the values of ΔD in table 5 are divided by the appropriate multiplier M, then the magnitude of $f\epsilon_t$ can be obtained for each value of ΔD, where ϵ_t is the angle between the plane of the plate in position I and that in position II. This was done and the results are shown in table 7.

TABLE 6. *Values of $\tan^2\beta$ and the multiplier, M, for a value of $f\epsilon_t = 1.00$ micron*

The multiplier, M, is so calculated that when it is multiplied by a given value of $f\epsilon_t$, it yields the distortion correction referred to the calibrated focal length.

Angular separation, β, from axis	$\tan^2\beta$	M
deg		
0	0.0000	0.0000
5	.0077	−.0690
10	.0311	−.1234
15	.0718	−.1630
20	.1325	−.1865
25	.2174	−.1913
30	.3334	−.1727
35	.4903	−.1234
40	.7041	−.0314
45	1.0000	−.1235

TABLE 7. *Computation of $\overline{f\epsilon_t}$ to determine effective amount of uncompensated plate tipping that may be present in method A*

Values of $f\epsilon_t$ are obtained for each value of ΔD given in table 5; the average $\overline{f\epsilon_t}$ for β ranging from 10° to 30° is −129 microns; this value is used to determine the probable contribution to distortion $M\overline{f\epsilon_t}$. The last column shows the magnitude of difference that remains. All values are given in microns.

β	ΔD	$\overline{f\epsilon_t} = D/M$	$M\overline{f\epsilon_t}$	$\Delta D + M\overline{f\epsilon_t}$
deg				
0	0	----	----	----
5	7	−101	−9	−2
10	13	−105	−16	−3
15	18	−110	−21	−3
20	24	−129	−24	0
25	28	−146	−25	3
30	27	−156	−22	5
35	9	−73	−16	−7
40	−4	127	4	0
45	−9	−73	16	7

The values of $f\epsilon_t$ that are shown in table 7 indicate that some effect of uncompensated plate tipping may be present in the values of distortion obtained by method A. All values of $f\epsilon_t$ are of the same sign and are of the same order of magnitude except that computed for $\beta = 40°$. The value of ΔD for this point is so small (4μ) that little weight can be given to the values of $f\epsilon_t$, derived from it. While there is appreciable variation in the remaining values of $f\epsilon_t$, it must be remembered that the warping that introduces this effect probably bends the plate slightly as well as tipping it. An average $f\epsilon_t$, for the range 10° to 30° was determined and found to be $f\epsilon_t = -129$ microns which indicates that the effective angle between the plates in positions I and II is approximately 3.0 min of arc. The quantity $\overline{Mf\epsilon_t}$ was then evaluated for each value of β. The degree of compensation achieved by assumption of this amount of uncompensated plate tipping is shown graphically in figure 4. The solid curve shows the variation of the quantity $-\overline{Mf\epsilon_t}$ with β while the circles show the corresponding values of ΔD. The quantity, $D+\overline{Mf\epsilon_t}$, would equal zero if $f\epsilon_t$ was invariant for all values of β. However, the departure from zero is sufficiently small that it is evident that uncompensated differential plate tipping makes an important contribution to the systematic error whose cause is being sought.

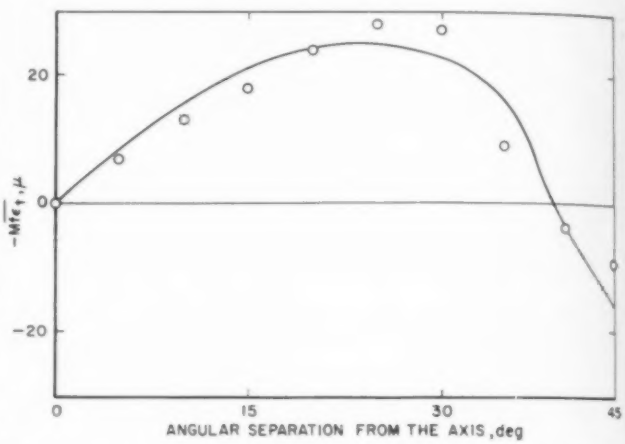

FIGURE 4. *Variation of the quantity $-M\overline{f\epsilon_t}$ with angular separation from the axis β.*

Compensation of the differences in distortion values ($\Delta D = D_B - D_A$) by an assumed differential plate tipping ϵ of approximately 3 min of arc. The solid line is a plot of the function, $-M\overline{f\epsilon_t}$; the circles are corresponding values of ΔD

Following this work careful measurements on the plate holder were made to determine if this warpage actually existed. While measurable values of warpage were found that were somewhat smaller than might be inferred from the results shown in table 7, they appeared large enough to warrant correction. Accordingly a new heavier plate holder has been constructed and has replaced the one in use during this experiment. Recent measurements show that the values of $\Delta D = D_B - D_A$ now obtained are less than one-fourth the values of ΔD obtained prior to the change.

In table 8, the correction $M\overline{f\epsilon_t}$ is applied directly to the values of distortion D_A. The corrected value $D_A' = D_A - M\overline{f\epsilon_t}$ is given in the table and agrees closely with the corresponding values of D_B. The last column shows the differences still remaining between values of D_A' and D_B. It is clear that the remaining discrepancies are so small in comparison with the values of D_A' and D_B that they can be neglected.

TABLE 8. *Comparison of D_A' (the value of D_A after correction for plate tipping) and D_B*

The values of D_A and D_B are taken from table 5; values of $Mf_{\epsilon t}$ are taken from table 7. The last column $\Delta D'$ shows that the discrepancies between the two methods have been reduced to tolerable values. All values are given in microns.

Angular separation from axis	D_A	$\overline{Mf_{\epsilon t}}$	$D_A'=D_A-\overline{Mf_{\epsilon t}}$	D_B	$\Delta D'=D_B-D_A'$
deg					
0	0	0	0	0	0
5	−14	−9	−5	−7	−2
10	−21	−16	−5	−8	−3
15	−17	−21	4	1	−3
20	−3	−24	21	21	0
25	24	−25	49	52	3
30	60	−22	82	87	5
35	97	−16	113	106	−7
40	83	4	79	79	0
45	−97	16	−113	−106	7

4. Conclusion

It is evident from the foregoing study that highly accurate values of distortion can be obtained by either the photographic method using the precision lens testing camera or the visual method using the nodal slide bench. For each method, values can be obtained that are precise to within ±4 microns. When proper care is taken, the values obtained by either of the methods do not depart from the common average by amounts exceeding ±5 microns.

It is however clear that to obtain and maintain such high accurarcy it is necessary to be constantly on the alert for various insidious sources of error such as plate curvature, differential plate tipping, and incorrect prime calibration of angles used in the determinations.

5. References

[1] I. C. Gardner and F. A. Case, Precision camera for testing lenses, J. Research NBS **18,** 449 (1937) RP984.

[2] F. E. Washer, Sources of error in various methods of airplane camera calibration, Photogrammetric Eng. XXII, p. 727 (1956).

[3] A. H. Bennett, The distortion of some typical photographic objectives, J. Opt. Soc. Am. and Rev. Sci. Instr. **14,** 245 (1927).

[4] F. E. Washer and F. A. Case, Calibration of precision airplane mapping cameras, Photogrammetric Eng. XVI, 502 (1950); J. Research NBS **45,** 1 (1950) RP2108.

[5] F. E. Washer, Effect of camera tipping on the location of the principal point, J. Research NBS **57,** 31 (1956) RP2691.

WASHINGTON, April 12, 1958.

INDEX TO VOLUME 61

July to December 1958—Research Papers 2877 to 2920

A

Page

Aberration, longitudinal spherical, optical T-bench method of measuring, RP2880 ... 31
Acoustic wave field, diffraction and reflection of, RP2906 ... 343
Alkali silicate glasses, density formula for, from annealing to glass-processing temperatures, RP2915 ... 463
Allen, H. C., Jr., E. K. Plyler, E. D. Tidwell, Emission spectrum of carbon monoxide from 2.3 to 2.5 microns, RP2883 ... 53
Ammonia, vibration-rotation bands of, RP2894 ... 123
An electrical-analog method for transient heat-flow analysis, RP2892 ... 105
Atmospheric transmittance of Mauna Loa, studies of, RP2910 ... 419

B

Benedict, W. S., E. K. Plyler, E. D. Tidwell, Vibration-rotation bands of ammonia: 1. The combination bands $\nu_2-(\nu_1, \nu_3)$, RP2894 ... 123
Black, I. A., L. H. Bolz, F. P. Brooks, F. A. Mauer, H. S. Peiser, A liquid-helium cold cell for use with an X-ray diffractometer, RP2907 ... 367
Bolz, L. H., I. A. Black, F. P. Brooks, F. A. Mauer, H. S. Peiser, A liquid-helium cold cell for use with an X-ray diffractometer, RP2907 ... 367
Brittle cermets, evaluation of tensile, compressive, torsional, transverse, and impact tests and correlation of results for, RP2895 ... 149
Brooks, F. P., I. A. Black, L. H. Bolz, F. A. Mauer, H. S. Peiser, A liquid-helium cold cell for use with an X-ray diffractometer RP2907 ... 367
Buckley, F., Dielectric constant of hydrogen-bonded liquids, RP2905 ... 325
Bunting, E. N., F. R. Lippincott, A. Van Valkenburg, C. E. Weir, Infrared studies on polymorphs of silicon dioxide and germanium dioxide, RP2885 ... 61

C

Calcia-titania, revision of the phase equilibrium diagram of the binary system showing the compound $Ca_4Ti_3O_{10}$, RP2913 ... 437
Calcium aluminate hydrates, a study of, RP2877 ... 1
Carbon-14 carboxy-labeled polysaccharides, RP2886 ... 71
Carbon monoxide from 2.3 to 2.5 microns, emission spectrum of, RP2883 ... 53
Carlson, E. T., The system lime-alumina-water at 1° C, RP2877 ... 1
Carpenter, L. H., On the motion of two cylinders in an ideal fluid, RP2889 ... 83
Carwile, N. L., G. W. Geil, Effect of strain-temperature history on the tensile behavior of titanium and a titanium alloy, RP2897 ... 173
Catalán, M. A., W. F. Meggers, M. Sales, Term analysis of the second spectrum of rhenium (Re II), RP2914 ... 441
Central notations for the revised ISCC–NBS color-name blocks, RP2911 ... 427
Chemical equilibrium among molecules, atoms, and atomic ions considered as clusters RP2916 ... 469
Cleek, G. W., E. H. Hamilton, Properties of sodium titanium silicate glasses, RP2890 ... 89
Clusters, chemical equilibrium among molecules, atoms, and atomic ions, considered as, RP2916 ... 469
Cold cell, liquid helium, for use with an X-ray diffractometer, RP2907 ... 367
Color-name blocks, revised ISCC–NBS, central notations for the, RP2911 ... 427
Corliss, C. H., W. F. Meggers, Improved description of hafnium spectra, RP2904 ... 269
Corliss, E. L. R., Uniform transient error, RP2879 ... 25
Correction for instrumental drift in flame photometry, RP2918 ... 499
Cristobalite, inversion temperature of, RP2902 ... 251

D

Darling, W. R., F. E. Washer, W. P. Tayman, Evaluation of lens distortion by visual and photographic methods, RP2920 ... 509
Density formula for alkali silicate glasses from annealing to glass-processing temperatures, RP2915 ... 463
Deuteromethanes, redetermination of mass spectra of, RP2896 ... 171
Dibeler, V. H., F. L. Mohler, E. Quinn, Redetermination of mass spectra of de uteromethanes, RP2896 ... 171
—, *J. L. Franklin, P. P. Morris Jr.*, Mass spectrometric study of the rate of thermal decomposition of hydrazoic acid, RP2881 ... 41
Diborane and pentaborane, heats of formation of, RP2901 ... 247
Dielectric constant of hydrogen-bonded liquids, RP2905 ... 325
Diffraction and reflection of waves and pulses by wedges and corners, RP2906 ... 343
Douglas, T. B., A. C. Victor, Heat content of zirconium and of five compositions of zirconium hydride from 0° to 900° C, RP2878 ... 13
Drift, instrumental, correction for, in flame photometry, RP2918 ... 499

E

Effect of crystal field and spin-orbit coupling on magnetic susceptibility of systems with f^2 electron configuration, RP2893 ... 117
Effect of strain-temperature history on the tensile behavior of titanium and a titanium alloy, RP2897 ... 173
Electromagnetic wave field, diffraction and reflection of, RP2906 ... 343
Electromagnetic waves in the presence of stratified media, transmission and reflection of, RP2899 ... 205
Emission spectrum of carbon monoxide from 2.3 to 2.5 microns, RP2883 ... 53
Engel, O. G., Erosion damage to solids caused by high-speed collision with rain, RP2882 ... 47
Erosion damage to solids caused by high-speed collison with rain, RP2882 ... 47
Evaluation of lens distortion by visual and photographic methods, RP2920 ... 509
Evaluation of tensile, compressive, torsional, transverse, and impact tests and correlation of results for brittle cermets, RP2895 ... 149

F

Franklin, J. L., V. H. Dibeler, P. P. Morris, Jr., Mass spectrometric study of the rate of thermal decomposition of hydrazoic acid, RP2881 ... 41
Further studies of the influence of a ridge on the low-frequency ground wave, RP2884 ... 57

G

Gases, thermodynamic properties of, at high temperature, RP2916 ... 469
Geil, G. W., N. L. Carwile, Effect of strain-temperature history on the tensile behavior of titanium and a titanium alloy, RP2897 ... 173
Glasses, alkali silicate, density formula for, RP2915 ... 463
Glasses, sodium titanium silicate, properties of, RP2890 ... 89
Gross, D., A. F. Robertson, An electrical-analog method for transient heat-flow analysis, RP2892 ... 105
—, —, Self-ignition temperatures of materials from kinetic-reaction data, RP2909 ... 413
Gross, L. J., R. F. Walker, S. Zerfoss, S. F. Holley, Temperature of the inversion in cristobalite, RP2902 ... 251

H

Hafnium spectra, improved description of, RP2904 ... 269
Hamilton, E. H., G. W. Cleek, Properties of sodium titanium silicate glasses, RP2890 ... 89
Hardy, R. C., Viscosity of *n*-hexadecane, RP2912 ... 433
Haught, A. F., B. W., Mulligan, Correction for instrumental drift in flame photometry, RP2918 ... 499
Heat content of zirconium and of five compositions of zirconium hydride from 0° to 900° C, RP2878 ... 13
Heat-flow analysis, transient, electrical-analog method for, RP2892 ... 105
Heat of formation of sodium calcium aluminate, RP2887 ... 75
Heats of formation of diborane and pentaborane, RP2901 ... 247
Herzfeld, C. M., D. B. Levine, Effect of crystal field and spin-orbit coupling on magnetic susceptibility of systems with f^2 electron configuration, RP2893 ... 117
n-Hexadecane, viscosity of, RP2912 ... 433
Holley, S. F., M. J. Kerper, L. E. Mong, M. B. Stiefel, Evaluation of tensile, compressive, torsional, transverse, and impact tests and correlation of results for brittle cermets, RP2895 ... 149
—, *R. F. Walker, S. Zerfoss, L. J. Gross*, Temperature of the inversion in cristobalite RP2902 ... 251
Hydrazoic acid, mass spectrometric study of the rate of thermal decomposition of, RP2881 ... 41
Hydrogen-bonded liquids, dielectric constant of, RP2905 ... 325

I

Improved description of hafnium spectra, RP2904 ... 269
Infrared emission spectra of flames under high resolution, RP2903 ... 263
Infrared flame spectra, emission of, under high resolution, RP2903 ... 263
Infrared spectrum of carbon monoxide, RP2883 ... 53
Infrared studies on polymorphs of silicon dioxide and germanium dioxide, RP2885 ... 61
Interferometer, parallel testing, RP2917 ... 491
Isbell, H. S., J. D. Moyer, Carbon-14 carboxy-labeled polysaccharides, RP2886 ... 71
ISCC–NBS color-name blocks, central notations for the revised, RP2911 ... 427

J

Johnson, W. H., F. J. Prosen, F. Y. Pergiel, Heats of formation of diborane and pentaborane, RP2901 ... 247
Johnston, R. G., R. Stair, Some studies of atmospheric transmittance on Mauna Loa, RP2910 ... 419

K

Kelly, K. L., Central notations for the revised ISCC–NBS color-name blocks, RP2911 ... 427
Kerper, M. J., L. E. Mong, M. B. Stiefel, S. F. Holley, Evaluation of tensile, compressive, torsional, transverse, and impact tests and correlation of results for brittle cermets, RP2895 ... 149

L

Lens distortion, evaluation of, by visual and photographic methods, RP2920 ... 509
Levine, D. B., C. M. Herzfeld, Effect of crystal field and spin-orbit coupling on magnetic susceptibility of systems with f^2 electron configuration, RP2893 ... 117
Lime-alumina-water, a study of the system at 1° C, RP2877 ... 1
Lippincott, E. R., A. Van Valkenburg, C. E. Weir, E. N. Bunting, Infrared studies on polymorphs of silicon dioxide and germanium dioxide, RP2885 ... 61
Liquid-helium cold cell for use with an X-ray diffractometer, RP2907 ... 367
Logan, H. L., Mechanism of stress-corrosion cracking in the AZ31B magnesium alloy, RP2919 ... 503
Longitudinal spherical aberration, optical T-bench method of measuring, RP2880 ... 31
Low-frequency ground wave, further studies of the influence of a ridge on, RP2884 ... 5

M

Madorsky, S. L., S. Straus, Thermal degradation of polyacrylonitrile, polybutadiene, and copolymers of butadiene with acrylonitrile and strene, RP2888 ... 77
Magnetic susceptibility of systems with f^2 electron configuration, effect of crystal field and spin-orbit coupling on, RP2893 ... 117
Mass spectrometric study of the rate of thermal decomposition of hydrazoic acid, RP2881 ... 41
Materials, self-ignition temperatures of, from kinetic-reaction data, RP2909 ... 413
Mauer, F. A., I. A. Black, L. H. Bolz, F. P. Brooks, H. S. Peiser, A liquid-helium cold cell for use with an X-ray diffractometer, RP2907 ... 367
Mechanism of stress-corrosion cracking in the AZ31B magnesium alloy, RP2919 ... 503
Meggers, W. F., A. G. Shenstone, The second spectrum of ruthenium (Ru II), RP2908 ... 373
—, *C. H. Corliss*, Improved description of hafnium spectra, RP2904 ... 269
—, *M. A. Catalán, M. Sales*, Term analysis of the second spectrum of rhenium (Re II), RP2914 ... 441
—, *R. W. Stanley*, Wavelengths from thorium-halide lamps, RP2891 ... 95
Mohler, F. L., V. H. Dibeler, F. Quinn, Redetermination of mass spectra of deuteromethanes, RP2896 ... 171
Mong, L. F., M. J. Kerper, M. B. Stiefel, S. F. Holley, Evaluation of tensile compressive, torsional, transverse, and impact tests and correlation of results for brittle cermets, RP2895 ... 149
Morris, P. P., Jr., V. H. Dibeler, J. L. Franklin, Mass spectrometric study of the rate of thermal decomposition of hydrazoic acid, RP2881 ... 41
Moyer, J. D., H. S. Isbell, Carbon-14 carboxy-labeled polysaccharides, RP2886 ... 71
Mulligan, B. W., A. F. Haught, Correction for instrumental drift in flame photometry, RP2918 ... 503
Murphy, A., J. R. Wait, Further studies of the influence of a ridge on the low-frequency ground wave, RP2884 ... 57

N

Newkirk, T. F., R. D. Thwaite, Pseudoternary system calcium oxide-monocalcium aluminate ($CaO \cdot Al_2O_3$)-dicalcium ferrite ($2CaO \cdot Fe_2O_3$), RP2900 ... 233
Newman, F. S., Heat of formation of sodium calcium aluminate, RP2887 ... 75

O

On the motion of two cylinders in an ideal fluid, RP2889 ... 83
Optical T-bench method of measuring longitudinal spherical aberration, RP2880 ... 31
Oxyacetylene flame spectra, emission of, under high resolution, RP2903 ... 263

P

Parallel testing interferometer, RP2917 ... 491
Pergiel, F. Y., E. J. Prosen, W. H. Johnson, Heats of formation of diborane and pentaborane, RP2901 ... 247
Phase equilibrium diagram of the binary system calcia-titania, showing the compound $Ca_4Ti_3O_{10}$, revision of, RP2913 ... 437
Plyler, E. K., F. D. Tidwell, Infrared emission spectra of flames under high resolution, RP2903 ... 263
—, *H. C. Allen, Jr., F. D. Tidwell*, Emission spectrum of carbon monoxide from 2.3 to 2.5 microns, RP2883 ... 53
—, *W. S. Benedict, F. D. Tidwell*, Vibration-rotation bands of ammonia: I. The combination bands $\nu_2-(\nu_1, \nu_3)$, RP2894 ... 123
Polyacrylonitrile, polybutadiene, and copolymers of butadiene with acrylonitrile and styrene, thermal degradation of, RP2888 ... 77
Polymorphs of silicon dioxide and germanium dioxide, infrared studies on, RP2885 ... 61
Polysaccharides, carbon-14, carboxy-labeled, RP2886 ... 71
Propagation of very-low-frequency pulses to great distances, RP2898 ... 187
Properties of sodium titanium silicate glasses, RP2890 ... 89
Prosen, F. J., W. H. Johnson, F. Y. Pergiel, Heats of formation of diborane and pentaborane, RP2901 ... 247
Pseudoternary system calcium oxide-monocalcium aluminate ($CaO \cdot Al_2O_3$)-dicalcium ferrite ($2CaO \cdot Fe_2O_3$), RP2900 ... 233

Q

Quinn, F., F. L. Mohler, V. H. Dibeler, Redetermination of mass spectra of deuteromethanes, RP2896 ... 171

R

Rain, erosion damage to solids caused by high-speed collision with, RP2882 ... 47
Redetermination of mass spectra of deuteromethanes, RP2896 ... 171
Revision of the phase equilibrium diagram of the binary system calcium-titania, showing the compound $Ca_4Ti_3O_{10}$, RP2913 ... 437
Rhenium (Re II), term analysis of the second spectrum of, RP2914 ... 441
Ridge, further studies of the influence of a, on the low-frequency ground wave, RP2884 ... 57
Robertson, A. F., D. Gross, An electrical-analog method for transient heat-flow analysis, RP2892 ... 105
—, —, Self-ignition temperatures of materials from kinetic-reaction data, RP2909 ... 413
Roth, R. S., Revision of the phase equilibrium diagram of the binary system calcia-titania, showing the compound $Ca_4Ti_3O_{10}$, RP2913 ... 437
Ruthenium (Ru II), second spectrum of, RP2908 ... 373

S

Sales, M., W. F. Meggers, M. A. Catalán, Term analysis of the second spectrum of rhenium (Re II), RP2914 ... 441
Saunders, J. B., Parallel testing interferometer, RP2917 ... 491
Second spectrum of ruthenium (Ru II), RP2908 ... 373
Self-ignition temperatures of materials from kinetic-reaction data, RP2909 ... 413
Shenstone, A. G., W. F. Meggers, The second spectrum of ruthenium (Ru II), RP2908 ... 373
Silicate glasses, alkali density formula for, RP2915 ... 463
Sodium calcium aluminate, heat of formation of, RP2887 ... 75
Some studies of atmospheric transmittance on Mauna Loa, RP2910 ... 479
Stair, R., R. G. Johnston, Some studies of atmospheric transmittance on Mauna Loa, RP2910 ... 479
Stanley, R. W., W. F. Meggers, Wavelengths from thorium-halide lamps, RP2891 ... 95
Stiefel, M. B., M. J. Kerper, L. F. Mong, S. F. Holley, Evaluation of tensile, compressive, torsional, transverse, and impact tests and correlation of results for brittle cermets, RP2895 ... 149
Straus, S., S. L. Madorsky, Thermal degradation of polyacrylonitrile, polybutadiene, and copolymers of butadiene with acrylonitrile and strene, RP2888 ... 77
Stress-corrosion cracking in the AZ31B magnesium alloy, mechanism of, RP2919 ... 503
System lime-alumina-water at 1° C, RP2877 ... 1

T

Tayman, W. P., F. F. Washer, W. R. Darling, Evaluation of lens distortion and photographic method, RP2920 ... 509
Temperature of the inversion in cristobalite, RP2902 ... 251
Tensile behavior of titanium and a titanium alloy, effect of strain-temperature on, RP2897 ... 173
Term analysis of the second spectrum of rhenium (Re II), RP2914 ... 441
Thermal decomposition rate of hydrazoic acid, mass spectrometric study of, RP2881 ... 41
Thermal degradation of polyacrylonitrile, polybutadiene, and copolymers of butadiene with acrylonitrile and strene, RP2888 ... 77
Thermodynamic properties of gases at high temperature: I. Chemical equilibrium among molecules, atoms, and atomic ions considered as clusters, RP2916 ... 469
Thorium-halide lamps, wavelengths from, RP2891 ... 95
Thwaite, R. D., T. F. Newkirk, Pseudoternary system calcium oxide-monocalcium aluminate ($CaO \cdot Al_2O_3$)-dicalcium ferrite ($2CaO \cdot Fe_2O_3$), RP2900 ... 233
Tidwell, F. D., E. K. Plyler, Infrared emission spectra of flames under high resolution, RP2903 ... 263
—, *H. C. Allen, E. K. Plyler*, Emission spectrum of carbon monoxide from 2.3 to 2.5 microns, RP2883 ... 53
—, *W. S. Benedict, E. K. Plyler*, Vibration-rotation bands of ammonia: I. The combination bands $\nu_2-(\nu_1, \nu_3)$, RP2894 ... 123
Tilton, L. W., Density formula for alkali silicate glasses from annealing to glass-processing temperatures, RP2915 ... 463
Titanium and a titanium alloy, effect of strain-temperature history on the tensile behavior of, RP2897 ... 173
Transient error, uniform, RP2879 ... 25
Transmission and reflection of electromagnetic waves in the presence of stratified media, RP2899 ... 205
Two cylinders in an ideal fluid, on the motion of, RP2889 ... 83

U

Uniform transient error, RP2879 ... 25

V

Van Valkenburg, A., E. R. Lippincott, C. E. Weir, E. N. Bunting, Infrared studies on polymorphs of silicon dioxide and germanium dioxide, RP2885 ... 61
Very-low-frequency pulses, propagation of to great distances, RP2898 ... 187
Vibration-rotation bands of ammonia: I. The combination bands $\nu_2-(\nu_1, \nu_3)$, RP2894 ... 123
Victor, A. C., T. B. Douglas, Heat content of zirconium and of five compositions of zirconium hydride from 0° to 900°C, RP2878 ... 13
Viscosity of *n*-hexadecane, RP2912 ... 433

W

Wait, J. R., A. Murphy, Further studies of the influence of a ridge on the low-frequency ground wave, RP2884 ... 57
—, Propagation of very-low-frequency pulses to great distances, RP2898 ... 187
—, Transmission and reflection of electromagnetic waves in the presence of stratified media, RP2899 ... 205
Walker, R. F., S. Zerfoss, S. F. Holley, L. J. Gross, Temperature of the inversion in cristobalite, RP2902 ... 251
Washer, F. F., Optical T-bench method of measuring longitudinal spherical aberration, RP2880 ... 31
—, *W. P. Tayman, W. R. Darling*, Evaluation of lens distortion by visual and photographic methods, RP2920 ... 509
Wavelengths from thorium-halide lamps, RP2891 ... 95
Waves and pulses, on the diffraction and reflection of by wedges and corners, RP2906 ... 343
Wedges and corners on the diffraction and reflection of waves and pulses by, RP2906 ... 343
Weir, C. E., E. R. Lippincott, A. Van Valkenburg, E. N. Bunting, Infrared studies on polymorphs of silicon dioxide and germanium dioxide, RP2885 ... 61
Woolley, H. W., Thermodynamic properties of gases at high temperature: I. Chemical equilibrium among molecules, atoms, and atomic ions considered as clusters, RP2916 ... 469

Z

Zerfoss, S., R. F. Walker, S. F. Holley, L. J. Gross, Temperature of the inversion in cristobalite, RP2902 ... 251
Zirconium and five compositions of zirconium hydride, heat content of from 0° to 900°C, RP2878 ... 13

U. S. GOVERNMENT PRINTING OFFICE: 1959

THE NATIONAL BUREAU OF STANDARDS

The scope of activities of the National Bureau of Standards at its headquarters in Washington, D. C., and its major laboratories in Boulder, Colorado, is suggested in the following listing of the divisions and sections engaged in technical work. In general, each section carries out specialized research, development, and engineering in the field indicated by its title. A brief description of the activities, and of the resultant publications, appears on the inside of the front cover.

WASHINGTON, D. C.

Electricity and Electronics. Resistance and Reactance. Electron Devices. Electrical Instruments. Magnetic Measurements. Dielectrics. Engineering Electronics. Electronic Instrumentation. Electrochemistry.

Optics and Metrology. Photometry and Colorimetry. Optical Instruments. Photographic Technology. Length. Engineering Metrology.

Heat. Temperature Physics. Thermodynamics. Cryogenic Physics. Rheology. Engine Fuels. Free Radicals Research.

Atomic and Radiation Physics. Spectroscopy. Radiometry. Mass Spectrometry. Solid State Physics. Electron Physics. Atomic Physics. Neutron Physics. Radiation Theory. Radioactivity. X-rays. High Energy Radiation. Nucleonic Instrumentation. Radiological Equipment.

Chemistry. Organic Coatings. Surface Chemistry. Organic Chemistry. Analytical Chemistry. Inorganic Chemistry. Electrodeposition. Molecular Structure and Properties of Gases. Physical Chemistry. Thermochemistry. Spectrochemistry. Pure Substances.

Mechanics. Sound. Mechanical Instruments. Fluid Mechanics. Engineering Mechanics. Mass and Scale. Capacity, Density, and Fluid Meters. Combustion Controls.

Organic and Fibrous Materials. Rubber. Textiles. Paper. Leather. Testing and Specifications. Polymer Structure. Plastics. Dental Research.

Metallurgy. Thermal Metallurgy. Chemical Metallurgy. Mechanical Metallurgy. Corrosion. Metal Physics.

Mineral Products. Engineering Ceramics. Glass. Refractories. Enameled Metals. Concreting Materials. Constitution and Microstructure.

Building Technology. Structural Engineering. Fire Protection. Air Conditioning, Heating, and Refrigeration. Floor, Roof, and Wall Coverings. Codes and Safety Standards. Heat Transfer.

Applied Mathematics. Numerical Analysis. Computation. Statistical Engineering. Mathematical Physics.

Data Processing Systems. SEAC Engineering Group. Components and Techniques. Digital Circuitry. Digital Systems. Analog Systems. Application Engineering.

• Office of Basic Instrumentation.

• Office of Weights and Measures.

BOULDER, COLORADO

Cryogenic Engineering. Cryogenic Equipment. Cryogenic Processes. Properties of Materials. Gas Liquefaction.

Radio Propagation Physics. Upper Atmosphere Research. Ionospheric Research. Regular Propagation Services. Sun-Earth Relationships. VHF Research. Ionospheric Communication Systems.

Radio Propagation Engineering. Data Reduction Instrumentation. Modulation Systems. Navigation Systems. Radio Noise. Tropospheric Measurements. Tropospheric Analysis. Radio Systems Application Engineering. Radio Meteorology.

Radio Standards. High Frequency Electrical Standards. Radio Broadcast Service. High Frequency Impedance Standards. Electronic Calibration Center. Microwave Physics. Microwave Circuit Standards.

Recent Publications of the National Bureau of Standards

Periodicals

Journal of Research of the National Bureau of Standards, Volume 61, No. 4, October 1958 (RP2900 to RP2905 incl.). 60 cents.

Technical News Bulletin, Volume 42, No. 10, October 1958. 10 cents. Annual subscription $1.50, 75 cents additional for foreign mailing.

Basic Radio Propagation Predictions for January 1959. Three months in advance. CRPL-D 170. Issued October 1958. 10 cents. Annual subscription $1.00, 50 cents additional for foreign mailing.

Miscellaneous Publications

M224. Hydraulic Research in the United States, 1958. $1.25.*

Available from the Superintendent of Documents, U. S. Government Printing Office, Washington 25, D. C. The three NBS periodicals are available on a 1-, 2-, or 3-year subscription basis, although no reduction in rates can be made.

**Foreign postage, one-fourth additional.*

OF MICHIGAN
LABORATORY

UNITED S
GOVERNMENT PRINTI
DIVISION OF PUBLIC DOCUMENTS
WASHINGTON 25, D. C.
OFFICIAL BUSINESS

PENALTY FOR PRIVATE USE TO AVOID PAYMENT OF POSTAGE, $300 (GPO)

Journal of Research of the National Bureau of Standards Vol. 61, No. 6 December 1958

Contents

Page

Term analysis of the second spectrum of rhenium (Re II). William F. Meggers, Miguel A. Catalán, and Manuel Sales. RP2914 441

Density formula for alkali silicate glasses from annealing to glass-processing temperatures. Leroy W. Tilton. RP2915 463

Thermodynamic properties of gases at high temperature: 1. Chemical equilibrium among molecules, atoms, and atomic ions considered as clusters. Harold W. Woolley. RP2916 469

Parallel testing interferometer. James B. Saunders. RP2917 491

Correction for instrumental drift in flame photometry. Barry W. Mulligan and Alan F. Haught. RP2918 499

Mechanism of stress-corrosion cracking in the AZ31B magnesium alloy. Hugh L. Logan. RP2919 503

Evaluation of lens distortion by visual and photographic methods. Francis E. Washer, William P. Tayman, and Walter R. Darling. RP2920 509

Index to volume 61 (July to December 1958, Research Papers RP2877 to RP2920). 517

[A list of recent NBS publications is given on page 3 of the cover.]

For sale by the Superintendent of Documents, U. S. Government Printing Office, Washington 25, D. C. Price 60 cents (single copy).
UNITED STATES GOVERNMENT PRINTING OFFICE, WASHINGTON : 1958

7480